NASA Technical Paper 1278

Effect of Rotor Meridional Velocity Ratio on Response to Inlet Radial and Circumferential Distortion

Nelson L. Sanger

JULY 1979

NASA

NASA Technical Paper 1278

Effect of Rotor Meridional Velocity Ratio on Response to Inlet Radial and Circumferential Distortion

Nelson L. Sanger
Lewis Research Center
Cleveland, Ohio

National Aeronautics
and Space Administration

**Scientific and Technical
Information Branch**

1979

CONTENTS

SUMMARY

Three single, transonic fan stages having differing meridional velocity ratios across the rotors were tested with two magnitudes of tip radial distortion and with a 90° circumferential distortion imposed on the inlet flow. The fan rotors were approximately 50.8 centimeters in diameter and had design operating tip speeds of 425 meters per second and a design pressure ratio of 1.60.

Of the three rotors tested the rotor having the lowest meridional velocity ratio (less than 0.9 at the tip) demonstrated the least degradation in performance from tip radial distortion. The rotor having the highest meridional velocity ratio (greater than 1.0 at the tip) suffered the largest losses in performance due to tip radial distortion.

Loss and deviation angle data (as needed for performance prediction with radial distortion) calculated along actual streamlines for radially distorted flow and correlated against diffusion factor, showed consistent agreement with data calculated along design streamlines for undistorted flow. The use of off-design calculation codes to predict radial distortion performance therefore appears feasible.

The tip region of the low meridional velocity ratio rotor displayed a stronger recovery response to the circumferential distortion than did the tip region of the high meridional velocity rotor. The hub sections all showed a typical low-recovery response with no significant effect of meridional velocity ratio apparent.

INTRODUCTION

A principal assumption in compressor and fan design procedure is that the inlet flow is uniform and axisymmetric. In actual aircraft applications the inlet flow is often nonuniform (i.e., distorted), a condition which can result in severe performance degradation. Ground-based turbomachinery can also experience distorted inflow produced by upstream duct geometry.

Distortion is characterized by distributions in the inlet flow parameters of velocity, pressure, temperature, flow angle, or gas constituency that are different from design intent. The variations in these parameters may have a principal bias in the radial direction, the circumferential direction, or in a combination of both directions. To simplify the analysis of the very complex, combined patterns that are encountered, variations in the radial and circumferential directions are usually considered separately.

Analysis of performance with radial distortion follows conventional compressor analysis procedures because the relative flow field is axisymmetric and steady; analysis

of performance with a circumferentially distorted flow field requires a more complex model because the flow field is nonaxisymmetric and therefore appears as unsteady to the rotor. Unsteady theoretical models applicable to the compressible flow field of high-speed compressors are still in the early stages of development. Thus, systematic experimental programs are currently necessary to reveal the aerodynamics of compressor flow with circumferential distortion and to permit more distortion-tolerant designs to be evolved. Distortion measurements are taken as part of a general program of fan and compressor research conducted at Lewis. Major attention is given to "steady-state" distortion patterns (the magnitude and extent are nonfluctuating with time), which are produced experimentally by wire mesh screens.

This report discusses the experimental tip radial and circumferential distortion performance of three transonic fan stages, each having different outlet-to-inlet ratios of meridional velocity (vector sum of axial and radial velocity components) across the rotor. The stages, each having an inlet hub-to-tip radius ratio of 0.5, were designed for a pressure ratio of 1.57 at a rotor tip speed of 425 meters per second. The velocity ratio was varied by changing the outer wall contour (tip) while maintaining the same inner wall (hub) contour for three stages. It is the objective of this study to examine the influence of meridional velocity ratio on the response of the rotors to the subject inlet distortions.

In exploring these matters the overall performances of each rotor and stage are compared with each other and with similar performances under undistorted flow conditions. Detailed flow measurements taken at various radial and axial positions are evaluated. Radial distributions of flow parameters and blade-element data are presented for design speed and 70 percent of design speed. Overall performance data are evaluated over the full range of flow conditions and for several speeds.

APPARATUS AND PROCEDURE

The apparatus consists of the test facility, single-stage fans, instrumentation, and distortion screens. The description of these items is followed by a discussion of test and calculation procedures.

TEST FACILITY

The tests were conducted in the Lewis single-stage compressor facility (ref. 1), a schematic of which is shown in figure 1. Air enters the facility through an inlet on the roof and passes through a measuring orifice and into the plenum. It then passes through the distortion screens, the test stage, and into a collector from which it is exhausted to

the atmosphere. Back pressure on the stage is controlled by a slide valve located in the collector. All tests were conducted with atmospheric inlet conditions.

SINGLE-STAGE FANS

The pertinent design features of each single-stage fan are presented in table I. Each rotor and stator have designated numbers, and the complete stage is described by a two-number code. Thus, stage 20-17 consists of rotor 20 and stator 17. All stages were designed for the same pressure ratio and temperature ratio at the same flow rate. And all stages have nearly the same rotor and stator solidities and aspect ratios as well as rotor tip speeds. The meridional velocity ratios were achieved by tapering the outer casing while maintaining the same hub contour for all stages. Since all the rotors were designed to produce the same overall pressure ratio, but each had differing amounts of contouring, some differences in geometric and aerodynamic design distributions (such as camber angle) occurred. The principal difference in the three designs, however, is the meridional velocity ratio.

Rotor and stator blade shapes were multiple circular arcs (MCA) for all stages. The rotor vibration dampers were located at 57, 50, and 58 percent of span from the tip for rotors 20, 11, and 19, respectively (corresponding to the low, reference, and high meridional velocity ratio). Stage 11-4 is referred to as the "reference" stage because it formed the basis for the study of several design parameters such as specific weight-flow, loading, solidity, and meridional velocity ratio. Using stage 11-4 as reference, other stages in a series were designed to vary (insofar as was practicable) only one principal parameter.

The design geometries and design blade-element parameters are in tables II to XIII. (Symbols are defined in appendix A, related equations in appendix B, and definitions used in the tables are presented in appendix C.) Because each stage performed differently from design to various degrees and because it is not pertinent to this report, no comparisons shall be made with design. The undistorted performances of stages 20-17 and 11-4 are presented in references 2 and 3. The performance of stage 19-16 has not previously been documented.

The actual meridional velocity ratios produced by each rotor for undistorted flow are plotted in figure 2 for the near-peak-efficiency flow condition. Meridional velocity ratio of the rotors differed in a clear manner across the whole blade span. The largest and most consistent difference occurred in the tip region where the outer casing was contoured. To determine the response of the stage with distortion to meridional velocity ratio changes, attention was directed to the tip region in the discussion that follows. For convenience the rotors (and rotor-stator combinations) will be classified according

to their general levels of meridional velocity ratio and referred to as low, reference, and high MVR, corresponding to rotors 20, 11, and 19.

INSTRUMENTATION

Compressor flow rate was measured using a calibrated thin-plate orifice located in the inlet piping (fig. 1). Rotative speed was measured by an electric speed counter in conjunction with a magnetic pickup.

For undistorted and radially distorted flow conditions, surveys were made at 11 radial locations and three axial locations (upstream of the rotor, downstream of rotor, and downstream of the stator (stations 1, 2, and 3 in fig. 3).) Total pressure, total temperature, and flow angle were measured with a combination probe (fig. 4(a)), and static pressure was measured with an 8° (included angle) wedge (fig. 4(b)). Each probe was positioned with a null-balancing, stream-direction-sensitive control system that automatically alined the probe to the direction of flow. One combination probe and one wedge static probe were used at each of the three measuring stations. A more complete description of the instrumentation is given in reference 1.

For circumferentially distorted flow, radial surveys of the flow field were made at five axial locations (stations -1, 0, 1, 2, and 3 in fig. 3), but at only three radial positions (near tip, midspan, and near hub). Because of the circumferential variation in flow properties, it was desirable to obtain all measurements at the same circumferential location. Therefore, a single combination probe was used. (The distortion screen was rotated with respect to the probe.) Static pressures were obtained by averaging the pressures measured from the taps on the two sides of the 60° (included angle) wedge and using calibration curves relating these readings with true static pressure. A more complete description of this instrumentation is presented in reference 2.

The estimated errors in the data, based on inherent accuracies of the instrumentation and recording systems, are as follows:

Weight flow, kg/sec	±0.3
Rotative speed, rpm	±30
Flow angle, deg	±1
Temperature, K	±0.6
Rotor-inlet total pressure, N/cm^2	±0.01
Rotor-outlet total pressure, N/cm^2	±0.10
Stator-outlet total pressure, N/cm^2	±0.10
Rotor-inlet static pressure, N/cm^2	±0.04
Rotor-outlet static pressure, N/cm^2	±0.07
Stator-outlet static pressure, N/cm^2	±0.07

DISTORTION SCREENS

The distortion screen assembly used in the investigation was located 36.25 centimeters upstream of the rotor hub leading edge (fig. 3). The distortion screens were secured to a backup screen having a 1.9- by 1.9-centimeter opening and a 0.27-centimeter wire diameter. The eight backup-screen struts were streamlined so that each cross section resembled an ellipse having a maximum thickness of 0.76 centimeter.

The circumferential distortion screen was composed of a 20 by 20 wire mesh (20 wires per in. or per 2.5 cm). The screen covered 85° at the outer radius and 135° at the inner radius. Wire diameter was 0.051 centimeter, resulting in a 36-percent open area. Interaction between the rotor and the resulting distorted flow field produces a distortion pattern at the rotor inlet plane that covered 90°. The screen (see fig. 5) was rotated to 12 equally spaced circumferential positions to obtain the distortion patterns measured by the survey probe.

The high magnitude, radial distortion was produced by a screen composed of 0.051-centimeter-diameter wire arranged in a 20 by 20 mesh (36 percent open area). The radial extent of the screen from the tip inward was 4.45 centimeters, which was equivalent to 35 percent of the flow area at the screen. The low magnitude, radial distortion was produced by a screen of 0.081-centimeter-diameter wire arranged in a 7 by 7 mesh (61 percent open area). The radial extent of the screen from the tip inward was 5.1 centimeters, which corresponds to 39.5 percent of the flow area at the screen.

TEST PROCEDURE

For tests with only the backup screen in place (reference undistorted inlet flow condition) and for radial distortion tests, radial surveys were taken for all stages over a range of weightflows from maximum flow to near stall at 70 and 100 percent of design equivalent speed $N/\sqrt{\theta}$. At 60, 80, and 90 percent of design equivalent speed surveys were taken only at the near-stall weight flow. (Hereinafter the adjective "equivalent" is implied.) Data were recorded at 11 radial positions for each operating condition. For tests with and without distortion the back pressure was increased for each speed by closing the outlet valve until a stalled condition was obtained. Stall or surge conditions were indicated by a sudden drop in stage outlet pressure (measured by a midpassage monitoring probe and recorded on an X-Y plotter), by large increases in measured blade stresses on both rotor and stator, and by a sudden increase in audible noise. Radial survey data were taken at a weight flow as close to actual stall as practicable. In general, this was within 0.5 kilogram per second of the actual stall weight flow.

The circumferential distortion test data were taken at 100 and 70 percent of design speed. The 100 percent of design speed data were taken at three weight flows, from

near stall to maximum weight flow; the 70 percent of design speed data were taken at near stall and midflow. Data were surveyed at 10, 45, and 90 percent span from the tip for each of the 12 screen positions.

CALCULATION PROCEDURE

All data presented in this report have been adjusted such that average rotor-inlet conditions correspond to standard-day conditions (total pressure, 10.13 N/cm^2; total temperature, 288 K). The calculation procedure used for undistorted tests with the backup screen (BUS) in place is the same as used for conventional clean inlet tests (see ref. 1). In particular, flow streamlines at all operating conditions are assumed to be the same as the design streamlines.

For operation with radial distortion, streamlines were assumed to pass through equal-weight-flow 0oints calculated on blade leading and trailing edges along a linear path. In this study streamlines across the rotor, for example, were defined by fixing radial locations at the trailing edge (same as determined by design streamlines) and calculating the corresponding weight flow locations at the leading edge.

Because of the asymmetric nature of the flow, circumferential distortion data are presented at the measuring stations only. No attempts were made to calculate blade-element parameters or to translate data to the blade edges. Further details on the calculating procedure for circumferential distortion data are given in reference 2.

Overall performance values with the backup screen (BUS) were obtained from a mass or energy average of the data taken at 11 radial positions. Values with circumferential distortion are obtained from three radial positions. To insure accurate comparison of circumferentially distorted and BUS overall performance data, the BUS data are recalculated from three radial points.

RESULTS AND DISCUSSION

The results of this investigation are presented in two main sections: Performance with radially distorted inlet flow and performance with circumferentially distorted flow.

The reader should note certain distinctions in terminology. Tests on the subject stages reported in references 3 and 4 were with truly undistorted or "clean" inlet flow (i.e., no backup screen). All tests discussed in this report were conducted with a backup screen in place; additionally, radial and circumferential distortion screens were secured to the backup screen for distortion tests. All tests without the distortion screens (but with the backup screens) are referred to as BUS tests, and represent flow

without distortion. Regions of the flow in which no distortion screens were secured to the backup screen are referred to as "undistorted" regions or sectors.

PERFORMANCE WITH RADIAL DISTORTION

Overall Performance

Two complete speed lines (100 and 70 percent of design speed) were obtained for each stage for flow with radial distortion. Two magnitudes of distortion were applied to the low MVR stage and the high MVR stage, and one magnitude to stage 11-4, the reference MVR stage. The magnitude of inlet radial distortion DM for each stage at 100 and 70 percent of design speed at the near stall condition is as follows:

Stage	Rotor meridional velocity ratio (a)		Magnitude of distortion, DM $\Big\vert_{\theta^{O}=\text{const}}$	
			100 Percent of design speed	70 Percent of design speed
20-17	Low	0.85	0.18	0.07
			.09	.04
11-4	Reference	.93	.16	.07
19-16	High	1.04	.16	.06
			.09	.03

[a]At 10 percent span from tip; experimental values (BUS).

Overall performance curves (efficiency and total pressure ratio) with and without tip radial distortion are shown in figures 6 to 8. With distortion, the low MVR rotor operated on the BUS speed line at an efficiency that was greater than BUS levels (fig. 6); the reference MVR rotor operated slightly below the BUS speed line at an efficiency that was about equal to the BUS levels (fig. 7); and the high MVR rotor operated below the BUS speed line at the lowest efficiency as compared with BUS values.

At design speed and the higher magnitude of radial distortion, all rotors and stages displayed essentially the same decrease in stall pressure ratio. This decrease is measured by the change in stall pressure-ratio parameter ΔPRS (see definition in appendix B) and is summarized in table XIV.

At speeds lower than design all stages stalled at weight flows higher than BUS values and displayed the same trends with respect to BUS conditions. However, the differ-

ences between distorted and BUS performance were smaller at 70 percent of design speed, mainly because DM was smaller.

Inlet radial distortion causes a rematching of the blade elements, which generally resulted in a performance penalty. This behavior is clearly displayed by the reference and high MVR rotors (11 and 19), which lost overall pressure ratio, efficiency, and stall pressure ratio with tip radial distortion. The rematching of the low MVR rotor elements was much less adversely affected: Overall pressure ratio was unaffected, efficiency increased slightly, but stall pressure ratio did decline.

Radial Distribution of Flow Parameters

Radial distributions in selected rotor flow parameters for the near-stall, tip-radial distortion and BUS points are presented in figures 9 to 11. Also presented are BUS performance data at approximately the same flow rate as the near-stall flow condition with distortion. The plots allow two types of comparisons of flows with and without distortion:

(1) Comparisons at the same weight flow indicate flow shifts and blade-element rematching, which translate into changes in overall performances.

(2) Comparisons at near-stall operation permit the indentification of highly loaded elements and help to explain losses in stall margin.

The discussion will center mainly on changes in performance and flow from BUS conditions caused by tip radial distortion. The low magnitude of distortion (DM) was chosen for discussion in figures 9 and 11 because data at the same flow rate are available for comparison. These data are not available for the high DM. The high DM data are presented in figures 24 and 25 where comparisons may be made at the near-stall condition only. Stator data for the low DM are presented in figure 12 and for the high DM in figure 26.

Because all rotors responded to the distortion in basically the same fashion, the initial portion of the discussion will describe the general response using figure 10 (reference MVR rotor 11) and specific differences will be noted later.

At the rotor inlet, distributions of the inlet specific weight flow parameter ρV_z show the effect of the screen in shifting flow from the rotor tip to the hub (fig. 10(i)). The lower than BUS values of V_z at the tip lead to higher incidence angles, while the hub section experiences high axial velocities and low incidence angles. High incidence angle tends to load a blade section, while low incidence unloads it.

A comparison of distorted and BUS temperature ratio distributions across the rotor (fig. 10(d)) at the same flow rate shows that the distorted flow energy addition is higher at the tip and lower at the hub than the BUS flow condition. This was anticipated from the incidence-angle distribution discussed previously. In the tip region, although total-

pressure ratio exceeds BUS levels, the magnitude of the outlet total pressure realized does not (cf., figs. 10(b) and (c)). The energy addition is high, but inlet total pressure is low because of the distortion. In the hub region, because of low energy addition, the outlet total pressure is also below the BUS levels. In general, then, the outlet total pressure with distortion is lower than outlet total pressure without distortion (BUS) over all or most of the blade span. Therefore, the overall pressure ratio with distortion is also lower. The lower average outlet total pressure (and density) also produces a higher average outlet axial velocity due to continuity requirements (see fig. 10(k)), a condition which tends to unload the blade. A further effect of distortion is that the higher energy addition in the distorted region and lower energy addition in the undistorted region tend to reduce the outlet-total-pressure distortion (compared with magnitude at the inlet) and the axial velocity distribution follows this behavior.

These flow and performance changes from BUS conditions discussed previously apply to all three rotors, with one notable exception: The low MVR rotor (20) produced outlet-total-pressure distributions that closely approximated the BUS distribution, particularly in the tip region (fig. 9(b)). This behavior enabled the low MVR rotor to operate on the BUS speed line. The high MVR rotor (19), however, was unable to meet the BUS total-pressure distribution (fig. 11(b)); consequently, overall, mass-averaged pressure ratio was less than BUS values. A significant difference in operation between the low MVR and the other rotors can be seen by comparing loss distributions in the tip region for BUS and distorted flow conditions (figs. 9(f), 10(f), and 11(f)). The low MVR rotor did not show a large increase in loss compared with BUS flow in this region, but the other rotors showed notably higher values. Although the reasons for this behavior cannot be determined with certainty, it should be observed that, the lower MVR rotor had the lowest camber over the outer span of the blade (see tables IV, VIII, and XII); thus its loading level was achieved with a relatively greater proportion of diffusion of meridional velocity and a lesser amount of fluid turning than the other rotors (see eq. (B3)). In addition, a lower camber tends to keep suction-surface Mach numbers, and consequent shock losses, lower.

When comparing near-stall operating points, it is significant that for each rotor, values of temperature ratio and D-factor at the tip were nearly the same for distorted and BUS flow conditions. This implies that a critical loading condition (measured by temperature-rise or D-factor) was reached in the tip region of each rotor. In each case of tip radially distorted flow the condition was reached at a higher flow rate than for BUS flow.

It should be noted that a general characteristic of all of the rotors is a tendency to "heal", or diminish, DM across the blade row. The ability to reduce DM suggests that the performance of any succeeding stages (in a multistage arrangement) would not be

penalized as much as any of the subject stages. The low MVR rotor displayed the strongest tendency to reduce the DM and to achieve undistorted outlet distributions.

For the stages under consideration the stator performance was generally not adversely affected by radial distortion. Since rotor-outlet axial velocities were greater than BUS values over most of the span, this led to high stator-inlet velocities and Mach number and to low incidence angles, particularly in the hub region. The stators therefore, operated in an unloaded manner as indicated by D-factor levels. The loss followed the general trend of incidence angle, and deviation angle was not significantly affected. In the midspan segment the effects of the rotor damper on stator flow parameters was obvious (see fig. 12). These data also indicate a sharp increase in loss coefficient and D-factor in the hub region of all stators (95 percent of span from tip), for which the cause is unknown. Possible causes are wall boundary-layer separation, local choking, or a measurement problem.

Blade-Element Performance

With the tip-radial distortion imposed herein, the flow is assumed to be axisymmetric, but with the blade elements along the span operating in an off-design mode. In principle, this flow can be predicted using off-design calculation codes, provided the pertinent relations for loss and fluid turning are known. In this section blade-element flow and performance parameters with and without distortion over an operating range are compared to determine whether similar relations for loss and deviation can be applied. Performance parameters for BUS flow are evaluated along design streamlines, as is common practice for undistorted-flow studies, and performance parameters with radially distorted flow are evaluated along streamlines calculated at each operating point.

Blade-element parameters are typically presented as functions of incidence angle as in figure 13(a). With tip radial distortion, however, the deficit in velocity near the tip caused the tip elements to operate at levels of incidence angle higher than BUS operation "limits" over most of the flow range (cf., solid and open points, fig. 13(a)). Whereas under normal conditions blade loading would become excessive at such high incidence angles, it did not in this case because of an acceleration of meridional velocity across the element (see eq. (B3)). The resulting levels of MVR were also beyond the range associated with BUS operation (see fig. 13(b)). Similar behavior was noted in a single rotor-blade row in reference 5.

An alternative method of correlation, principally used for blade-element loss coefficient, is to present the blade-element parameters as functions of diffusion factor D. Parameters correlated in this fashion are presented in figures 14 to 16 for selected

blade elements. Additional blade-element data for rotors at 70 percent of design speed are presented in figures 27 to 29 and for stators at design speed in figures 30 to 32.

An examination of rotor data reveals that of the parameters considered, incidence angle and MVR were significantly affected by tip radial distortion. All rotors showed similar response characteristics. Because of the deficiency in inlet velocity, the tip elements operated at levels of incidence angle significantly higher than BUS operation over the entire operating range (represented by D-factor range) shown in figures 14 to 16. Conversely, higher velocities at the hub caused it to operate at lower incidence angles than BUS operation. Despite the high incidence in the tip, the D-factor (loading) level remained similar to BUS levels because the element operated at much higher MVR's (figs. 14 to 16), which act to unload the element. The hub elements operated with a slight decrease in MVR, but the resultant diffusion was not strong enough to compensate for the unloading effect of low incidence. Hub D-factors were therefore generally lower than BUS values. Energy addition, pressure ratio, deviation angle, and loss coefficient responded to blade loading D at nearly the same levels, with and without distortion (figs. 14 to 16). An examination of the same parameters at 70 percent speed (figs. 27 to 29) shows no significant effect of rotative speed (or Mach number) on the distortion response.

The two parameters of greatest interest for use in predicting radial distortion performance are deviation angle and loss coefficient. The agreement between the deviation angle against D-factor correlation with and without distortion (BUS), with little exception, is very good for all three rotors over the entire span (figs. 14 to 16). The loss coefficient correlation shows the best agreement for the reference and low MVR rotors. The greatest difference between BUS and radially distorted-flow curves occurs at the 30-percent-of-span-from-tip location. This location is approximately at the edge of the screen and is where the largest differences occur between design streamline slope and calculated streamline slope with radial distortion. (See fig. 17(a), which is representative of conditions for all rotors.) At 70 percent of design speed (figs. 27 to 29), agreement between BUS loss against D-factor curves and radial distortion curves is quite good.

The velocity distribution entering the stator was still lower in the tip and higher at the hub than BUS data at the same weight flow (stator inlet = rotor outlet; see figs. 9(j), and 11(j)). The stator blade-element performance shows a bit more scatter than corresponding rotor results, but the general behavior with distortion was similar to behavior with BUS flow (see figs. 30 to 32). Design streamline slopes and streamline slopes calculated for stators from the radial distortion data were quite close (see fig. 17(b) which is representative of conditions for all stators).

As noted earlier, since radial distortion presents an axisymmetric, steady flow field to a compressor stage, it is possible, in principle, to predict performance of a

known stage design using streamline curvature, off-design analysis codes. The input to these codes includes empirical correlations of loss coefficient and deviation angle. The results of this study indicate that if experimental distortion data are evaluated along calculated streamlines, the blade-element deviation angles and loss coefficients correlated against D-factor show a generally good, although not perfect, agreement with undistorted-flow data. Where differences between distorted- and undistorted-flow data did occur, it was at spanwise locations where calculated streamline slopes diverged greatly from design streamline slopes (fig. 17). There accordingly appears to be some promise in the use of undistorted-flow loss coefficient and deviation angle parameters correlated against D-factor to predict rotor and stator performance when operating with inlet radial distortion.

PERFORMANCE WITH CIRCUMFERENTIAL DISTORTION

Overall Performance

Overall performance maps for rotor and stage performances are presented in figure 18. Pressure ratio is plotted as a function of weight flow for performance with undistorted flow (BUS) and circumferentially distorted inlet flow. Efficiencies are not presented because efficiency is particularly sensitive to the accuracy of the measured temperatures, and a radial mass average based on only three points is not sufficiently accurate.

The greatest effects of distortion occur at design speed where the flow is greatest, the pressure drop across the screen is greatest, and the corresponding DM is greatest. The DM for each stage at 100 and 70 percent of design speed at the near-stall condition is given in the following table:

Stage	Rotor meridional velocity ratio (a)		Magnitude of distortion, DM, r=const, midspan	
			100 Percent of design speed	70 Percent of design speed
20-17	Low	0.85	0.13	0.06
11-4	Reference	.93	.12	.04
19-16	High	1.04	.13	.05

[a]At 10 percent span from tip; experimental values (BUS).

All rotors and stages showed similar overall responses to circumferentially distorted flow. At design speed, distortion degraded performance: Pressure ratio levels were lower; and stall occurred at higher flow rates.

The change in stall pressure ratio from BUS to circumferentially distorted flow indicated in figure 18 is summarized in tabel XV. This change is indicated by a change in the stall pressure ratio parameter ΔPRS (see definition in appendix B). The BUS values of pressure ratio for comparison with circumferential distortion data are based on a three-point radial mass average, rather than the usual 11-point average. The losses in stall pressure ratio due to circumferential distortion are sustained by the rotors in the reference and low MVR stages. The high MVR stage (19-16) suffered a further loss in ΔPRS through the stator, as evidence by a larger ΔPRS for the stage than for the rotor. This is also observable in figure 18(c). Thus the high MVR stage was the most adversely affected by circumferential distortion. At 70 percent of design speed stall pressure ratio was essentially unaffected by circumferential distortion except in the high MVR stage (fig. 18(c) and table XV, ΔPRS).

Circumferential Flow Distributions

Conventional compressor data analysis is established on the premise of steady, axisymmetric inlet and outlet flow conditions. When the inlet flow is circumferentially distorted, some important compressor parameters cannot be accurately calculated because (1) the rotor relative flow field is unsteady and (2) the inlet and outlet flow fields are nonaxisymmetric. The implication of the latter condition is that blade-element parameters such as diffusion factor, loss coefficient, MVR, and efficiency cannot be accurately calculated because the circumferential location of corresponding inlet and outlet conditions cannot be determined with certainty. Even if these parameters could be calculated, their applicability would be questionable because of the unsteadiness of the flow field. Data analysis is consequently directed toward behavior of selected parameters measured or calculated at each axial station, rather than between two stations.

The near-stall point at design speed has been selected for detailed data presentation and discussion.

Circumferential distortion has certain characteristic effects on flow through a stage. In this section these effects will be noted as they are observed through the reference MVR in figures 19 to 21. (The circumferential distributions for the low and high MVR stages are presented in figs. 33 and 34. See ref. 2 for a more detailed discussion of response characteristics.)

Flow to rotor inlet. - Flow behind the screen (station -1 of fig. 19) possesses square-wave type of total-pressure and axial-velocity distortions. There is essentially no tangential component of velocity (fig. 20). At the rotor inlet (station 1 of fig. 19)

total-pressure distortion is still essentially a square wave (fig. 19); axial velocity distortion (fig. 19) is attenuated; and, because of the interaction between the rotor and the distorted flow field, tangential velocity components have been induced (fig. 20). The induced tangential velocities are strongest in the hub region and, in combination with the axial-velocity distribution there, produce the largest circumferential variation in incidence angle.

In the undistorted sector the incidence angle (fig. 21(h)) is lower than BUS levels (solid symbols along the vertical axis), a condition which tends to unload the blade sections. In the distorted sector the increasing incidence angle tends to load the blade sections to greater than BUS levels. For near-stall operation the rotor-blade sections operate momentarily during each revolution at incidence angles higher than those associated with BUS stall conditions.

Rotor response. - The circumferential distribution of energy addition to the air by the rotor is indicated by the rotor-outlet total temperature (fig. 21(g)). Because inlet total temperature is circumferentially constant, the temperature distribution at the outlet is representative of temperature rise or temperature ratio. The energy addition tends to follow the incidence angle distribution but is also related to the induced-inlet-tangential velocity because energy addition is proportional to the change in absolute tangential velocity across the blade row.

In the undistorted sector temperature rise is less than BUS level. In the distorted sector temperature rise is higher than the BUS level and, for the near-stall condition, exceeds the BUS level associated with stall.

The rotor-outlet-total-pressure distribution (fig. 21(b)) tends to follow the total-temperature distribution (θ^{o} increasing). In the distorted sector, however, a critical condition is reached, after which total pressure decreases even though total temperature continues to increase. This is interpreted as a dynamic stall condition and can be seen clearly in the tip region and to a lesser degree at midspan.

The rotor-outlet-axial-velocity distribution (fig. 21(e)) tends to follow the total-pressure variation. The low values of V_{z2} at the screen edge ($\theta = 130^{o} - 150^{o}$) near the hub result from the momentary unloading experienced by the rotor due to induced tangential velocity and low incidence at the rotor inlet. These low axial velocities at the rotor outlet produce locally higher stator incidence angles (fig. 21(i)).

In the undistorted sector the rotor adds less energy (lower outlet total temperature, fig. 21(h)) and produces a lower than BUS density rise. Continuity requires higher axial velocities and therefore high Mach numbers (fig. 21(j)). These higher Mach numbers at the stator inlet can lead to choking and increased profile and shock losses across the stators.

Stator response. - Stators experience a spatial or steady-state distortion. Since no work is done through the stator, the total-pressure distributions are largely un-

changed, except for stator-loss contributions. Axial velocity distributions are changed, and the most notable effects were observed in the hub region. The flow field downstream of the stator must adjust to a circumferentially constant static pressure and, in the presence of a total-pressure distortion, the axial velocity distribution experiences the adjustment. Because this adjustment produces a larger axial velocity distortion, the effects can be very significant. (See parts (b) of figs. 21, 33, and 34.)

Discussion of Circumferential Distortion Performance

A comparison of the responses of the high and low MVR rotors to circumferential distortion is made from circumferential plots of total pressure at rotor outlet. These total-pressure plots for tip and hub elements operating at three flow conditions at design speed and a constant DM of 0.13 are presented in figure 22. The hub and tip elements are selected for review because they are removed from the influence of the damper and because, comparing one rotor with another (see fig. 2), the tip and hub elements show similar changes in MVR (e.g., rotor 19's MVR is greater than rotor 20's near the tip (1.04 against 0.85) and near the hub (0.95 against 0.84)).

The outlet-total-pressure responses of the hub elements to the circumferential distortion were essentially the same, regardless of MVR; the tip elements, however, differed. The low MVR rotor (20) responded strongly in the distorted sector. It compensated for the imposed total-pressure deficit by overpressuring the flow in part of the distorted region. In contrast, the high MVR rotor (19) did not compensate for the imposed total-pressure deficit and, instead tended to pass it downstream.

The difference between tip and hub responses was expected and is related to the differences in velocity triangles associated with blade stagger. The tip is highly staggered ($>60^{\circ}$), and the hub is considerably less so ($<30^{\circ}$), which is typical of fan rotors. The velocity triangles shown in figure 23 are representative of the tip, the hub, and a hypothetical hub section that turns completely to the axial direction. For simplicity, no axial velocity ratio change is shown across the rotor. In the figures solid lines indicate undistorted flow (design), and dashed lines a reduction of flow due to a distortion (off-design). Deviation angle is assumed not to change with distorted flow. It is apparent from the figure that, for an equal change in inlet V_z, the greatest change in energy addition, ΔV_θ or ΔT_T (and, disregarding losses, ΔP_T) is realized in the highly staggered case (a). A smaller energy addition occurs in case (b), and no change occurs in a rotor which turns to the axial direction (case (c)). Therefore, the ineffectiveness of the rotor-hub elements to remove the distortion, regardless of velocity ratio, was predictable, as was the stronger response of the tip elements. What was not predictable was that tip elements with low MVR's (like rotor 20) displayed a stronger response to circumferential distortion than did those with higher MVR's (like rotor 19) as shown in

figure 22. The same trend in recovery with velocity ratio was observed for tip elements exposed to a tip radial distortion (see figs. 9(a) and 11(a)).

The decrease in overall pressure ratio (fig. 18) observed with circumferential distortion can be explained in large part by quasi-steady reasoning from the circumferential distribution data. For operation with circumferential distortion redistribution of flow must occur because of the presence of the screen. At the same flow rate for BUS and distorted flows (for comparison, near-stall points are considered sufficiently close), the undistorted sector of the annulus must pass flow at a higher axial velocity than the corresponding BUS level. Incidence angle and energy addition are therefore lower than BUS levels in the undistorted sector. With less energy addition the outlet total pressure and density are also lower. Outlet axial velocity must be greater than BUS levels because of continuity requirements. The circumferential and radial distribution of parameters are translated into overall performance by a mass-averaging process. Since axial velocity is greater than average in the larger undistorted sector (270°), this sector is weighted more heavily in calculating overall performance, and it is in this sector that energy addition and total pressure are lower than BUS levels. Therefore, lower overall pressure ratio will be realized from circumferentially distorted flow simply because of flow redistributions associated with continuity, mass averaging, and radial equilibrium requirements.

For all rotors tested the stalling weight flow at design speed was slightly higher with circumferential distortion than without it. Stall is apparently initiated when critical flow is attained in the tip region of the rotor (as was the case for tip radial distortion, see p. 9). With circumferential distortion the critical flow condition is reached in the distorted sector for a very short time during each evolution of the rotor. The process described is essentially the dynamic stalling process, but its precise role in setting the overall stall limits of a compressor blade row is not clear or predictable at present. The fact that the circumferential extent of increased energy addition (in the distorted sector) exceeds the circumferential extent of increased total pressure (cf. figs. 20(c) and (a)) at the near-stall point suggests that additional losses from steady-state levels are being incurred and may be the source of the flow breakdown.

As noted in the previous section, stator inlet Mach numbers are significantly increased with distortion as a result of flow redistributions. This was a particularly critical problem in stator 16 (operated with the high MVR rotor). To maintain an adequate choke margin, stator 16 was designed with greater amounts of front camber and consequently higher suction-surface Mach numbers. The combination of this condition with the higher than normal inlet Mach number due to distortion most likely produced increased shock losses. This is the probable cause for the large difference in overall pressure ratio between rotor 19 (high MVR) and stage 19-16 at high weight flows (design speed) in figure 18(c).

SUMMARY OF RESULTS

Three transonic fan stages having differing meridional velocity ratios across the rotors were tested with two magnitudes of tip radial distortion with a 90° circumferential distortion imposed on the inlet flow. Distortions were produced by wire mesh screens secured to a support (or backup) screen. The fan rotors were approximately 50.8 centimeters in diameter and had design operating tip speeds of 425 meters per second and a design pressure ratio of 1.60. Overall performance and detailed flow parameters at several radial positions were measured. The following results were obtained:

1. The rotor having the lowest meridional velocity ratio (less than 0.9 at the tip) demonstrated the least degradation of performance from a tip radial distortion. Its ability to almost achieve undistorted-flow outlet-total-pressure distributions enabled it to operate essentially on the undistorted-flow design speed line. The rotor having the highest meridional velocity ratio (greater than 1.0 at the tip) sustained the largest losses in performance due to tip radial distortion.

2. When correlated against diffusion factor, tip radial distortion data evaluated along calculated streamlines compared well with undistorted blade-element data evaluated along design streamlines. It therefore appears feasible to predict radial distortion performance with axisymmetric, streamline-curvature, off-design calculation codes using correlations of loss and deviation angle against diffusion factor obtained from undistorted flow tests.

3. The tip region of the low-meridional-velocity-ratio rotor displayed a stronger recovery to the circumferential distortion than did the tip region of the high-meridional-velocity rotor. The hub sections all showed a typical low recovery with no significant effect of meridional velocity ratio apparent.

Lewis Research Center,
National Aeronautics and Space Administration,
Cleveland, Ohio, January 3, 1979,
505-04.

APPENDIX A

SYMBOLS

BUS	backup screen
D	diffusion factor (D-factor)
DM	distortion magnitude, $(P_{max} - P_{min})/P_{max}$
i_{ss}	suction-surface incidence angle, angle between inlet air direction and line tangent to blade suction surface at leading edge, deg
M	Mach number
MVR	meridional velocity ratio, outlet to inlet
N	rotative speed, rpm
P	total pressure, N/cm^2
ΔP	$P_{max} - P_{min}$, N/cm^2
PR	total pressure ratio
p	static pressure, N/cm^2
r	radius, cm
SPFT	span from tip
T	total temperature, K
TR	total temperature ratio
U	wheel speed, m/sec
V	air velocity, m/sec
W	weight flow, kg/sec
Z	axial distance from rotor blade hub leading edge, cm
α_c	cone angle, deg
α_s	slope of streamline, deg
β	air angle, angle between air velocity and axial direction, deg
β'_c	relative meridional air angle based on cone angle, arctan $(\tan \beta'_m \cos \alpha_c / \cos \alpha_s)$, deg
γ	ratio of specific heats
δ	ratio of rotor inlet total pressure to standard pressure of 10.13 N/cm^2

δ^o deviation angle, angle between outlet air direction and tangent to blade mean camber line at trailing edge, deg

η efficiency

θ ratio of rotor inlet total temperature to standard temperature of 288.2 K

θ^o circumferential position, deg

κ_{mc} angle between blade mean camber line and meridional plane, deg

κ_{ss} angle between blade suction-surface camber line at leading edge and meridional plane, deg

ρ density, kg/m^3

σ solidity, ratio of chord to spacing

ω total loss coefficient

Subscripts:

ad adiabatic (temperature-rise)

d distortion

id ideal

LE blade leading edge

m meridional direction

max maximum

min minimum

ref reference

s stall

ss suction surface

TE blade trailing edge

u undistorted

z axial direction

θ tangential direction

-1 first instrumentation plane between distortion screen and rotor (fig. 3)

0 second instrumentation plane between distortion screen and rotor (fig. 3)

1 third instrumentation plane upstream of rotor (rotor inlet) (fig. 3)

2 instrumentation plane between rotor and stator (fig. 3)

3 instrumentation plane downstream of stator (fig. 3)

Superscript:

' relative to blade

APPENDIX B

EQUATIONS

Suction-surface incidence angle:

$$i_{ss} = \left(\beta'_c\right)_{LE} - \kappa_{ss} \tag{B1}$$

Deviation angle:

$$\delta^o = \left(\beta'_c\right)_{TE} - \left(\kappa_{mc}\right)_{TE} \tag{B2}$$

Diffusion factor:

$$D = \underbrace{1 - \frac{V'_{TE}}{V'_{LE}}}_{\substack{\text{Velocity} \\ \text{diffusion} \\ \text{term}}} + \underbrace{\left| \frac{\left(rV_\theta\right)_{TE} - \left(rV_\theta\right)_{LE}}{(r_{TE} + r_{LE})\sigma(V'_{LE})} \right|}_{\text{Fluid turning term}} \tag{B3}$$

Total-loss coefficient:

$$\overline{\omega} = \frac{\left(P'_{id}\right)_{TE} - (P')_{TE}}{(P')_{LE} - (p)_{LE}} \tag{B4}$$

Adiabatic (temperature rise) efficiency:

$$\eta_{ad} = \frac{PR^{(\gamma-1)/\gamma} - 1}{TR - 1} \tag{B5}$$

Equivalent weight flow:

$$\frac{W\sqrt{\theta}}{\delta} \tag{B6}$$

Equivalent rotative speed:

$$\frac{N}{\sqrt{\theta}} \tag{B7}$$

Loss in stall pressure ratio:

$$\Delta PRS = 1 - \frac{PR_{d,s}}{PR_{u,s}}\Bigg|_{\frac{N}{\sqrt{\theta}} = \text{Constant}} \tag{B8}$$

APPENDIX C

DEFINITIONS AND UNITS USED IN TABLES

ABS	absolute
AERO CHORD	aerodynamic chord, cm
AREA RATIO	ratio of actual flow area to critical area (where local Mach number is 1)
BETAM	meridional air angle, deg
CONE ANGLE	angle between axial direction and conical surface representing blade element, deg
DELTA INC	difference between mean camber blade angle and suction-surface blade angle at leading edge, deg
DEV	deviation angle (defined by eq. (B2)), deg
D-FACT	diffusion factor (defined by eq. (B3))
EFF	adiabatic efficiency (defined by eq. (B5))
IN	inlet (leading edge of blade)
INCIDENCE	incidence angle (defined by eq. (B1))
KIC	angle between blade mean camber line at leading edge and meridional plane, deg
KOC	angle between blade mean camber line at trailing edge and meridional plane, deg
KTC	angle between blade mean camber line at transition point and meridional plane, deg
LOSS COEFF	loss coefficient (total defined by eq. (B4) and profile defined by eq. (B6))
LOSS PARAM	loss parameter, $\overline{\omega} \cos\left(\beta'_m\right)_{TE} \Big/ 2\sigma$
MERID	meridional
MERID VEL R	meridional velocity ratio
OUT	outlet (trailing edge of blade)
PERCENT SPAN	percent of blade span from tip at rotor outlet
PHISS	suction-surface camber ahead of assumed shock location, deg

PRESS	pressure, N/cm^2
PROF	profile
RADII	radius, cm
REL	relative to blade
RI	inlet radius (leading edge of blade), cm
RO	outlet radius (trailing edge of blade), cm
RP	radial position
SETTING ANGLE	angle between aerodynamic chord and meridional plane, deg
SOLIDITY	ratio of aerodynamic chord to blade spacing
SPEED	speed, m/sec
SS	suction surface
STREAMLINE SLOPE	slope of streamline, deg
TANG	tangential
TEMP	temperature, K
TI	thickness of blade at leading edge, cm
TM	thickness of blade at maximum thickness, cm
TO	thickness of blade at trailing edge, cm
TOT	total
TOTAL CAMBER	difference between inlet and outlet blade mean camber lines, deg
VEL	velocity, m/sec
X FACTOR	ratio of suction-surface camber ahead of assumed shock location of a multiple-circular-arc blade section to that of a double-circular-arc blade section
ZIC	axial distance to blade leading edge from inlet, cm
ZMC	axial distance to blade maximum thickness point from inlet, cm
ZOC	axial distance to blade trailing edge from inlet, cm
ZTC	axial distance to transition point from inlet, cm

REFERENCES

1. Urasek, Donald C.; and Janetzke, David C.: Performance of Tandem-Bladed Transonic Compressor Rotor with Tip Speed of 1375 Feet Per Second. NASA TM X-2484, 1972.

2. Sanger, Nelson L.: Performance of a 1.57-Pressure-Ratio Transonic Fan Stage with a Screen-Induced 90° Circumferential Inlet Flow Distortion. NASA TN D-8163, 1976.

3. Moore, Royce D.; Lewis, George W.; and Osborn, Walter M.: Performance of a Transonic Fan Stage Designed for a Low Meridional Velocity Ratio. NASA TP-1298, 1978.

4. Kovich, George; Moore, Royce D.; and Urasek, Donald C.: Performance of Transonic Fan Stage with Weight Flow per Unit Annulus Area of 198 Kilograms per Second per Square Meter (40.6 (lb/sec)ft^2). NASA TM X-2905, 1973.

5. Sandercock, Donald M.; and Sanger, Nelson L.: Some Observations of the Effects of Radial Distortions on Performance of a Transonic Rotating Blade Row. NASA TN D-7824, 1974.

TABLE I. - STAGE DESIGN FEATURES

Parameter	Meridional velocity ratio		
	Low	Reference	High
	Stage		
	20-17	11-4	19-16
Rotor pressure ratio	1.60	1.60	1.60
Stage pressure ratio	1.57	1.57	1.57
Rotor temperature ratio	1.16	1.16	1.16
Rotor adiabatic efficiency	0.881	0.889	0.899
Stage adiabatic efficiency	0.847	0.855	0.859
Equivalent flow rate, kg/sec	29.48	29.48	29.48
Solidity, rotor tip	1.31	1.30	1.31
Solidity, stator tip	1.31	1.27	1.31
Aspect ratio, rotor	2.5	2.5	2.5
Aspect ratio, stator	2.4	2.4	2.4
Rotor tip speed, m/sec	426	425	423
Rotor tip radius at inlet, cm	25.28	25.20	25.09
Stator tip radius at exit, cm	25.15	24.38	23.81
Rotor inlet hub-to-tip radius ratio	0.5	0.5	0.5
Rotor meridional velocity ratio (at tip)	0.73	0.81	0.90

TABLE II. - DESIGN BLADE-ELEMENT PARAMETERS

FOR LOW MVR ROTOR 20

	RADII		ABS BETAM		REL BETAM		TOTAL TEMP		TOTAL PRESS	
RP	IN	OUT	IN	OUT	IN	OUT	IN	RATIO	IN	RATIO
TIP	25.281	25.171	0.	45.7	66.5	64.6	288.2	1.204	10.13	1.601
1	24.724	24.614	-0.	43.4	65.7	63.6	288.2	1.190	10.13	1.601
2	24.156	24.057	0.	41.9	64.9	62.6	288.2	1.181	10.13	1.601
3	21.810	21.829	0.	40.8	61.9	58.1	288.2	1.164	10.13	1.601
4	19.385	19.601	0.	42.0	58.9	51.8	288.2	1.157	10.13	1.601
5	18.764	19.044	0.	42.5	58.1	49.8	288.2	1.155	10.13	1.601
6	18.451	18.766	0.	42.7	57.7	48.7	288.2	1.155	10.13	1.601
7	18.136	18.487	0.	43.0	57.3	47.5	288.2	1.154	10.13	1.601
8	17.819	18.209	0.	43.2	56.9	46.3	288.2	1.154	10.13	1.601
9	16.851	17.373	0.	44.1	55.6	42.3	288.2	1.153	10.13	1.601
10	14.130	15.145	0.	47.7	51.8	27.1	288.2	1.154	10.13	1.601
11	13.408	14.568	0.	49.1	50.6	21.6	288.2	1.155	10.13	1.601
HUB	12.700	14.031	0.	50.6	49.4	15.3	288.2	1.158	10.13	1.601

	ABS VEL		REL VEL		MERID VEL		TANG VEL		WHEEL SPEED	
RP	IN	OUT	IN	OUT	IN	OUT	IN	OUT	IN	OUT
TIP	185.6	194.1	464.9	316.0	185.6	135.6	0.	138.9	426.2	424.4
1	188.4	193.1	457.5	315.1	188.4	140.2	-0.	132.6	416.9	415.0
2	190.9	193.0	449.8	311.8	190.9	143.7	0.	128.9	407.3	405.6
3	196.3	197.1	416.8	282.0	196.3	149.2	0.	128.8	367.7	368.0
4	196.9	204.9	381.6	246.1	196.9	152.3	0.	137.1	336.8	330.5
5	196.6	207.6	372.5	237.0	196.6	153.1	0.	140.2	316.4	321.1
6	196.3	208.9	367.9	232.5	196.3	153.5	0.	141.8	311.1	316.4
7	196.0	210.4	363.2	228.1	196.0	153.9	0.	143.4	305.8	311.7
8	195.7	211.9	358.5	223.7	195.7	154.4	0.	145.2	300.4	307.0
9	194.2	217.0	344.2	210.7	194.2	155.8	0.	151.1	284.1	292.9
10	187.7	235.7	303.3	178.0	187.7	158.5	0.	174.4	238.2	255.3
11	185.7	242.3	292.6	170.6	185.7	158.7	0.	183.1	226.1	246.0
HUB	183.8	249.9	282.2	164.5	183.8	158.6	0.	193.1	214.1	236.6

	ABS MACH NO		REL MACH NO		MERID MACH NO		STREAMLINE SLOPE		MERID PEAK SS	
RP	IN	OUT	IN	OUT	IN	OUT	IN	OUT	VEL R	MACH NO
TIP	0.563	0.535	1.409	0.871	0.563	0.373	-2.68	-1.58	0.730	1.528
1	0.572	0.535	1.388	0.873	0.572	0.388	-2.24	-1.43	0.724	1.519
2	0.580	0.537	1.366	0.867	0.580	0.400	-1.70	-1.14	0.753	1.510
3	0.597	0.553	1.268	0.791	0.597	0.419	1.22	1.06	0.760	1.490
4	0.599	0.578	1.161	0.695	0.599	0.430	4.65	3.98	0.773	1.477
5	0.598	0.587	1.133	0.670	0.598	0.433	5.88	4.80	0.779	1.476
6	0.597	0.591	1.119	0.658	0.597	0.434	6.43	5.23	0.782	1.476
7	0.596	0.596	1.105	0.646	0.596	0.436	7.00	5.66	0.785	1.476
8	0.595	0.600	1.090	0.634	0.595	0.437	7.58	6.11	0.789	1.477
9	0.590	0.616	1.046	0.598	0.590	0.442	9.47	7.54	0.802	1.481
10	0.569	0.673	0.920	0.509	0.569	0.453	15.94	11.97	0.844	1.403
11	0.563	0.694	0.887	0.488	0.563	0.454	18.03	13.24	0.854	1.365
HUB	0.557	0.717	0.855	0.472	0.557	0.455	20.24	14.58	0.863	1.328

	PERCENT	INCIDENCE		DEV	D-FACT	EFF	LOSS COEFF		LOSS PARAM	
RP	SPAN	MEAN	SS				TOT	PROF	TOT	PROF
TIP	0.	2.5	0.0	5.4	0.435	0.706	0.235	0.148	0.039	0.024
1	5.00	2.8	-0.0	4.8	0.420	0.755	0.191	0.108	0.032	0.018
2	10.00	3.0	0.0	4.4	0.412	0.796	0.156	0.078	0.026	0.013
3	30.00	4.1	0.0	2.9	0.427	0.878	0.094	0.035	0.017	0.006
4	50.00	5.2	0.0	2.6	0.462	0.919	0.068	0.025	0.012	0.005
5	55.00	5.5	0.0	2.8	0.473	0.925	0.065	0.026	0.012	0.005
6	57.50	5.6	0.0	2.9	0.478	0.928	0.063	0.026	0.012	0.005
7	60.00	5.7	0.0	2.9	0.483	0.931	0.061	0.025	0.011	0.005
8	62.50	5.9	0.0	3.0	0.488	0.934	0.059	0.025	0.011	0.005
9	70.00	6.3	0.0	3.6	0.504	0.941	0.056	0.027	0.011	0.005
10	90.00	7.2	0.0	6.2	0.543	0.935	0.074	0.065	0.014	0.013
11	95.00	7.5	0.0	7.0	0.552	0.925	0.092	0.087	0.018	0.017
HUB	100.00	7.7	0.0	7.8	0.558	0.911	0.117	0.115	0.022	0.022

TABLE III. - DESIGN BLADE-ELEMENT PARAMETERS FOR STATOR 17

	RADII		ABS BETAM		REL BETAM		TOTAL TEMP		TOTAL PRESS	
RP	IN	OUT	IN	OUT	IN	OUT	IN	RATIO	IN	RATIO
TIP	25.146	25.146	44.7	0.	44.7	0.	347.0	1.001	16.22	0.976
1	24.587	24.600	42.0	-0.	42.0	-0.	343.0	1.000	16.22	0.982
2	24.057	24.110	40.3	0.	40.3	0.	340.2	1.000	16.22	0.985
3	21.962	22.133	38.6	0.	38.6	0.	335.3	1.000	16.22	0.989
4	19.882	20.160	39.4	0.	39.4	0.	333.3	1.000	16.22	0.987
5	19.364	19.670	39.8	0.	39.8	0.	333.0	1.000	16.22	0.986
6	19.105	19.426	40.0	0.	40.0	0.	332.8	1.000	16.22	0.986
7	18.846	19.182	40.2	0.	40.2	0.	332.7	1.000	16.22	0.986
8	18.588	18.939	40.5	0.	40.5	0.	332.5	1.000	16.22	0.985
9	17.812	18.213	41.2	0.	41.2	0.	332.2	1.000	16.22	0.984
10	15.750	16.298	44.5	0.	44.5	0.	332.5	1.000	16.22	0.970
11	15.238	15.815	45.7	0.	45.7	0.	333.0	1.000	16.22	0.959
HUB	14.732	15.240	47.1	-0.	47.1	-0.	333.6	1.000	16.22	0.942

	ABS VEL		REL VEL		MERID VEL		TANG VEL		WHEEL SPEED	
RP	IN	OUT	IN	OUT	IN	OUT	IN	OUT	IN	OUT
TIP	198.2	151.4	198.2	151.4	140.9	151.4	139.4	0.	0.	0.
1	198.5	153.8	198.5	153.8	147.4	153.8	132.9	-0.	0.	0.
2	199.4	155.6	199.4	155.6	152.2	155.6	128.9	0.	0.	0.
3	205.3	158.8	205.3	158.8	160.5	158.8	128.0	0.	0.	0.
4	212.8	160.3	212.8	160.3	164.4	160.3	135.2	0.	0.	0.
5	215.2	160.7	215.2	160.7	165.3	160.7	137.8	0.	0.	0.
6	216.5	161.0	216.5	161.0	165.7	161.0	139.2	0.	0.	0.
7	217.8	161.3	217.8	161.3	166.2	161.3	140.7	0.	0.	0.
8	219.1	161.7	219.1	161.7	166.7	161.7	142.2	0.	0.	0.
9	223.5	162.5	223.5	162.5	168.1	162.5	147.4	0.	0.	0.
10	239.4	158.7	239.4	158.7	170.9	158.7	167.7	0.	0.	0.
11	245.0	155.1	245.0	155.1	171.1	155.1	175.5	0.	0.	0.
HUB	251.2	149.6	251.2	149.6	171.1	149.6	183.9	-0.	0.	0.

	ABS MACH NO		REL MACH NO		MERID MACH NO		STREAMLINE SLOPE		MERID PEAK SS	
RP	IN	OUT	IN	OUT	IN	OUT	IN	OUT	VEL R	MACH NO
TIP	0.547	0.412	0.547	0.412	0.389	0.412	0.13	-0.53	1.075	0.850
1	0.551	0.422	0.551	0.422	0.409	0.422	0.75	0.02	1.044	0.827
2	0.556	0.428	0.556	0.428	0.424	0.428	1.26	0.44	1.022	0.814
3	0.578	0.441	0.578	0.441	0.452	0.441	2.86	1.67	0.989	0.815
4	0.602	0.447	0.602	0.447	0.465	0.447	4.50	2.65	0.975	0.841
5	0.610	0.448	0.610	0.448	0.468	0.448	4.96	2.88	0.973	0.851
6	0.614	0.449	0.614	0.449	0.470	0.449	5.21	3.00	0.972	0.856
7	0.618	0.450	0.618	0.450	0.472	0.450	5.46	3.12	0.971	0.861
8	0.622	0.451	0.622	0.451	0.473	0.451	5.72	3.24	0.970	0.866
9	0.636	0.454	0.636	0.454	0.478	0.454	6.57	3.62	0.967	0.885
10	0.685	0.443	0.685	0.443	0.489	0.443	9.30	4.55	0.929	0.958
11	0.702	0.432	0.702	0.432	0.490	0.432	10.06	4.62	0.906	0.986
HUB	0.721	0.416	0.721	0.416	0.491	0.416	10.83	4.62	0.875	1.020

	PERCENT	INCIDENCE		DEV	D-FACT	EFF	LOSS COEFF		LOSS PARAM	
RP	SPAN	MEAN	SS				TOT	PROF	TOT	PROF
TIP	0.	6.1	0.0	14.2	0.513	0.	0.141	0.141	0.056	0.056
1	5.00	6.1	0.0	12.3	0.483	0.	0.098	0.098	0.038	0.038
2	10.00	6.2	0.0	11.1	0.463	0.	0.077	0.077	0.029	0.029
3	30.00	6.2	0.0	9.4	0.441	0.	0.055	0.055	0.019	0.019
4	50.00	6.2	0.0	8.9	0.444	0.	0.060	0.060	0.019	0.019
5	55.00	6.2	0.0	8.8	0.447	0.	0.062	0.062	0.019	0.019
6	57.50	6.2	0.0	8.8	0.448	0.	0.063	0.063	0.019	0.019
7	60.00	6.1	0.0	8.8	0.449	0.	0.064	0.064	0.019	0.019
8	62.50	6.1	0.0	8.7	0.450	0.	0.065	0.065	0.019	0.019
9	70.00	6.1	0.0	8.7	0.456	0.	0.067	0.067	0.019	0.019
10	90.00	6.1	0.0	8.8	0.509	0.	0.110	0.110	0.027	0.027
11	95.00	6.1	0.0	8.9	0.536	0.	0.146	0.146	0.035	0.035
HUB	100.00	6.1	0.1	9.1	0.572	0.	0.202	0.202	0.047	0.047

TABLE IV. - BLADE GEOMETRY FOR LOW MVR ROTOR 20

RP	PERCENT SPAN	RADII RI	RADII RO	BLADE ANGLES KIC	BLADE ANGLES KTC	BLADE ANGLES KOC	DELTA INC	CONE ANGLE
TIP	0.	25.281	25.171	63.94	63.97	59.17	2.52	-3.006
1	5.	24.724	24.614	62.90	62.83	58.74	2.77	-2.925
2	10.	24.156	24.057	61.85	61.62	58.16	3.03	-2.520
3	30.	21.810	21.829	57.80	56.14	55.16	4.11	0.434
4	50.	19.385	19.601	53.76	50.05	49.12	5.19	4.227
5	55.	18.764	19.044	52.71	48.42	46.96	5.46	5.281
6	58.	18.451	18.766	52.18	47.58	45.80	5.59	5.834
7	60.	18.136	18.487	51.64	46.73	44.57	5.73	6.399
8	63.	17.819	18.209	51.09	45.86	43.29	5.86	6.974
9	70.	16.851	17.373	49.43	43.22	38.64	6.26	8.822
10	90.	14.130	15.145	44.69	36.03	20.60	7.25	14.611
11	95.	13.408	14.588	43.40	34.05	14.33	7.46	16.271
HUB	100.	12.700	14.031	42.12	32.06	7.30	7.64	17.597

RP	BLADE THICKNESSES TI	BLADE THICKNESSES TM	BLADE THICKNESSES TO	AXIAL DIMENSIONS ZIC	AXIAL DIMENSIONS ZMC	AXIAL DIMENSIONS ZTC	AXIAL DIMENSIONS ZOC
TIP	0.051	0.153	0.051	1.017	2.032	2.437	3.097
1	0.051	0.163	0.051	0.980	2.034	2.409	3.135
2	0.051	0.173	0.051	0.942	2.035	2.376	3.175
3	0.051	0.217	0.051	0.780	2.037	2.204	3.340
4	0.051	0.261	0.051	0.609	2.037	1.957	3.534
5	0.051	0.272	0.051	0.563	2.035	1.882	3.590
6	0.051	0.278	0.051	0.539	2.034	1.842	3.619
7	0.051	0.284	0.051	0.514	2.033	1.800	3.648
8	0.051	0.290	0.051	0.490	2.032	1.757	3.678
9	0.051	0.307	0.051	0.410	2.025	1.617	3.775
10	0.051	0.358	0.051	0.163	1.991	1.161	4.058
11	0.051	0.372	0.051	0.084	1.977	1.021	4.128
HUB	0.051	0.385	0.051	0.000	1.961	0.875	4.196

RP	AERO CHORD	SETTING ANGLE	TOTAL CAMBER	SOLIDITY	X FACTOR	PHISS	AREA RATIO
TIP	4.676	63.24	4.77	1.298	0.646	3.50	1.043
1	4.676	62.19	4.16	1.327	0.710	3.82	1.044
2	4.676	61.10	3.69	1.358	0.775	4.20	1.044
3	4.675	56.39	2.64	1.500	1.023	6.30	1.041
4	4.680	50.68	4.64	1.681	1.140	8.60	1.040
5	4.683	48.98	5.74	1.735	1.152	9.18	1.040
6	4.686	48.09	6.38	1.763	1.158	9.47	1.040
7	4.688	47.16	7.07	1.793	1.163	9.77	1.040
8	4.691	46.19	7.81	1.824	1.167	10.06	1.041
9	4.704	42.98	10.79	1.925	1.173	10.91	1.042
10	4.784	31.74	24.09	2.289	1.135	12.65	1.046
11	4.820	27.96	29.07	2.412	1.131	13.07	1.048
HUB	4.862	23.78	34.82	2.547	1.130	13.46	1.050

TABLE V. - BLADE GEOMETRY FOR STATOR 17

RP	PERCENT SPAN	RADII RI	RADII RO	BLADE ANGLES KIC	BLADE ANGLES KTC	BLADE ANGLES KOC	DELTA INC	CONE ANGLE
TIP	0.	25.146	25.146	38.58	30.24	-14.15	6.11	0.057
1	5.	24.587	24.600	35.90	28.80	-12.31	6.14	0.190
2	10.	24.057	24.110	34.10	27.85	-11.10	6.16	0.763
3	30.	21.962	22.133	32.40	27.20	-9.40	6.18	2.467
4	50.	19.882	20.160	33.28	28.23	-8.88	6.16	4.012
5	55.	19.364	19.670	33.70	28.63	-8.82	6.15	4.418
6	58.	19.105	19.426	33.91	28.84	-8.78	6.15	4.632
7	60.	18.846	19.182	34.13	29.05	-8.75	6.15	4.852
8	63.	18.588	18.939	34.35	29.27	-8.72	6.14	5.077
9	70.	17.812	18.213	35.15	30.01	-8.66	6.13	5.805
10	90.	15.750	16.298	38.48	32.94	-8.79	6.07	7.976
11	95.	15.238	15.815	39.76	34.02	-8.93	6.05	8.430
HUB	100.	14.732	15.240	41.21	35.22	-9.14	6.03	7.472

RP	BLADE THICKNESSES TI	BLADE THICKNESSES TM	BLADE THICKNESSES TO	AXIAL DIMENSIONS ZIC	AXIAL DIMENSIONS ZMC	AXIAL DIMENSIONS ZTC	AXIAL DIMENSIONS ZOC
TIP	0.051	0.279	0.051	7.612	9.388	9.114	11.507
1	0.051	0.279	0.051	7.578	9.395	9.003	11.507
2	0.051	0.279	0.051	7.556	9.400	8.919	11.507
3	0.051	0.279	0.051	7.537	9.407	8.755	11.508
4	0.051	0.279	0.051	7.543	9.405	8.668	11.506
5	0.051	0.279	0.051	7.546	9.404	8.651	11.505
6	0.051	0.279	0.051	7.547	9.404	8.642	11.504
7	0.051	0.279	0.051	7.549	9.403	8.633	11.504
8	0.051	0.279	0.051	7.551	9.403	8.625	11.504
9	0.051	0.279	0.051	7.559	9.401	8.601	11.503
10	0.051	0.279	0.051	7.593	9.394	8.557	11.500
11	0.051	0.279	0.051	7.607	9.391	8.552	11.499
HUB	0.051	0.279	0.051	7.624	9.387	8.549	11.497

RP	AERO CHORD	SETTING ANGLE	TOTAL CAMBER	SOLIDITY	X FACTOR	PHISS	AREA RATIO
TIP	4.179	19.35	52.73	1.270	0.600	13.51	1.339
1	4.178	17.85	48.20	1.298	0.600	11.95	1.311
2	4.180	16.88	45.20	1.326	0.600	10.86	1.290
3	4.183	15.86	41.80	1.449	0.600	9.31	1.244
4	4.189	16.23	42.16	1.598	0.600	8.87	1.207
5	4.191	16.42	42.51	1.640	0.600	8.83	1.198
6	4.192	16.52	42.69	1.662	0.600	8.80	1.193
7	4.193	16.62	42.88	1.685	0.600	8.78	1.188
8	4.194	16.73	43.08	1.708	0.600	8.76	1.183
9	4.199	17.10	43.81	1.781	0.600	8.73	1.167
10	4.216	18.70	47.27	2.010	0.600	8.93	1.132
11	4.220	19.32	48.69	2.076	0.600	9.10	1.123
HUB	4.209	20.02	50.35	2.146	0.600	9.31	1.114

TABLE VI. - DESIGN BLADE-ELEMENT PARAMETERS FOR

REFERENCE MVR ROTOR 11

	RADII		ABS BETAM		REL BETAM		TOTAL TEMP		TOTAL PRESS	
RP	IN	OUT	IN	OUT	IN	OUT	IN	RATIO	IN	RATIO
TIP	25.197	24.816	0.	43.1	67.1	62.6	288.2	1.198	10.13	1.601
1	24.628	24.280	-0.	41.3	66.1	61.7	288.2	1.186	10.13	1.601
2	24.060	23.744	0.	40.0	65.1	60.7	288.2	1.177	10.13	1.601
3	21.741	21.600	0.	39.3	61.5	56.0	288.2	1.163	10.13	1.601
4	19.980	19.992	0.	40.0	59.1	51.5	288.2	1.157	10.13	1.601
5	19.658	19.724	0.	40.2	58.7	50.6	288.2	1.157	10.13	1.601
6	19.356	19.456	0.	40.4	58.2	49.7	288.2	1.156	10.13	1.601
7	19.052	19.188	0.	40.7	57.8	48.7	288.2	1.156	10.13	1.601
8	18.747	18.920	0.	40.9	57.4	47.6	288.2	1.155	10.13	1.601
9	16.871	17.313	0.	42.5	54.9	40.4	288.2	1.153	10.13	1.601
10	14.202	15.169	0.	45.8	51.1	26.0	288.2	1.153	10.13	1.601
11	13.492	14.633	0.	47.1	50.0	21.0	288.2	1.155	10.13	1.601
HUB	12.700	14.097	0.	48.4	48.7	15.4	288.2	1.157	10.13	1.601

	ABS VEL		REL VEL		MERID VEL		TANG VEL		WHEEL SPEED	
RP	IN	OUT	IN	OUT	IN	OUT	IN	OUT	IN	OUT
TIP	179.2	199.9	461.1	317.2	179.2	145.9	0.	136.7	424.8	418.4
1	184.1	199.1	454.2	315.8	184.1	149.7	-0.	131.3	415.2	409.4
2	188.4	199.2	447.3	312.2	188.4	152.7	0.	127.9	405.7	400.3
3	198.8	204.3	417.0	283.2	198.8	158.2	0.	129.3	366.5	364.2
4	201.7	210.0	392.3	258.2	201.7	160.8	0.	135.1	336.5	337.1
5	201.9	211.2	388.1	253.9	201.9	161.2	0.	136.4	331.4	332.6
6	202.0	212.4	383.8	249.7	202.0	161.6	0.	137.8	326.3	328.0
7	202.0	213.6	379.4	245.4	202.0	162.0	0.	139.2	321.2	323.5
8	201.9	215.0	375.0	241.2	201.9	162.5	0.	140.8	316.1	319.0
9	200.0	224.2	347.7	216.9	200.0	165.3	0.	151.5	284.4	291.9
10	192.9	241.9	307.5	187.6	192.9	168.6	0.	173.5	259.4	255.7
11	190.6	248.1	296.8	181.1	190.6	169.0	0.	181.7	227.5	246.7
HUB	188.0	255.2	284.9	175.6	188.0	169.3	0.	191.0	214.1	237.7

	ABS MACH NO		REL MACH NO		MERID MACH NO		STREAMLINE SLOPE		MERID PEAK SS	
RP	IN	OUT	IN	OUT	IN	OUT	IN	OUT	VEL R	MACH NO
TIP	0.542	0.553	1.394	0.878	0.542	0.404	-5.69	-8.84	0.814	1.582
1	0.558	0.554	1.376	0.878	0.558	0.416	-5.12	-7.72	0.813	1.549
2	0.571	0.556	1.357	0.872	0.571	0.426	-4.46	-6.60	0.810	1.539
3	0.605	0.575	1.270	0.797	0.605	0.445	-0.98	-2.24	0.796	1.519
4	0.615	0.594	1.196	0.730	0.615	0.455	2.14	0.87	0.797	1.509
5	0.615	0.597	1.183	0.718	0.615	0.456	2.70	1.39	0.799	1.508
6	0.616	0.601	1.170	0.707	0.616	0.457	3.28	1.92	0.800	1.507
7	0.616	0.605	1.157	0.695	0.616	0.459	3.86	2.44	0.802	1.506
8	0.615	0.609	1.143	0.683	0.615	0.460	4.46	2.97	0.805	1.506
9	0.609	0.638	1.059	0.617	0.609	0.470	8.45	6.33	0.826	1.501
10	0.586	0.693	0.954	0.537	0.586	0.483	15.38	11.44	0.874	1.467
11	0.579	0.712	0.901	0.520	0.579	0.485	17.58	12.87	0.887	1.431
HUB	0.570	0.734	0.864	0.505	0.570	0.487	20.23	14.35	0.901	1.379

	PERCENT	INCIDENCE		DEV	D-FACT	EFF	LOSS COEFF		LOSS PARAM	
RP	SPAN	MEAN	SS				TOT	PROF	TOT	PROF
TIP	0.	2.5	-0.0	4.8	0.425	0.728	0.212	0.119	0.038	0.021
1	5.00	2.8	-0.0	4.4	0.413	0.774	0.171	0.085	0.031	0.015
2	10.00	3.0	0.0	4.0	0.407	0.813	0.140	0.058	0.025	0.010
3	30.00	4.1	-0.0	2.9	0.424	0.884	0.088	0.024	0.017	0.004
4	45.00	4.9	0.0	2.7	0.449	0.914	0.069	0.016	0.013	0.003
5	47.50	5.1	0.0	2.7	0.453	0.918	0.067	0.016	0.013	0.003
6	50.00	5.2	0.0	2.7	0.458	0.921	0.065	0.016	0.013	0.003
7	52.50	5.4	0.0	2.8	0.462	0.924	0.063	0.016	0.012	0.003
8	55.00	5.5	-0.0	2.8	0.467	0.927	0.062	0.016	0.012	0.003
9	70.00	6.3	0.0	3.5	0.492	0.942	0.054	0.020	0.011	0.004
10	90.00	7.3	0.0	5.6	0.519	0.938	0.069	0.052	0.014	0.010
11	95.00	7.5	0.0	6.3	0.524	0.929	0.084	0.073	0.017	0.014
HUB	100.00	7.6	-0.1	7.1	0.523	0.917	0.107	0.102	0.020	0.019

TABLE VII. - DESIGN BLADE-ELEMENT PARAMETERS

FOR STATOR 4

	RADII		ABS BETAM		REL BETAM		TOTAL TEMP		TOTAL PRESS	
RP	IN	OUT	IN	OUT	IN	OUT	IN	RATIO	IN	RATIO
TIP	24.394	24.384	38.3	0.	38.3	0.	345.2	1.000	16.22	0.983
1	23.919	23.908	36.7	-0.	36.7	-0.	341.7	1.000	16.22	0.981
2	23.453	23.459	35.7	0.	35.7	0.	339.1	1.000	16.22	0.982
3	21.557	21.636	35.5	0.	35.5	0.	335.0	1.000	16.22	0.989
4	20.113	20.265	36.3	0.	36.3	0.	333.5	1.000	16.22	0.988
5	19.872	20.038	36.5	0.	36.5	0.	333.3	1.000	16.22	0.987
6	19.630	19.810	36.7	0.	36.7	0.	333.2	1.000	16.22	0.987
7	19.388	19.582	36.9	0.	36.9	0.	333.0	1.000	16.22	0.987
8	19.146	19.355	37.2	0.	37.2	0.	332.9	1.000	16.22	0.986
9	17.692	18.004	38.6	0.	38.6	0.	332.2	1.000	16.22	0.984
10	15.755	16.239	41.6	0.	41.6	0.	332.3	1.000	16.22	0.974
11	15.273	15.805	42.8	0.	42.8	0.	332.8	1.000	16.22	0.966
HUB	14.643	15.240	44.4	-0.	44.4	-0.	333.5	1.000	16.22	0.953

	ABS VEL		REL VEL		MERID VEL		TANG VEL		WHEEL SPEED	
RP	IN	OUT	IN	OUT	IN	OUT	IN	OUT	IN	OUT
TIP	224.5	177.1	224.5	177.1	176.1	177.1	139.3	0.	0.	0.
1	222.9	176.2	222.9	176.2	178.7	176.2	133.3	-0.	0.	0.
2	222.1	176.0	222.1	176.0	180.5	176.0	129.5	0.	0.	0.
3	223.4	179.2	223.4	179.2	181.9	179.2	129.6	0.	0.	0.
4	226.7	179.9	226.7	179.9	182.6	179.9	134.3	0.	0.	0.
5	227.5	180.0	227.5	180.0	182.8	180.0	135.4	0.	0.	0.
6	228.3	180.2	228.3	180.2	183.0	180.2	136.5	0.	0.	0.
7	229.3	180.4	229.3	180.4	183.2	180.4	137.8	0.	0.	0.
8	230.2	180.6	230.2	180.6	183.5	180.6	139.1	0.	0.	0.
9	237.4	182.3	237.4	182.3	185.4	182.3	148.2	0.	0.	0.
10	251.3	182.5	251.3	182.5	187.8	182.5	167.0	0.	0.	0.
11	256.2	181.4	256.2	181.4	188.1	181.4	174.0	0.	0.	0.
HUB	263.6	179.3	263.6	179.3	188.3	179.3	184.4	-0.	0.	0.

	ABS MACH NO		REL MACH NO		MERID MACH NO		STREAMLINE SLOPE		MERID PEAK SS	
RP	IN	OUT	IN	OUT	IN	OUT	IN	OUT	VEL R	MACH NO
TIP	0.626	0.487	0.626	0.487	0.491	0.487	-1.16	-0.06	1.006	0.905
1	0.625	0.487	0.625	0.487	0.501	0.487	-0.70	0.11	0.986	0.884
2	0.625	0.488	0.625	0.488	0.508	0.488	-0.29	0.26	0.975	0.870
3	0.633	0.501	0.633	0.501	0.515	0.501	1.23	0.91	0.985	0.885
4	0.644	0.504	0.644	0.504	0.519	0.504	2.59	1.54	0.985	0.878
5	0.647	0.504	0.647	0.504	0.520	0.504	2.84	1.65	0.985	0.882
6	0.650	0.505	0.650	0.505	0.521	0.505	3.09	1.77	0.985	0.886
7	0.653	0.506	0.653	0.506	0.522	0.506	3.36	1.89	0.984	0.890
8	0.656	0.506	0.656	0.506	0.523	0.506	3.63	2.01	0.984	0.894
9	0.679	0.512	0.679	0.512	0.530	0.512	5.48	2.81	0.983	0.925
10	0.723	0.512	0.723	0.512	0.540	0.512	8.68	4.02	0.972	0.992
11	0.738	0.509	0.738	0.509	0.542	0.509	9.65	4.30	0.964	1.017
HUB	0.761	0.502	0.761	0.502	0.543	0.502	10.99	4.64	0.952	1.055

	PERCENT	INCIDENCE		DEV	D-FACT	EFF	LOSS COEFF		LOSS PARAM	
RP	SPAN	MEAN	SS				TOT	PROF	TOT	PROF
TIP	0.	6.4	-0.0	10.7	0.455	0.	0.080	0.080	0.032	0.032
1	5.00	6.4	0.0	9.7	0.441	0.	0.082	0.082	0.031	0.031
2	10.00	6.4	-0.0	9.0	0.428	0.	0.079	0.079	0.030	0.030
3	30.00	6.4	0.0	8.2	0.399	0.	0.047	0.047	0.016	0.016
4	45.00	6.4	0.0	8.0	0.399	0.	0.051	0.051	0.017	0.017
5	47.50	6.4	0.0	8.0	0.399	0.	0.052	0.052	0.017	0.017
6	50.00	6.4	0.0	8.0	0.400	0.	0.053	0.053	0.017	0.017
7	52.50	6.4	0.0	8.0	0.401	0.	0.054	0.054	0.017	0.017
8	55.00	6.4	0.0	8.0	0.402	0.	0.055	0.055	0.017	0.017
9	70.00	6.4	0.0	7.9	0.410	0.	0.060	0.060	0.017	0.017
10	90.00	6.3	0.0	8.1	0.442	0.	0.088	0.088	0.023	0.023
11	95.00	6.3	0.0	8.3	0.458	0.	0.111	0.111	0.027	0.027
HUB	100.00	6.2	-0.0	8.5	0.483	0.	0.146	0.146	0.035	0.035

TABLE VIII. - BLADE GEOMETRY FOR REFERENCE

MVR ROTOR 11

	PERCENT	RADII		BLADE ANGLES			DELTA	CONE
RP	SPAN	RI	RO	KIC	KTC	KOC	INC	ANGLE
TIP	0.	25.197	24.816	64.37	62.97	57.71	2.53	-10.431
1	5.	24.628	24.280	63.11	61.83	57.26	2.78	-9.182
2	10.	24.060	23.744	61.90	60.58	56.65	3.04	-8.035
3	30.	21.741	21.600	57.36	54.88	53.15	4.13	-3.095
4	45.	19.960	19.992	54.13	50.29	48.79	4.95	0.651
5	48.	19.658	19.724	53.59	49.49	47.87	5.09	1.291
6	50.	19.536	19.456	53.05	48.68	46.91	5.22	1.935
7	53.	19.052	19.188	52.51	47.86	45.89	5.36	2.581
8	55.	18.747	18.920	51.97	47.02	44.82	5.49	3.232
9	70.	16.871	17.313	48.65	42.07	36.74	6.30	7.403
10	90.	14.202	15.169	44.05	34.00	20.19	7.28	13.919
11	95.	13.492	14.633	42.82	31.93	14.48	7.49	15.774
HUB	100.	12.700	14.097	41.44	29.85	8.02	7.69	18.485

	BLADE THICKNESSES			AXIAL DIMENSIONS			
RP	TI	TM	TO	ZIC	ZMC	ZTC	ZOC
TIP	0.051	0.152	0.051	1.046	2.039	2.444	3.116
1	0.051	0.162	0.051	1.002	2.040	2.415	3.156
2	0.051	0.172	0.051	0.955	2.040	2.381	3.198
3	0.051	0.215	0.051	0.761	2.027	2.191	3.363
4	0.051	0.248	0.051	0.621	2.021	2.003	3.502
5	0.051	0.254	0.051	0.598	2.019	1.967	3.527
6	0.051	0.260	0.051	0.574	2.018	1.930	3.553
7	0.051	0.265	0.051	0.550	2.017	1.892	3.579
8	0.051	0.271	0.051	0.526	2.016	1.852	3.606
9	0.051	0.306	0.051	0.377	2.003	1.588	3.774
10	0.051	0.356	0.051	0.147	1.989	1.143	4.050
11	0.051	0.370	0.051	0.079	1.983	1.013	4.116
HUB	0.051	0.385	0.051	0.000	1.972	0.861	4.179

	AERO	SETTING	TOTAL		X		AREA
RP	CHORD	ANGLE	CAMBER	SOLIDITY	FACTOR	PHISS	RATIO
TIP	4.634	62.67	6.66	1.298	0.704	4.94	1.040
1	4.623	61.53	5.85	1.325	0.747	5.04	1.040
2	4.625	60.35	5.25	1.355	0.799	5.30	1.040
3	4.616	55.20	4.21	1.492	1.011	7.12	1.039
4	4.614	50.86	5.34	1.618	1.110	8.71	1.039
5	4.615	50.06	5.72	1.641	1.122	8.99	1.039
6	4.615	49.24	6.15	1.665	1.132	9.27	1.039
7	4.616	48.39	6.62	1.691	1.142	9.55	1.039
8	4.618	47.52	7.16	1.717	1.151	9.85	1.039
9	4.655	41.66	11.91	1.899	1.165	11.30	1.039
10	4.716	30.45	25.86	2.249	1.242	13.97	1.040
11	4.755	26.85	28.34	2.367	1.256	14.51	1.040
HUB	4.830	22.79	33.41	2.525	1.251	14.85	1.041

TABLE IX. - BLADE GEOMETRY FOR STATOR 4

RP	PERCENT SPAN	RADII RI	RADII RO	BLADE ANGLES KIC	BLADE ANGLES KTC	BLADE ANGLES KOC	DELTA INC	CONE ANGLE
TIP	0.	24.394	24.384	31.97	26.38	-10.67	6.38	-0.151
1	5.	23.919	23.908	30.32	25.41	-9.67	6.40	-0.160
2	10.	23.453	23.459	29.26	24.80	-9.00	6.41	0.092
3	30.	21.557	21.636	29.04	24.96	-8.21	6.41	1.158
4	45.	20.113	20.265	29.94	25.83	-8.02	6.40	2.248
5	48.	19.872	20.038	30.14	26.01	-8.01	6.39	2.450
6	50.	19.630	19.810	30.35	26.20	-7.99	6.39	2.659
7	53.	19.388	19.582	30.57	26.40	-7.98	6.39	2.874
8	55.	19.146	19.355	30.81	26.61	-7.97	6.38	3.096
9	70.	17.692	18.004	32.31	27.97	-7.93	6.36	4.621
10	90.	15.755	16.239	35.44	30.68	-8.11	6.30	7.232
11	95.	15.273	15.805	36.61	31.66	-8.25	6.28	7.960
HUB	100.	14.643	15.240	38.35	33.10	-8.48	6.25	8.954

RP	BLADE THICKNESSES TI	BLADE THICKNESSES TM	BLADE THICKNESSES TO	AXIAL DIMENSIONS ZIC	AXIAL DIMENSIONS ZMC	AXIAL DIMENSIONS ZTC	AXIAL DIMENSIONS ZOC
TIP	0.051	0.279	0.051	7.085	8.897	8.415	10.935
1	0.051	0.279	0.051	7.068	8.901	8.355	10.955
2	0.051	0.279	0.051	7.056	8.902	8.273	10.953
3	0.051	0.279	0.051	7.047	8.898	8.167	10.928
4	0.051	0.279	0.051	7.052	8.896	8.121	10.926
5	0.051	0.279	0.051	7.053	8.895	8.115	10.925
6	0.051	0.279	0.051	7.055	8.894	8.108	10.925
7	0.051	0.279	0.051	7.056	8.894	8.102	10.924
8	0.051	0.279	0.051	7.057	8.893	8.096	10.924
9	0.051	0.279	0.051	7.066	8.886	8.057	10.919
10	0.051	0.279	0.051	7.095	8.880	8.025	10.916
11	0.051	0.279	0.051	7.106	8.876	8.022	10.914
HUB	0.051	0.279	0.051	7.123	8.871	8.020	10.911

RP	AERO CHORD	SETTING ANGLE	TOTAL CAMBER	SOLIDITY	X FACTOR	PHISS	AREA RATIO
TIP	4.053	15.81	42.63	1.270	0.600	10.33	1.194
1	4.053	14.90	40.00	1.295	0.600	9.41	1.184
2	4.053	14.33	38.27	1.320	0.600	8.77	1.176
3	4.054	14.15	37.26	1.434	0.600	8.05	1.157
4	4.056	14.54	37.96	1.535	0.600	7.92	1.141
5	4.056	14.64	38.14	1.553	0.600	7.92	1.138
6	4.057	14.74	38.34	1.572	0.600	7.91	1.135
7	4.058	14.84	38.55	1.591	0.600	7.91	1.132
8	4.058	14.96	38.78	1.611	0.600	7.91	1.129
9	4.065	15.67	40.24	1.740	0.600	7.92	1.106
10	4.083	17.19	43.55	1.950	0.600	8.18	1.077
11	4.088	17.76	44.86	2.010	0.600	8.35	1.070
HUB	4.098	18.62	46.83	2.095	0.600	8.62	1.061

TABLE X. - DESIGN BLADE-ELEMENT PARAMETERS FOR HIGH MVR ROTOR 19

	RADII		ABS BETAM		REL BETAM		TOTAL TEMP		TOTAL PRESS	
RP	IN	OUT	IN	OUT	IN	OUT	IN	RATIO	IN	RATIO
TIP	25.088	24.447	0.	40.4	67.8	60.9	288.2	1.189	10.13	1.601
1	24.477	23.926	-0.	39.1	66.4	59.9	288.2	1.180	10.13	1.601
2	23.910	23.405	0.	38.2	65.2	58.8	288.2	1.174	10.13	1.601
3	21.602	21.319	0.	37.6	61.0	53.8	288.2	1.161	10.13	1.601
4	19.229	19.233	0.	38.8	57.4	47.3	288.2	1.155	10.13	1.601
5	18.927	18.972	0.	39.1	57.0	46.3	288.2	1.154	10.13	1.601
6	18.623	18.711	0.	39.3	56.6	45.3	288.2	1.154	10.13	1.601
7	18.317	18.451	0.	39.6	56.2	44.2	288.2	1.154	10.13	1.601
8	18.010	18.190	0.	39.8	55.7	43.1	288.2	1.153	10.13	1.601
9	16.759	17.147	0.	41.0	54.0	38.0	288.2	1.152	10.13	1.601
10	14.106	15.061	0.	44.2	50.3	24.2	288.2	1.152	10.13	1.601
11	13.399	14.540	0.	45.4	49.2	19.5	288.2	1.154	10.13	1.601
HUB	12.700	14.018	0.	46.6	48.1	14.3	288.2	1.156	10.13	1.601

	ABS VEL		REL VEL		MERID VEL		TANG VEL		WHEEL SPEED	
RP	IN	OUT	IN	OUT	IN	OUT	IN	OUT	IN	OUT
TIP	172.9	204.4	456.9	320.0	172.9	155.5	0.	132.6	423.0	412.2
1	180.3	204.8	450.3	316.8	180.3	158.9	-0.	129.3	412.7	403.4
2	186.2	205.8	444.1	312.3	186.2	161.7	0.	127.4	403.1	394.6
3	201.6	212.2	416.3	284.9	201.6	168.1	0.	129.5	364.2	359.4
4	206.9	220.5	384.6	253.1	206.9	171.7	0.	138.3	324.2	324.3
5	207.1	221.8	380.4	249.1	207.1	172.1	0.	139.8	319.1	319.9
6	207.2	223.1	376.2	245.1	207.2	172.5	0.	141.4	314.0	315.5
7	207.1	224.4	371.9	241.2	207.1	173.0	0.	143.0	308.8	311.1
8	207.0	225.8	367.5	237.3	207.0	173.4	0.	144.6	303.6	306.7
9	205.4	232.0	349.3	222.4	205.4	175.2	0.	152.1	282.5	289.1
10	197.6	249.3	309.2	195.8	197.6	178.7	0.	173.8	237.8	253.9
11	195.0	255.2	298.4	190.3	195.0	179.3	0.	181.6	225.9	245.1
HUB	192.2	262.0	287.8	185.8	192.2	180.0	0.	190.4	214.1	236.3

	ABS MACH NO		REL MACH NO		MERID MACH NO		STREAMLINE SLOPE		MERID PEAK SS	
RP	IN	OUT	IN	OUT	IN	OUT	IN	OUT	VEL R	MACH NO
TIP	0.522	0.568	1.379	0.890	0.522	0.433	-8.47	-13.66	0.900	1.580
1	0.545	0.572	1.362	0.885	0.545	0.444	-7.76	-12.10	0.881	1.571
2	0.564	0.577	1.346	0.875	0.564	0.453	-6.99	-10.43	0.868	1.563
3	0.614	0.599	1.269	0.805	0.614	0.475	-2.92	-4.61	0.834	1.549
4	0.632	0.626	1.175	0.719	0.632	0.488	2.00	0.49	0.830	1.548
5	0.633	0.630	1.162	0.708	0.633	0.489	2.67	1.11	0.831	1.545
6	0.633	0.634	1.149	0.697	0.633	0.491	3.35	1.73	0.833	1.542
7	0.633	0.639	1.136	0.686	0.633	0.492	4.05	2.37	0.835	1.541
8	0.632	0.643	1.122	0.676	0.632	0.494	4.76	3.00	0.838	1.539
9	0.627	0.663	1.066	0.635	0.627	0.500	7.82	5.59	0.853	1.539
10	0.601	0.717	0.941	0.563	0.601	0.514	15.37	11.31	0.904	1.495
11	0.593	0.735	0.907	0.548	0.593	0.517	17.73	12.89	0.920	1.454
HUB	0.584	0.756	0.874	0.536	0.584	0.519	20.23	14.54	0.936	1.412

	PERCENT	INCIDENCE		DEV	D-FACT	EFF	LOSS COEFF		LOSS PARAM	
RP	SPAN	MEAN	SS				TOT	PROF	TOT	PROF
TIP	0.	2.4	-0.1	4.1	0.409	0.762	0.179	0.085	0.033	0.016
1	5.00	2.8	-0.0	4.0	0.404	0.798	0.150	0.060	0.028	0.011
2	10.00	3.1	0.0	3.7	0.401	0.828	0.126	0.041	0.024	0.008
3	30.00	4.2	-0.0	2.8	0.419	0.895	0.079	0.008	0.016	0.002
4	50.00	5.3	-0.0	2.6	0.450	0.928	0.058	0.001	0.012	0.000
5	52.50	5.4	-0.0	2.7	0.455	0.931	0.057	0.002	0.012	0.000
6	55.00	5.6	0.0	2.7	0.459	0.933	0.055	0.003	0.011	0.001
7	57.50	5.7	0.0	2.8	0.463	0.936	0.054	0.003	0.011	0.001
8	60.00	5.9	0.0	2.8	0.466	0.939	0.052	0.004	0.011	0.001
9	70.00	6.4	0.0	3.3	0.480	0.947	0.049	0.007	0.010	0.002
10	90.00	7.4	-0.0	5.4	0.497	0.943	0.062	0.041	0.013	0.008
11	95.00	7.6	-0.0	6.1	0.497	0.936	0.076	0.062	0.015	0.012
HUB	100.00	7.8	0.0	6.9	0.494	0.925	0.094	0.087	0.018	0.017

TABLE XI. - DESIGN BLADE-ELEMENT PARAMETERS

FOR STATOR 16

	RADII		ABS BETAM		REL BETAM		TOTAL TEMP		TOTAL PRESS	
RP	IN	OUT	IN	OUT	IN	OUT	IN	RATIO	IN	RATIO
TIP	23.812	23.812	33.2	0.	33.2	0.	342.7	1.000	16.22	0.969
1	23.362	23.334	32.5	-0.	32.5	-0.	340.1	1.000	16.22	0.975
2	22.938	22.911	32.1	0.	32.1	0.	338.2	1.000	16.22	0.980
3	21.173	21.202	32.7	0.	32.7	0.	334.5	1.000	16.22	0.986
4	19.347	19.475	34.3	0.	34.3	0.	332.8	1.000	16.22	0.984
5	19.117	19.260	34.5	0.	34.5	0.	332.7	1.000	16.22	0.984
6	18.886	19.045	34.7	0.	34.7	0.	332.6	1.000	16.22	0.983
7	18.655	18.831	35.0	0.	35.0	0.	332.4	1.000	16.22	0.983
8	18.424	18.618	35.2	0.	35.2	0.	332.3	1.000	16.22	0.983
9	17.498	17.769	36.3	0.	36.3	0.	331.9	1.000	16.22	0.981
10	15.647	16.115	39.2	0.	39.2	0.	332.1	1.000	16.22	0.972
11	15.186	15.712	40.3	0.	40.3	0.	332.5	1.000	16.22	0.966
HUB	14.735	15.240	41.4	-0.	41.4	-0.	333.0	1.000	16.22	0.957

	ABS VEL		REL VEL		MERID VEL		TANG VEL		WHEEL SPEED	
RP	IN	OUT	IN	OUT	IN	OUT	IN	OUT	IN	OUT
TIP	249.7	190.8	249.7	190.8	209.1	190.8	136.6	0.	0.	0.
1	246.6	194.0	246.6	194.0	207.9	194.0	132.5	-0.	0.	0.
2	244.3	196.3	244.3	196.3	206.9	196.3	130.0	0.	0.	0.
3	241.4	200.5	241.4	200.5	203.1	200.5	130.4	0.	0.	0.
4	244.2	201.6	244.2	201.6	201.8	201.6	137.5	0.	0.	0.
5	245.0	201.9	245.0	201.9	201.9	201.9	138.8	0.	0.	0.
6	245.8	202.1	245.8	202.1	201.9	202.1	140.1	0.	0.	0.
7	246.6	202.4	246.6	202.4	202.0	202.4	141.4	0.	0.	0.
8	247.5	202.7	247.5	202.7	202.2	202.7	142.8	0.	0.	0.
9	251.9	204.3	251.9	204.3	203.0	204.3	149.1	0.	0.	0.
10	264.6	206.6	264.6	206.6	205.0	206.6	167.3	0.	0.	0.
11	269.1	206.7	269.1	206.7	205.4	206.7	173.9	0.	0.	0.
HUB	274.1	206.6	274.1	206.6	205.7	206.6	181.2	-0.	0.	0.

	ABS MACH NO		REL MACH NO		MERID MACH NO		STREAMLINE SLOPE		MERID PEAK SS	
RP	IN	OUT	IN	OUT	IN	OUT	IN	OUT	VEL R	MACH NO
TIP	0.706	0.528	0.706	0.528	0.591	0.528	-1.33	0.05	0.913	0.961
1	0.699	0.540	0.699	0.540	0.589	0.540	-1.10	-0.00	0.933	0.942
2	0.694	0.548	0.694	0.548	0.588	0.548	-0.85	0.00	0.949	0.929
3	0.689	0.564	0.689	0.564	0.580	0.564	0.53	0.47	0.987	0.915
4	0.700	0.569	0.700	0.569	0.578	0.569	2.46	1.30	0.999	0.931
5	0.702	0.570	0.702	0.570	0.579	0.570	2.74	1.42	1.000	0.935
6	0.705	0.571	0.705	0.571	0.579	0.571	3.04	1.55	1.001	0.939
7	0.708	0.572	0.708	0.572	0.580	0.572	3.34	1.68	1.002	0.948
8	0.711	0.573	0.711	0.573	0.581	0.573	3.66	1.82	1.003	0.959
9	0.725	0.578	0.725	0.578	0.584	0.578	5.06	2.42	1.006	1.013
10	0.766	0.585	0.766	0.585	0.593	0.585	8.59	3.83	1.008	1.137
11	0.780	0.585	0.780	0.585	0.595	0.585	9.66	4.21	1.006	1.178
HUB	0.795	0.584	0.795	0.584	0.597	0.584	10.79	4.65	1.004	1.224

	PERCENT	INCIDENCE		DEV	D-FACT	EFF	LOSS COEFF		LOSS PARAM	
RP	SPAN	MEAN	SS				TOT	PROF	TOT	PROF
TIP	0.	6.6	-0.0	8.2	0.451	0.	0.116	0.116	0.046	0.046
1	5.00	6.6	0.0	7.8	0.421	0.	0.089	0.089	0.034	0.034
2	10.00	6.6	-0.0	7.5	0.398	0.	0.073	0.073	0.028	0.028
3	30.00	6.6	0.0	7.2	0.359	0.	0.052	0.052	0.018	0.018
4	50.00	6.6	0.0	7.2	0.354	0.	0.058	0.058	0.018	0.018
5	52.50	6.6	0.0	7.2	0.355	0.	0.058	0.058	0.019	0.019
6	55.00	6.6	0.0	7.2	0.356	0.	0.059	0.059	0.019	0.019
7	57.50	6.6	0.0	7.1	0.356	0.	0.060	0.060	0.019	0.019
8	60.00	6.6	0.0	7.1	0.356	0.	0.061	0.061	0.019	0.019
9	70.00	6.5	0.0	6.9	0.360	0.	0.063	0.063	0.018	0.018
10	90.00	6.4	0.0	6.8	0.382	0.	0.087	0.087	0.023	0.023
11	95.00	6.4	0.0	6.9	0.393	0.	0.103	0.103	0.026	0.026
HUB	100.00	6.4	0.1	6.9	0.406	0.	0.130	0.130	0.032	0.032

TABLE XII. - BLADE GEOMETRY FOR HIGH MVR ROTOR 19

RP	PERCENT SPAN	RADII RI	RO	BLADE ANGLES KIC	KTC	KOC	DELTA INC	CONE ANGLE
TIP	0.	25.088	24.447	64.62	62.17	56.39	2.55	-17.424
1	5.	24.477	23.926	63.10	60.79	55.67	2.82	-14.384
2	10.	23.910	23.405	61.74	59.42	54.90	3.08	-12.669
3	30.	21.602	21.319	56.75	53.37	50.92	4.18	-6.094
4	50.	19.229	19.233	52.16	46.69	44.64	5.30	0.076
5	53.	18.927	18.972	51.60	45.90	43.61	5.44	0.841
6	55.	18.623	18.711	51.04	45.12	42.53	5.58	1.608
7	58.	18.317	18.451	50.48	44.30	41.40	5.72	2.390
8	60.	18.010	18.190	49.91	43.48	40.22	5.86	3.177
9	70.	16.759	17.147	47.66	40.01	34.70	6.41	6.425
10	90.	14.106	15.061	43.08	32.44	18.55	7.40	13.722
11	95.	13.399	14.540	41.88	30.52	13.15	7.61	15.792
HUB	100.	12.700	14.018	40.70	28.65	7.18	7.79	17.622

RP	BLADE THICKNESSES TI	TM	TO	AXIAL DIMENSIONS ZIC	ZMC	ZTC	ZOC
TIP	0.051	0.152	0.051	1.067	2.031	2.428	3.106
1	0.051	0.163	0.051	1.009	2.032	2.399	3.156
2	0.051	0.173	0.051	0.956	2.033	2.366	3.206
3	0.051	0.216	0.051	0.751	2.029	2.182	3.400
4	0.051	0.260	0.051	0.556	2.026	1.913	3.601
5	0.051	0.266	0.051	0.533	2.025	1.875	3.627
6	0.051	0.271	0.051	0.510	2.025	1.835	3.652
7	0.051	0.277	0.051	0.487	2.024	1.794	3.678
8	0.051	0.283	0.051	0.463	2.022	1.752	3.704
9	0.051	0.306	0.051	0.364	2.015	1.566	3.813
10	0.051	0.357	0.051	0.134	1.987	1.114	4.047
11	0.051	0.371	0.051	0.068	1.976	0.984	4.100
HUB	0.051	0.386	0.051	0.000	1.964	0.850	4.150

RP	AERO CHORD	SETTING ANGLE	TOTAL CAMBER	SOLIDITY	X FACTOR	PHISS	AREA RATIO
TIP	4.625	62.14	8.22	1.308	0.725	6.00	1.041
1	4.584	60.73	7.43	1.326	0.765	6.10	1.039
2	4.578	59.38	6.85	1.355	0.810	6.33	1.039
3	4.559	53.77	5.83	1.488	1.012	8.03	1.040
4	4.550	47.41	7.52	1.657	1.174	10.36	1.042
5	4.550	46.56	7.99	1.681	1.179	10.59	1.041
6	4.550	45.70	8.51	1.707	1.181	10.80	1.040
7	4.552	44.80	9.08	1.734	1.187	11.04	1.039
8	4.553	43.87	9.69	1.762	1.192	11.28	1.038
9	4.566	39.76	12.96	1.886	1.217	12.32	1.035
10	4.650	28.87	24.54	2.233	1.277	14.52	1.030
11	4.691	25.45	28.73	2.351	1.289	14.94	1.028
HUB	4.739	21.75	33.52	2.484	1.300	15.29	1.025

TABLE XIII. - BLADE GEOMETRY FOR

STATOR 16

RP	PERCENT SPAN	RADII RI	RADII RO	BLADE ANGLES KIC	BLADE ANGLES KTC	BLADE ANGLES KOC	DELTA INC	CONE ANGLE
TIP	0.	23.812	23.812	26.57	22.91	-8.24	6.58	0.057
1	5.	23.362	23.334	25.91	22.51	-7.79	6.59	-0.433
2	10.	22.938	22.911	25.55	22.31	-7.51	6.59	-0.402
3	30.	21.173	21.202	26.10	22.92	-7.17	6.59	0.427
4	50.	19.347	19.475	27.70	24.33	-7.16	6.57	1.931
5	53.	19.117	19.260	27.94	24.55	-7.17	6.57	2.161
6	55.	18.886	19.045	28.20	24.74	-7.17	6.57	2.401
7	58.	18.655	18.831	28.45	24.75	-7.14	6.56	2.654
8	60.	18.424	18.618	28.70	24.68	-7.10	6.55	2.918
9	70.	17.498	17.769	29.81	24.24	-6.92	6.51	4.085
10	90.	15.647	16.115	32.91	24.46	-6.82	6.41	7.029
11	95.	15.186	15.712	34.00	24.75	-6.86	6.37	7.890
HUB	100.	14.735	15.240	35.21	25.11	-6.94	6.34	7.603

RP	BLADE THICKNESSES TI	BLADE THICKNESSES TM	BLADE THICKNESSES TO	AXIAL DIMENSIONS ZIC	AXIAL DIMENSIONS ZMC	AXIAL DIMENSIONS ZTC	AXIAL DIMENSIONS ZOC
TIP	0.051	0.279	0.051	7.529	9.359	8.689	11.338
1	0.051	0.279	0.051	7.524	9.360	8.643	11.337
2	0.051	0.279	0.051	7.521	9.361	8.610	11.338
3	0.051	0.279	0.051	7.523	9.360	8.548	11.336
4	0.051	0.279	0.051	7.534	9.358	8.515	11.335
5	0.051	0.279	0.051	7.535	9.357	8.511	11.335
6	0.051	0.279	0.051	7.536	9.356	8.506	11.334
7	0.051	0.279	0.051	7.536	9.355	8.498	11.334
8	0.051	0.279	0.051	7.536	9.355	8.488	11.334
9	0.051	0.279	0.051	7.534	9.356	8.446	11.334
10	0.051	0.279	0.051	7.538	9.353	8.389	11.334
11	0.051	0.279	0.051	7.542	9.352	8.380	11.333
HUB	0.051	0.279	0.051	7.546	9.351	8.374	11.333

RP	AERO CHORD	SETTING ANGLE	TOTAL CAMBER	SOLIDITY	X FACTOR	PHISS	AREA RATIO
TIP	3.958	12.95	34.81	1.270	0.600	7.92	1.103
1	3.958	12.58	33.70	1.295	0.600	7.50	1.100
2	3.959	12.38	33.06	1.319	0.600	7.23	1.097
3	3.958	12.61	33.27	1.427	0.600	6.95	1.088
4	3.960	13.38	34.86	1.559	0.600	7.01	1.075
5	3.961	13.50	35.11	1.577	0.600	7.02	1.072
6	3.962	13.61	35.37	1.596	0.602	7.07	1.070
7	3.962	13.62	35.59	1.615	0.618	7.27	1.069
8	3.963	13.60	35.81	1.635	0.641	7.55	1.069
9	3.968	13.40	36.73	1.719	0.749	8.91	1.070
10	3.986	13.66	39.73	1.918	0.923	11.46	1.068
11	3.994	13.87	40.86	1.975	0.962	12.20	1.069
HUB	3.991	14.14	42.15	2.034	0.999	12.98	1.071

TABLE XIV. - LOSS IN STALL PRESSURE RATIO DUE TO TIP RADIAL DISTORTION

Stage	Meridional velocity ratio	Rotor speed, percent of design	Magnitude of distortion, DM	Rotor			Stage		
				Stall pressure ratio		Pressure ratio parameter, ΔPRS, percent	Stall pressure ratio		Pressure ratio parameter, ΔPRS, percent
				Undistorted flow	Distorted flow		Undistorted flow	Distorted flow	
19-16	High	100	0.16	1.657	1.568	5.4	1.591	1.513	4.9
		70	.06	1.27	1.246	1.9	1.245	1.228	1.4
		100	.09	1.657	1.60	3.4	1.591	1.558	2.1
		70	.03	1.27	1.258	.9	1.245	1.24	.4
11-4	Reference	100	0.16	1.68	1.584	5.7	1.628	1.556	4.4
		70	.07	1.279	1.257	1.7	1.257	1.247	.8
20-17	Low	100	0.18	1.664	1.563	6.1	1.618	1.533	5.3
		70	.07	1.271	1.251	1.6	1.252	1.239	1.0
		100	.09	1.664	1.615	1.8	1.618	1.592	1.6
		70	.04	1.271	1.259	.9	1.252	1.248	.3

TABLE XV. - LOSS IN STALL PRESSURE RATIO DUE TO CIRCUMFERENTIAL DISTORTION

Stage	Meridional velocity	Rotor speed, percent of design	Rotor			Stage		
			Stall pressure ratio		ΔPRS, percent	Stall pressure ratio		ΔPRS, percent
			Undistorted flow	Distorted flow		Undistorted flow	Distorted flow	
19-16	High	100	1.666	1.584	4.9	1.599	1.504	5.9
		70	1.274	1.271	.2	1.249	1.25	-.1
11-4	Reference	100	1.701	1.60	5.9	1.638	1.564	4.5
		70	1.287	1.29	-.2	1.262	1.274	-1.0
20-17	Low	100	1.672	1.572	6.0	1.626	1.534	5.7
		70	1.274	1.279	-.4	1.254	1.262	-.6

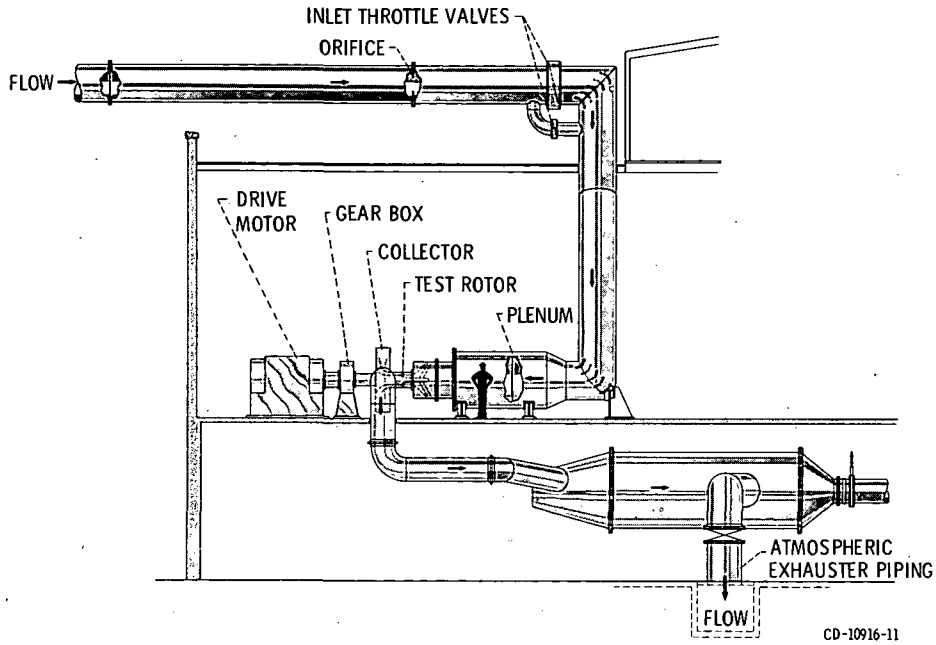

Figure 1. - Test facility.

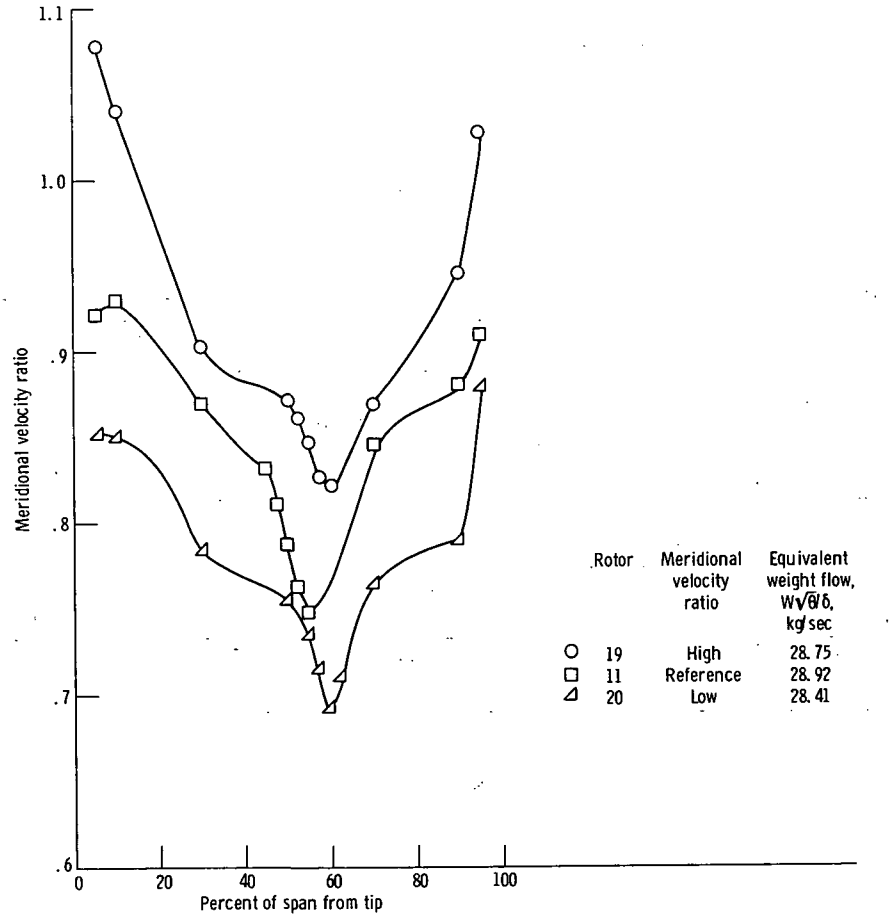

Figure 2. - Distribution of meridional velocity ratio at peak efficiency flow conditions for design speed and undistorted flow.

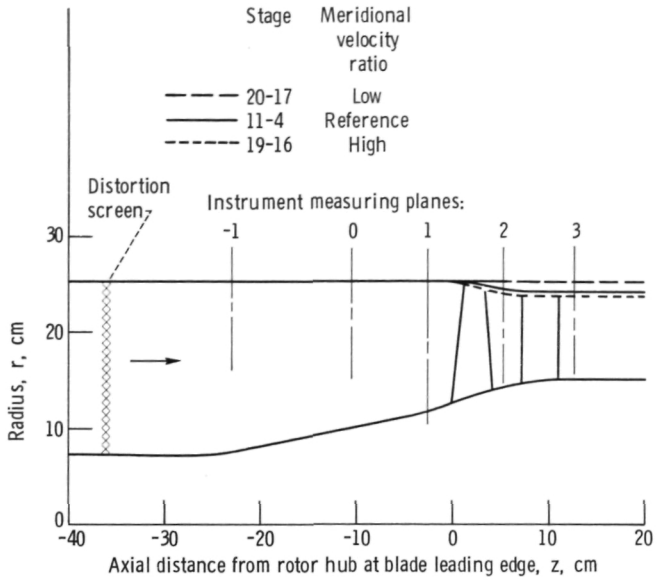

Figure 3. - Flow path schematic showing location of instrumentation and outer casing contours for each stage.

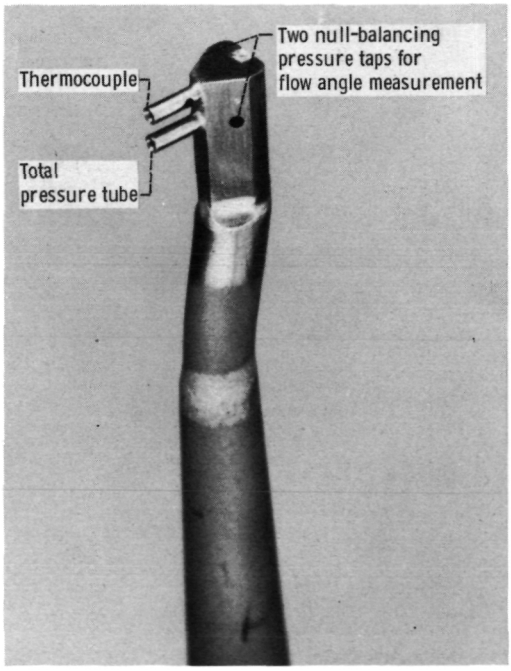

(a) Combination total pressure, total temperature, and flow angle probe.

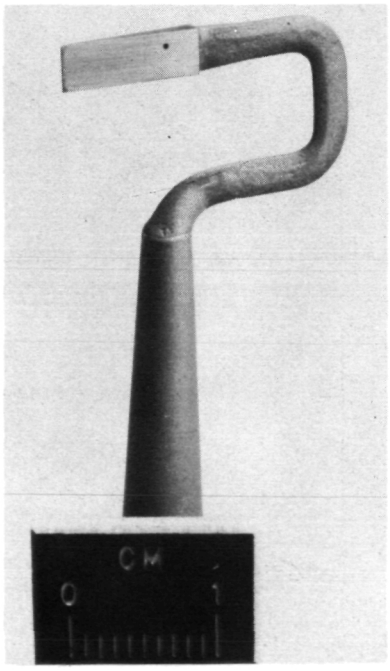

(b) Static pressure probe; 8^0 C-shaped wedge.

Figure 4. - Survey probes.

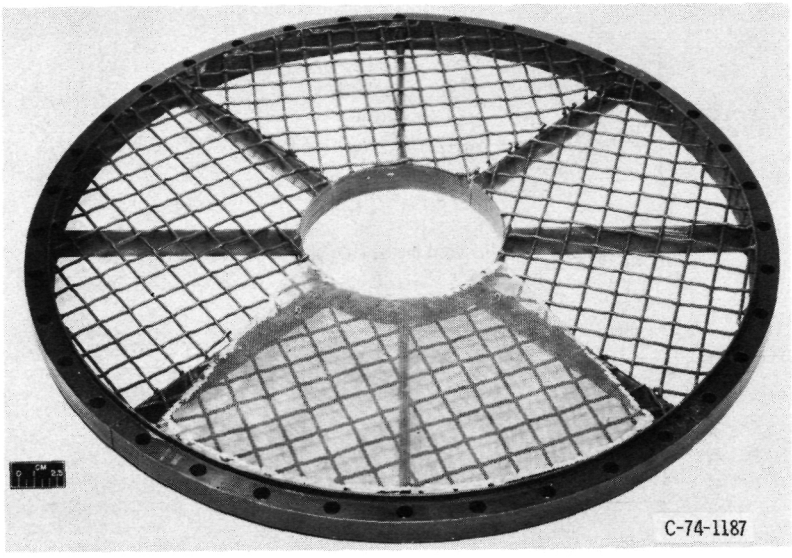

Figure 5. - Distortion screen and backup screen assembly.

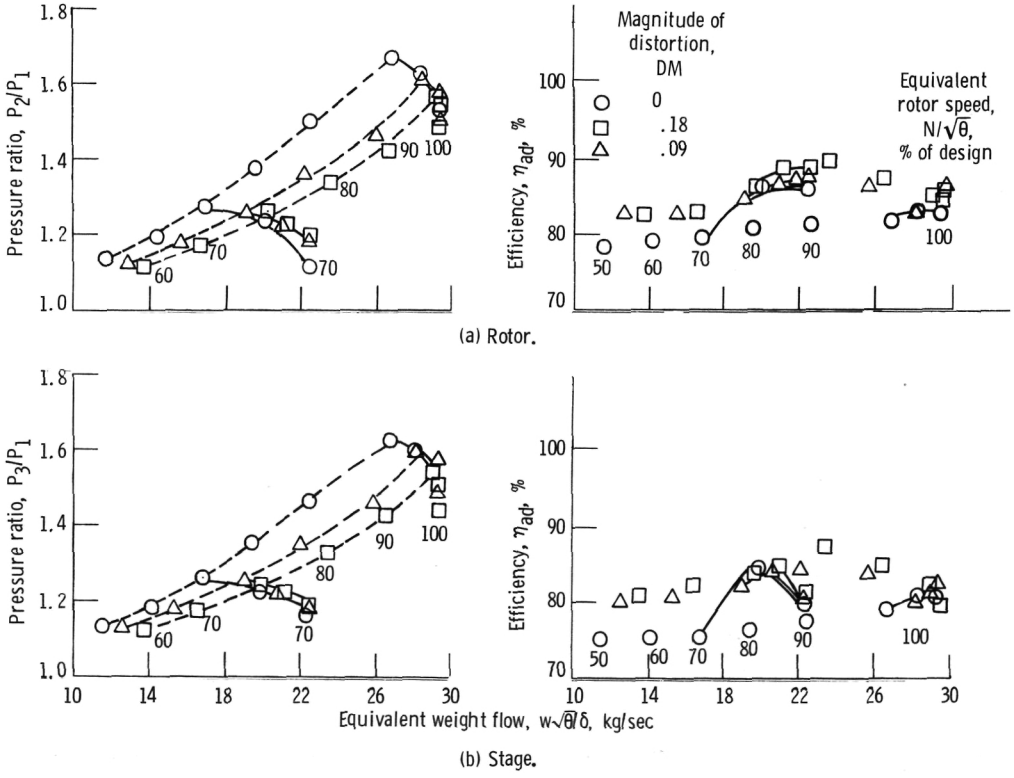

Figure 6. - Overall performance for undistorted and tip radially distorted inlet flows for low MVR stage 20-17.

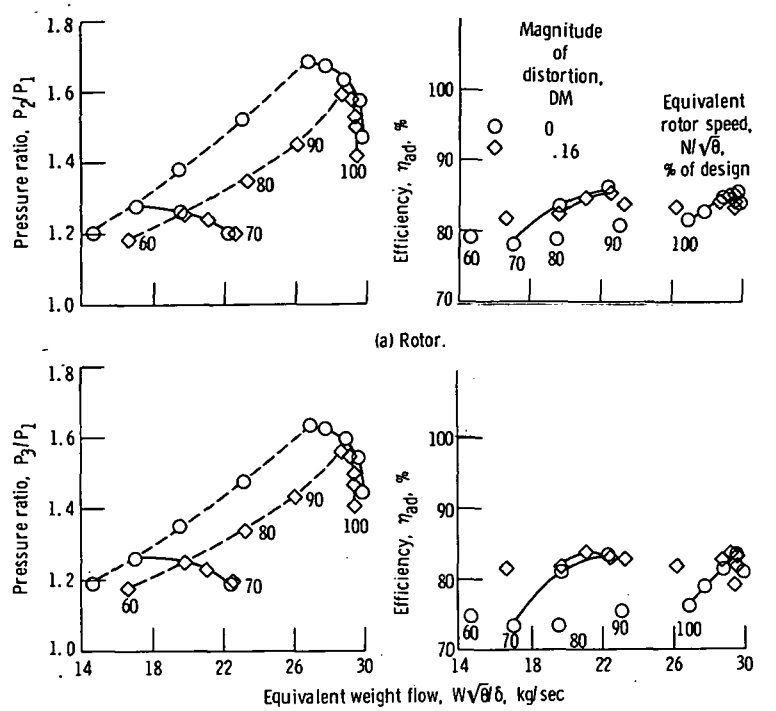

(a) Rotor.

(b) Stage.

Figure 7. - Overall performance for undistorted and tip radially distorted inlet flows for reference MVR stage 11-4.

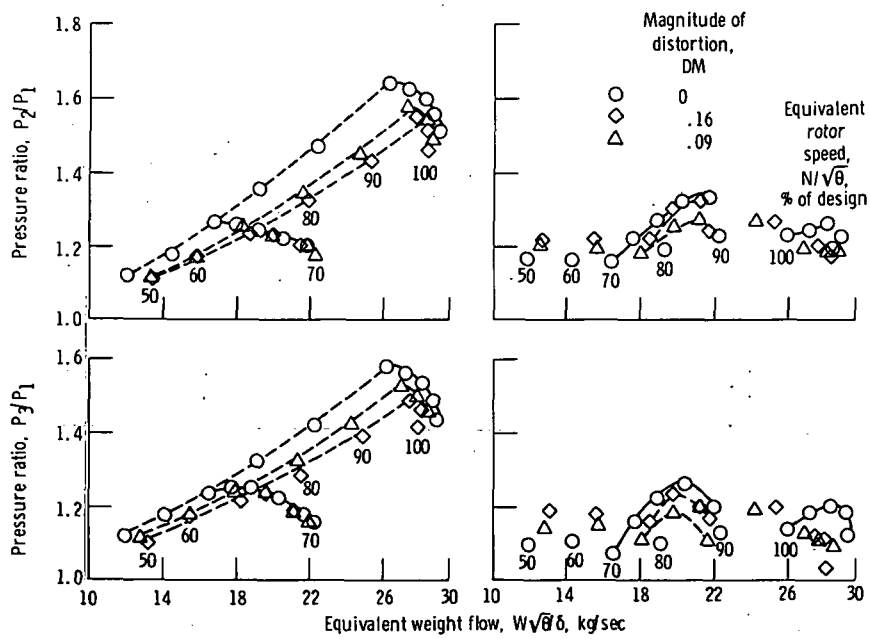

(b) Stage.

Figure 8. - Overall performance for undistorted and tip radially distorted inlet flows for high MVR stage 19-16.

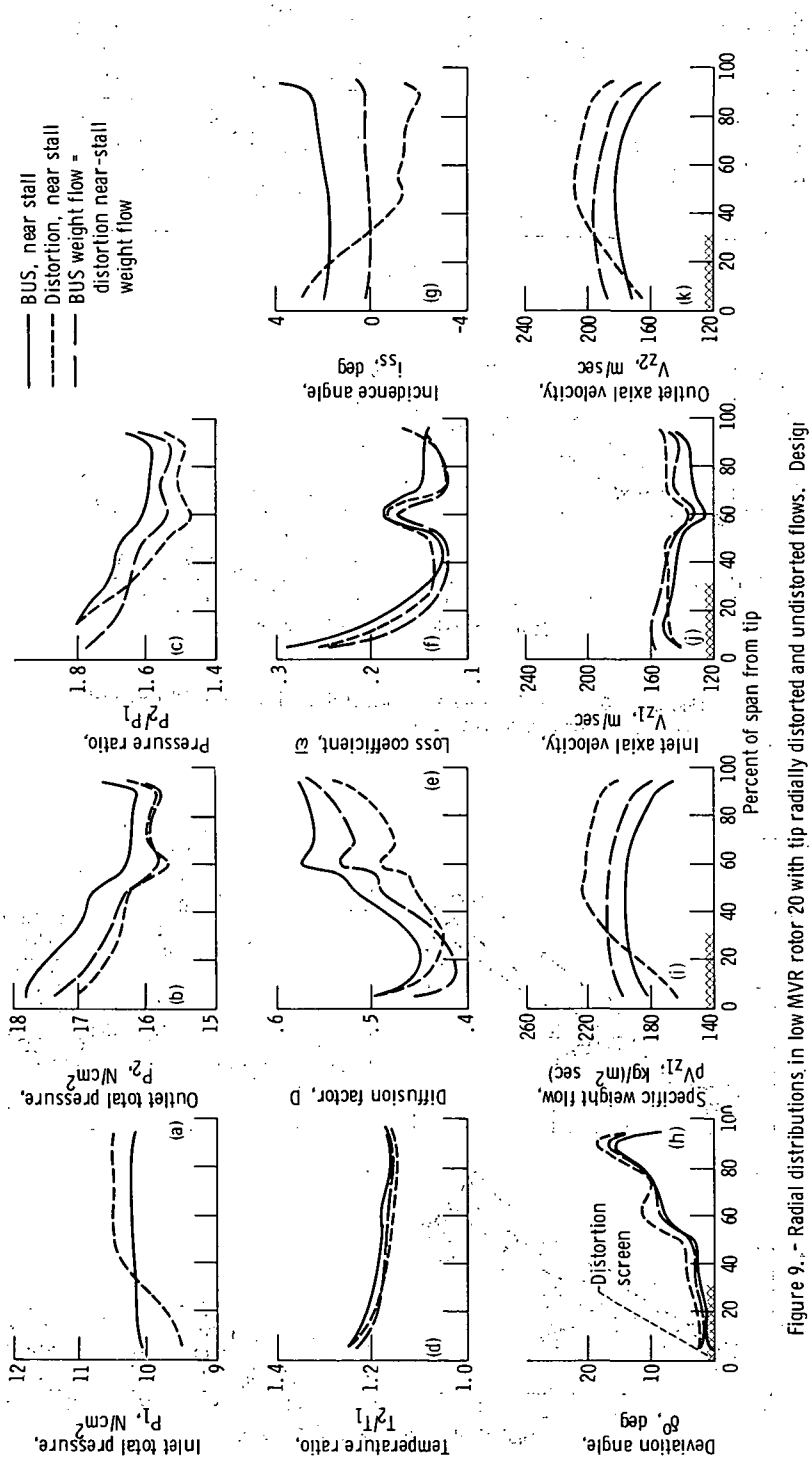

Figure 9. - Radial distributions in low MVR rotor 20 with tip radially distorted and undistorted flows. Desig

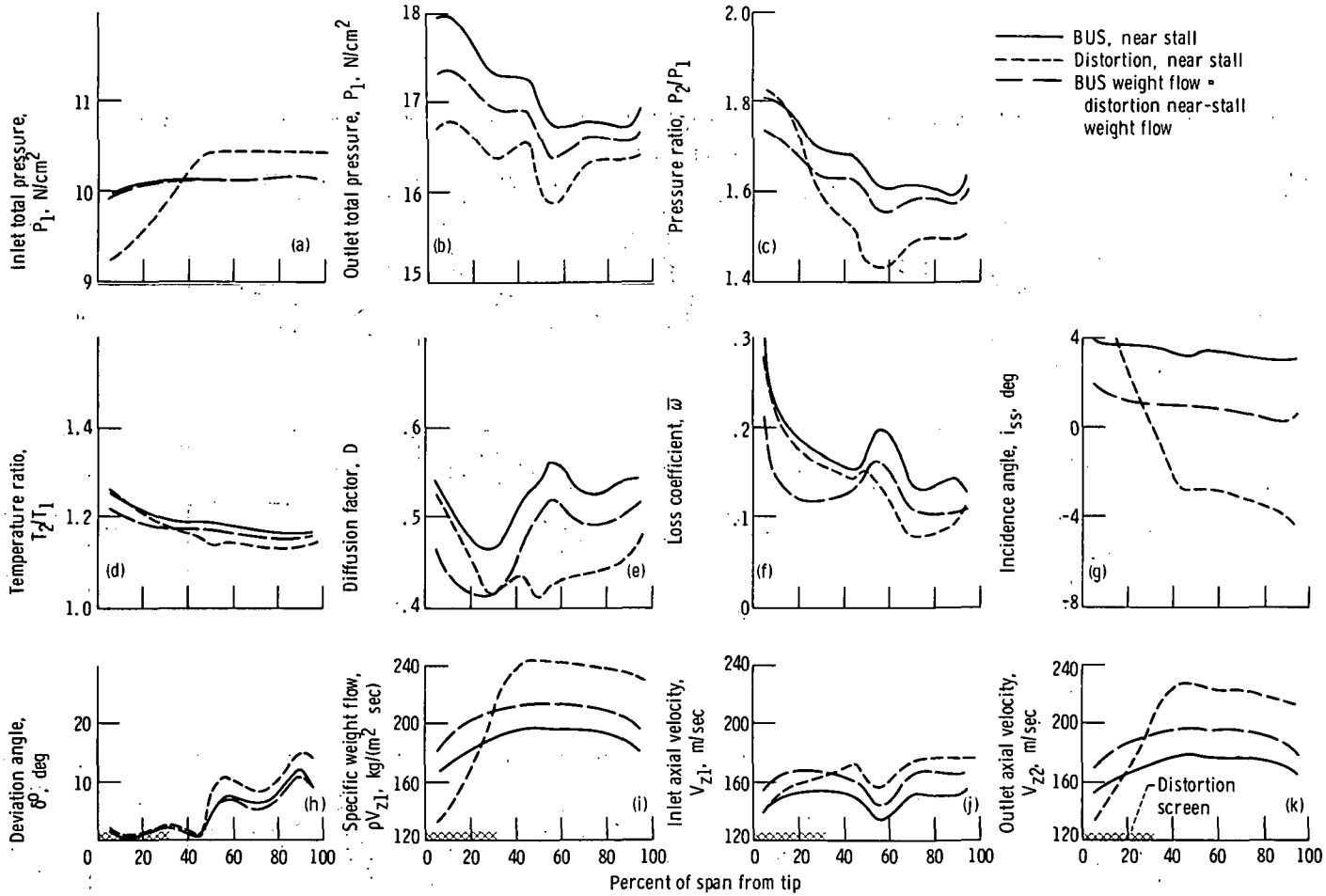

Figure 10. - Radial distributions in reference MVR rotor 11 with tip radially distorted and undistorted flows. Design speed; magnitude of distortion, 0.16.

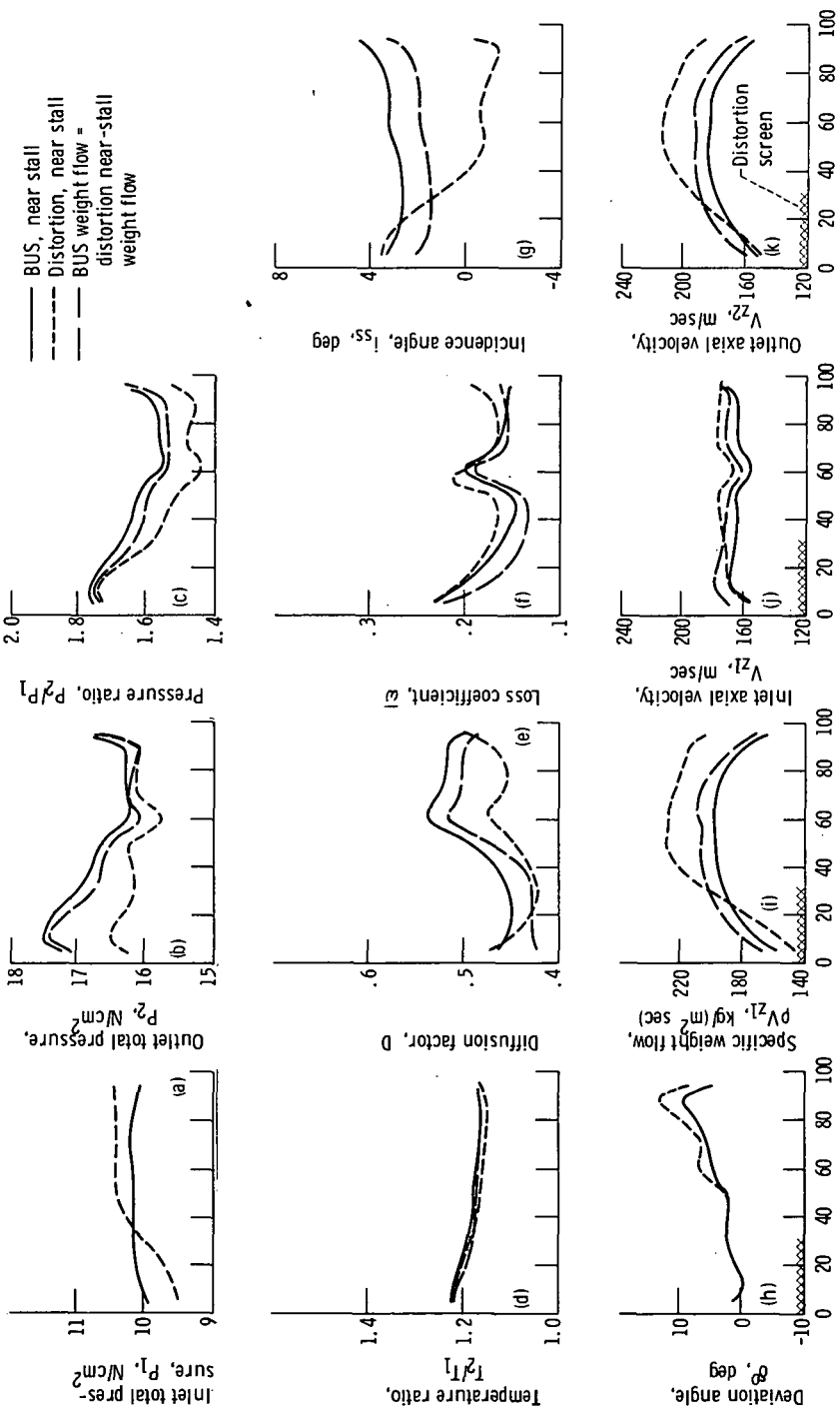

Figure 11. - Radial distributions in high MVR rotor 19 with tip radially distorted and undistorted flows. Design speed; magnitude of distortion, 0.09.

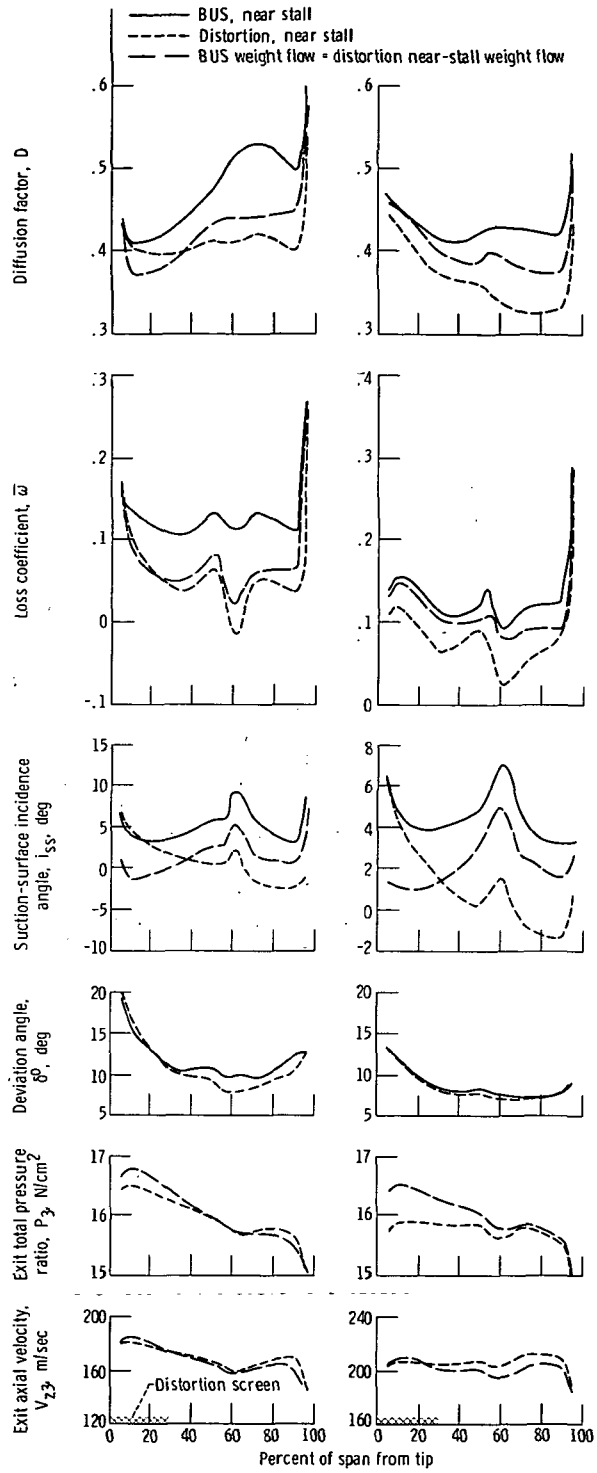

(a) Low MVR stator 17. (b) High MVR stator 16.

Figure 12. - Radial distributions in stators run with tip radially distorted and undistorted flows. Design speed; magnitude of distortion, 0.09.

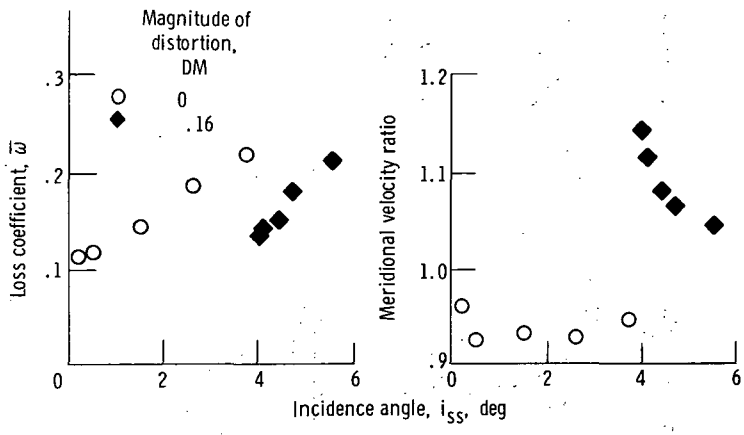

Figure 13. - Correlation of blade-element parameters with incidence angle for tip radially distorted and undistorted flows in rotor 11. 10 Percent of span from tip; design speed.

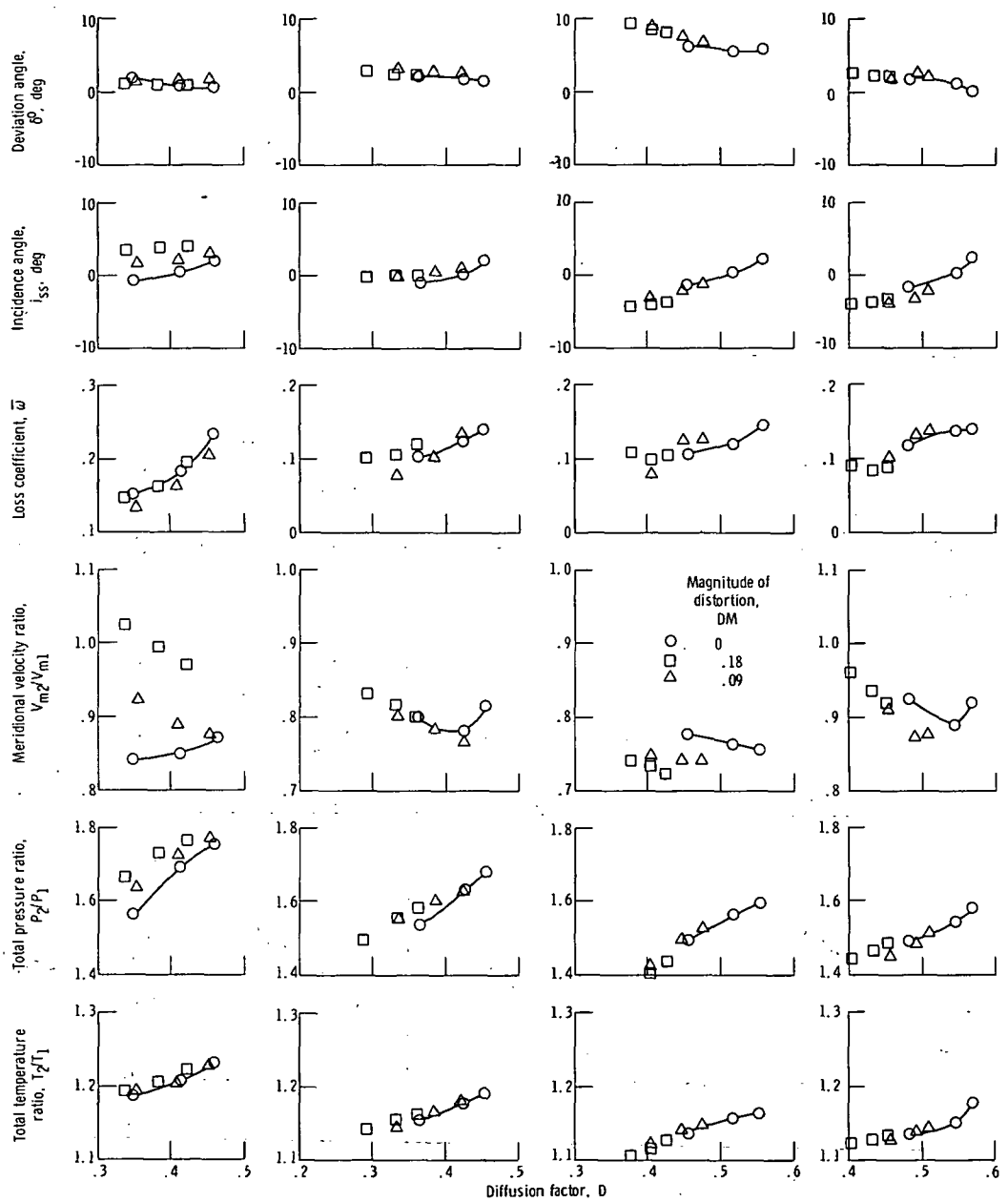

(a) 10 Percent of span from tip.

(b) 30 Percent of span from tip.

(c) 70 Percent of span from tip.

(d) 90 Percent of span from tip.

Figure 14. - Blade-element performance of rotor 20 at design speed.

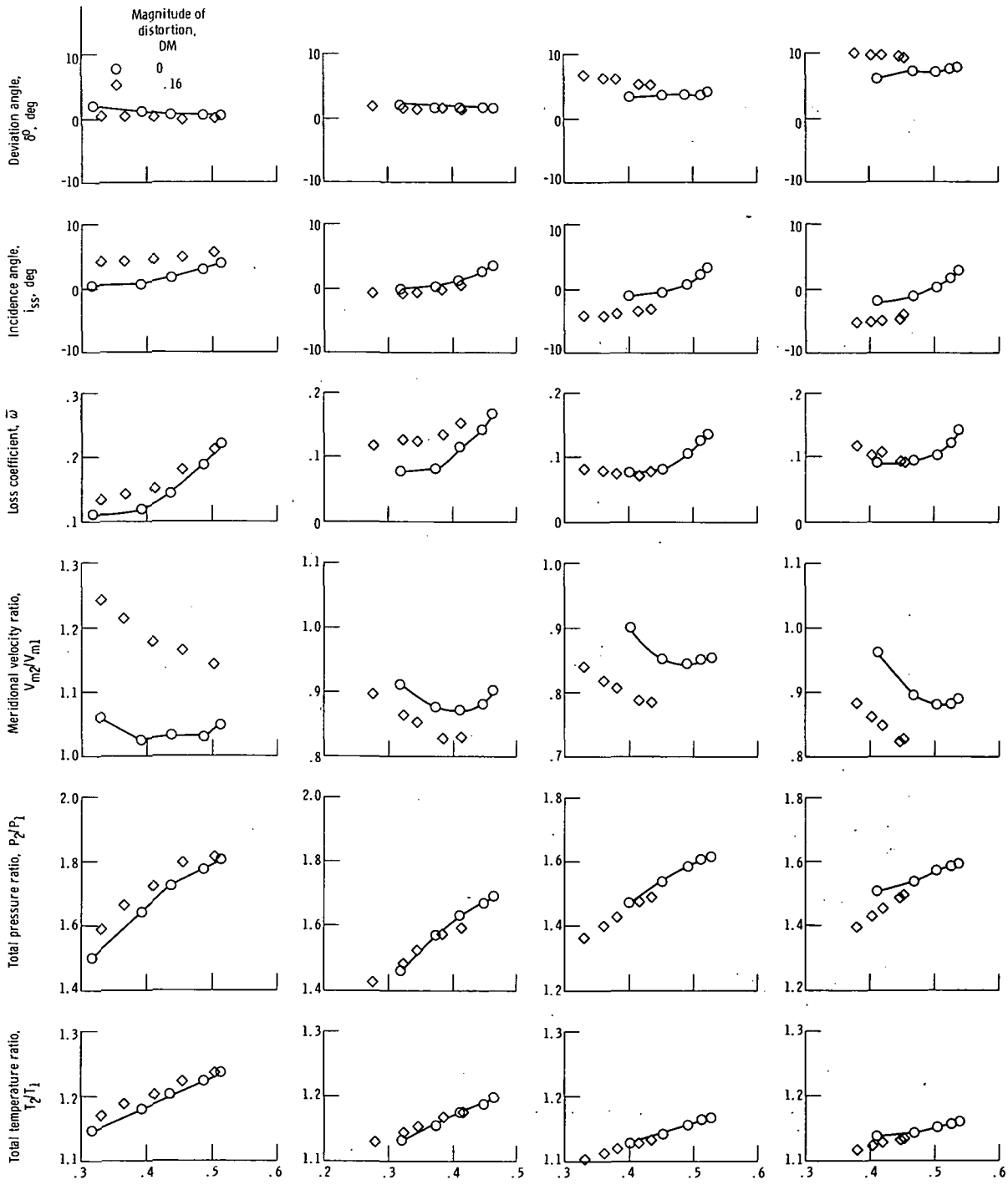

(a) 10 Percent of span from tip. (b) 30 Percent of span from tip. (c) 70 Percent of span from tip. (d) 90 Percent of span from tip.

Figure 15. - Blade-element performance of rotor 11 at design speed.

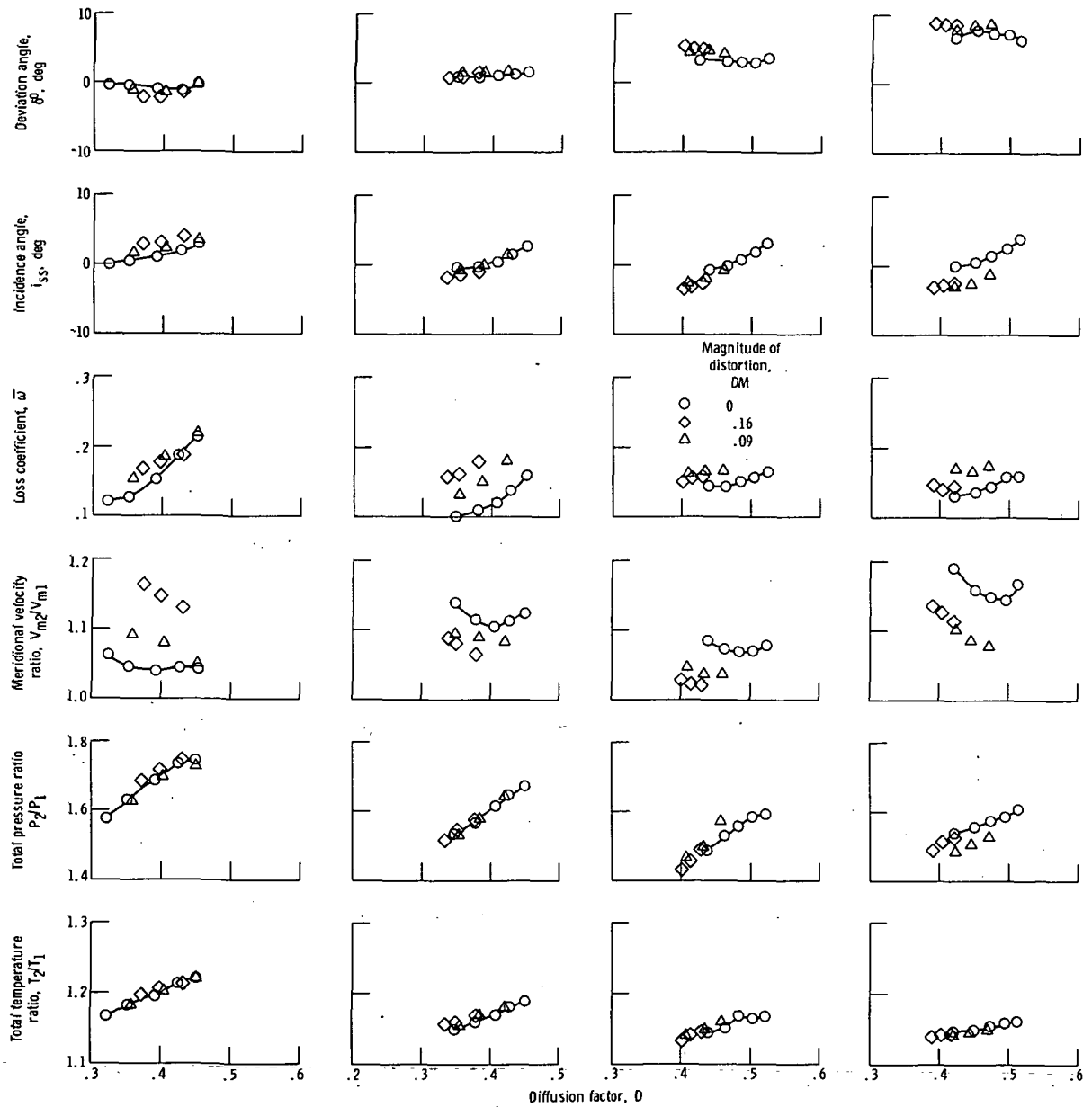

(a) 10 Percent of span from tip. (b) 30 Percent of span from tip. (c) 70 Percent of span from tip. (d) 90 Percent of span from tip.

Figure 16. - Blade-element performance of rotor 19 at design speed.

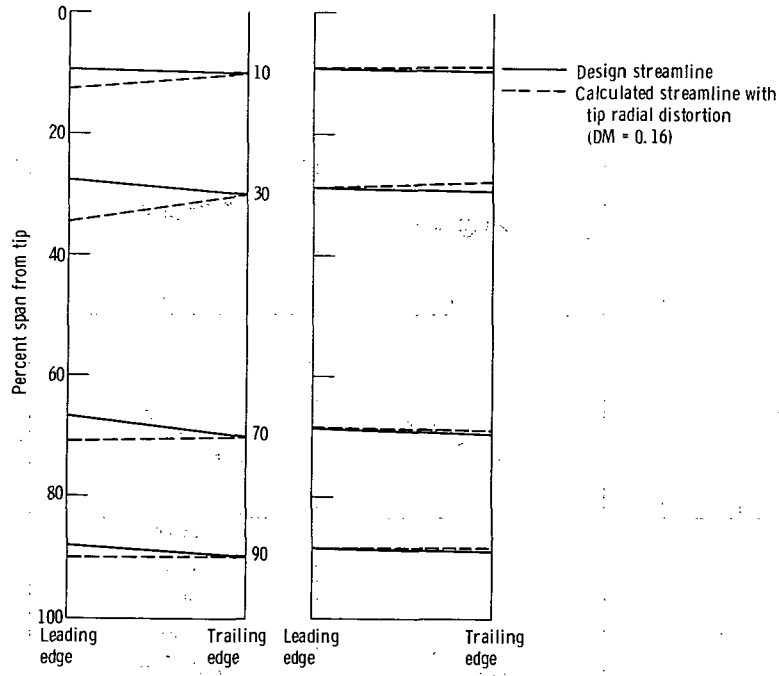

(a) Reference MVR rotor 11.

(b) Stator 4.

Figure 17. - Effect of tip radial distortion on streamline slope for rotor 11 and stator 4. Equivalent rotor speed, 100 percent of design; equivalent weight flow, 29.52 kilograms per second.

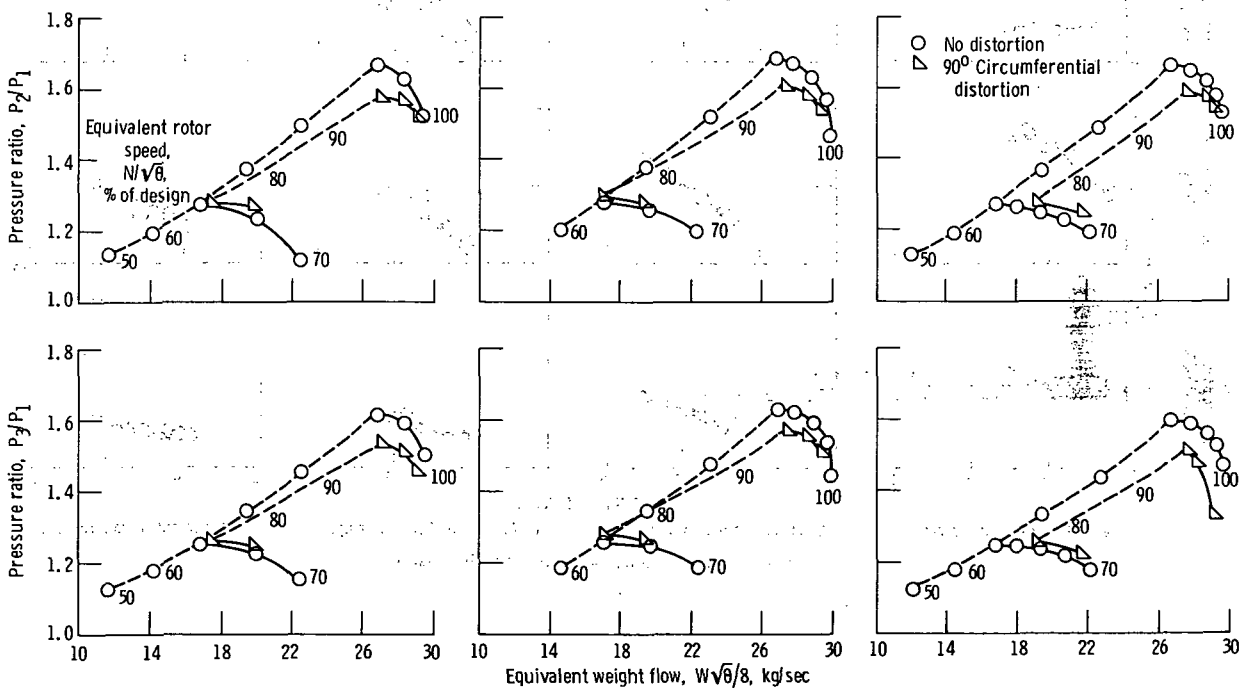

(a) Low MVR stage 20-17.

(b) Reference MVR stage 11-4.

(c) High MVR stage 19-16.

Figure 18. - Overall performance with undistorted and 90° circumferentially distorted inlet flow.

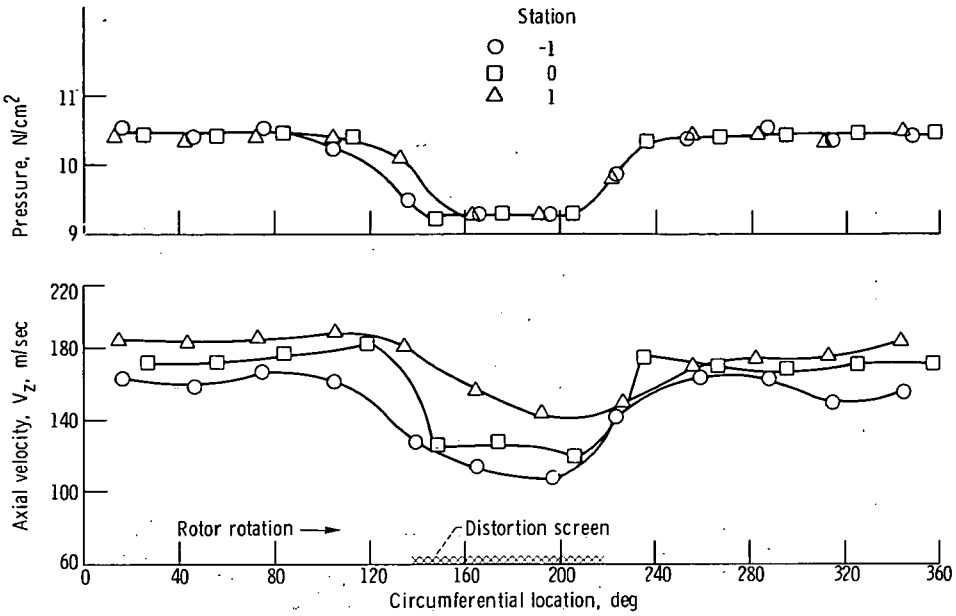

Figure 19. - Circumferential distributions of flow parameters between screen and rotor in reference MVR stage 11-4. Near stall; design speed; 90^0 circumferential distortion; midspan.

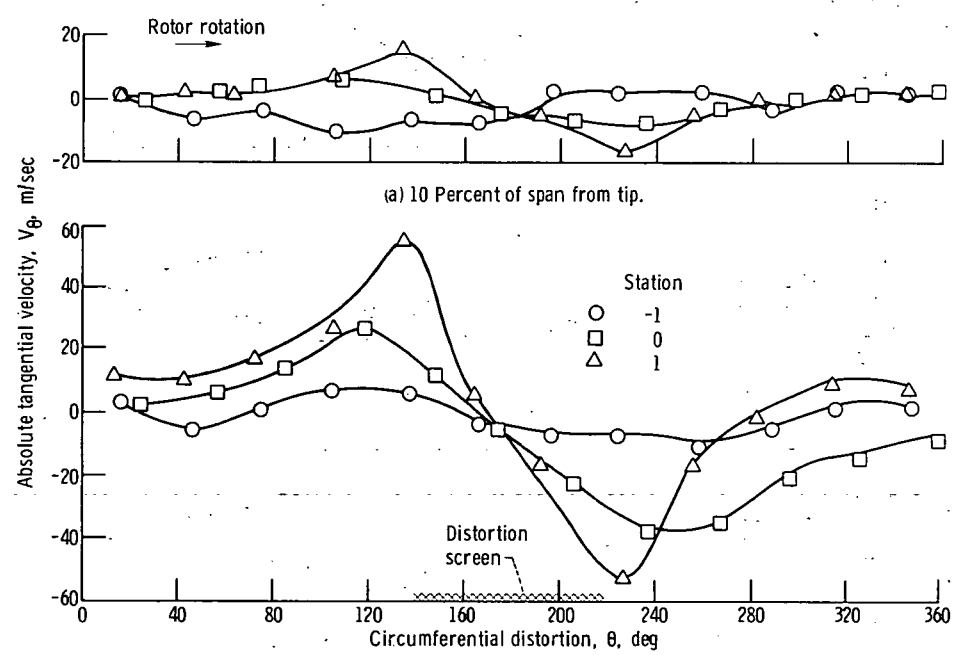

Figure 20. - Circumferential distributions of absolute tangential velocity between screen and rotor in reference MVR stage 11-4. Near stall; design speed; 90^0 circumferential distortion; midspan.

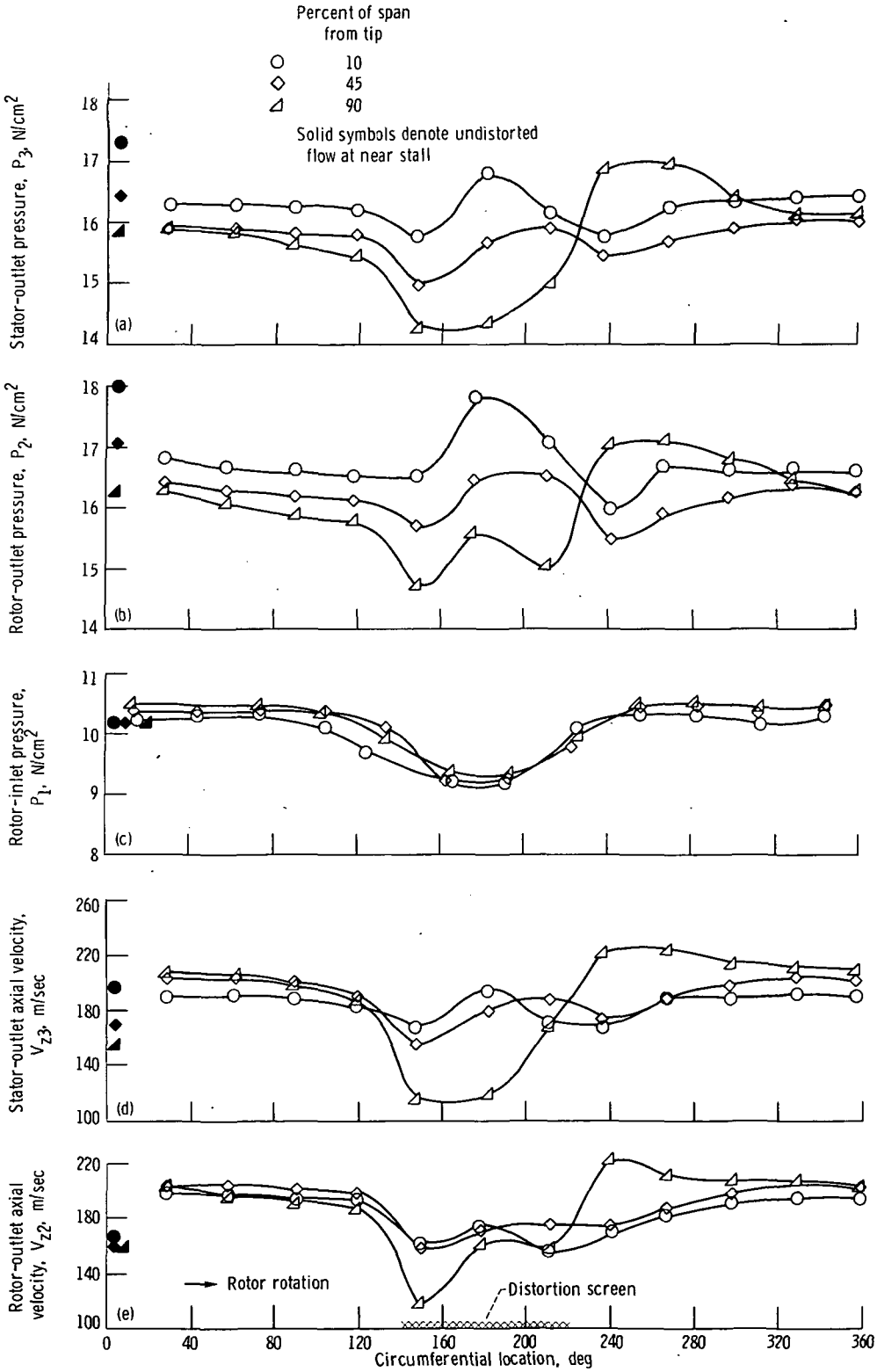

Figure 21. - Circumferential distributions of flow parameters at rotor inlet, rotor outlet, and stator outlet planes in reference MVR stage 11-4. Near-stall conditions; 100 percent of design speed; 90^0 circumferential distortion.

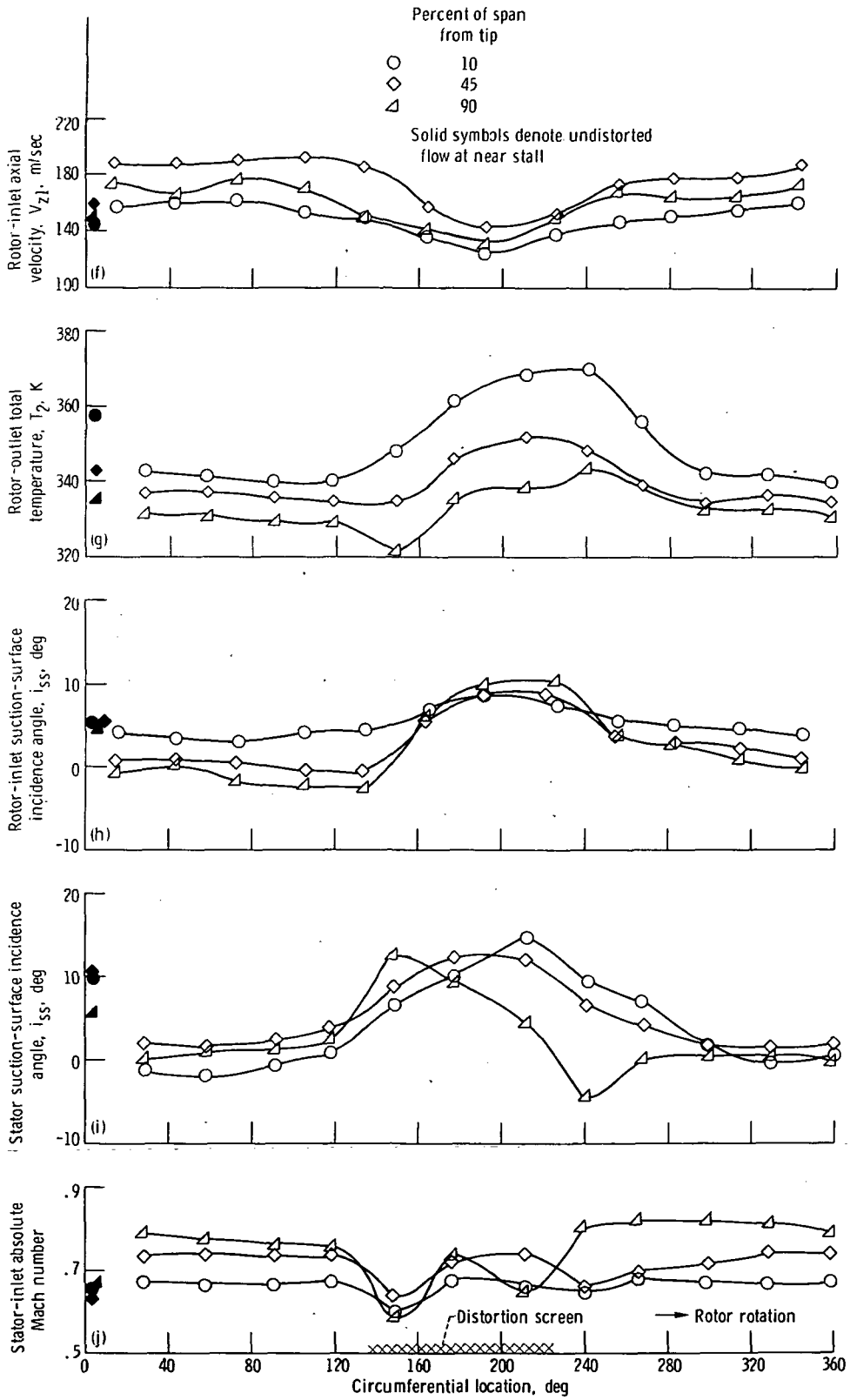

Figure 21. - Concluded.

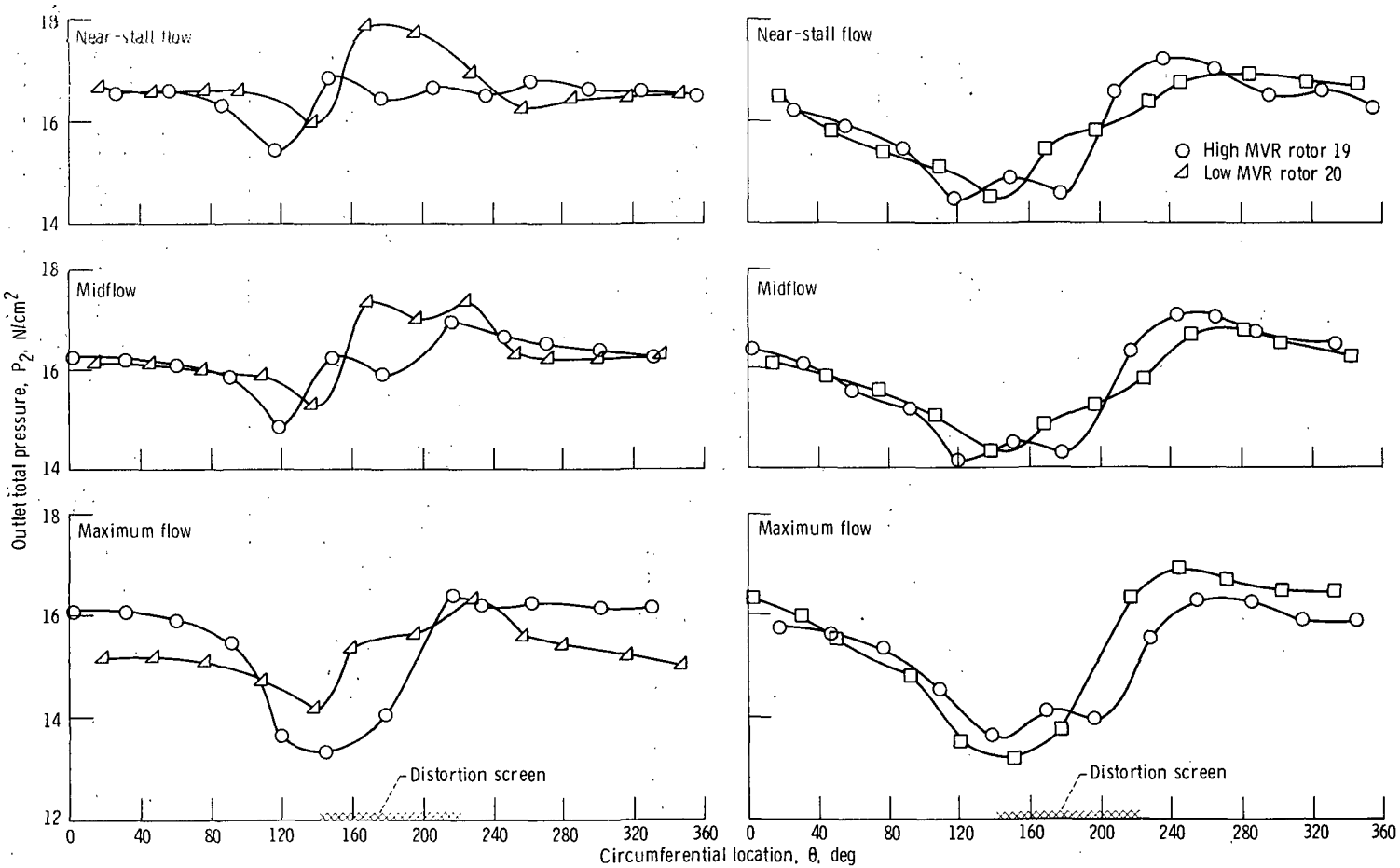

Figure 22. - Exit-total-pressure distributions at three flow rates for 90^0 circumferential distortion. Magnitude of distortion, 0.13.

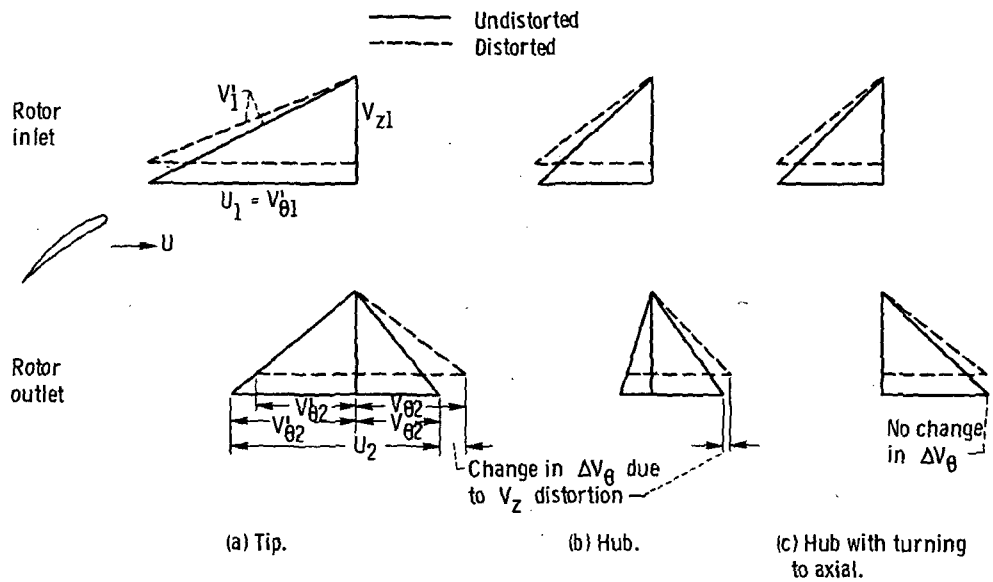

Figure 23. - Effect of velocity triangles on response to inlet distortion.

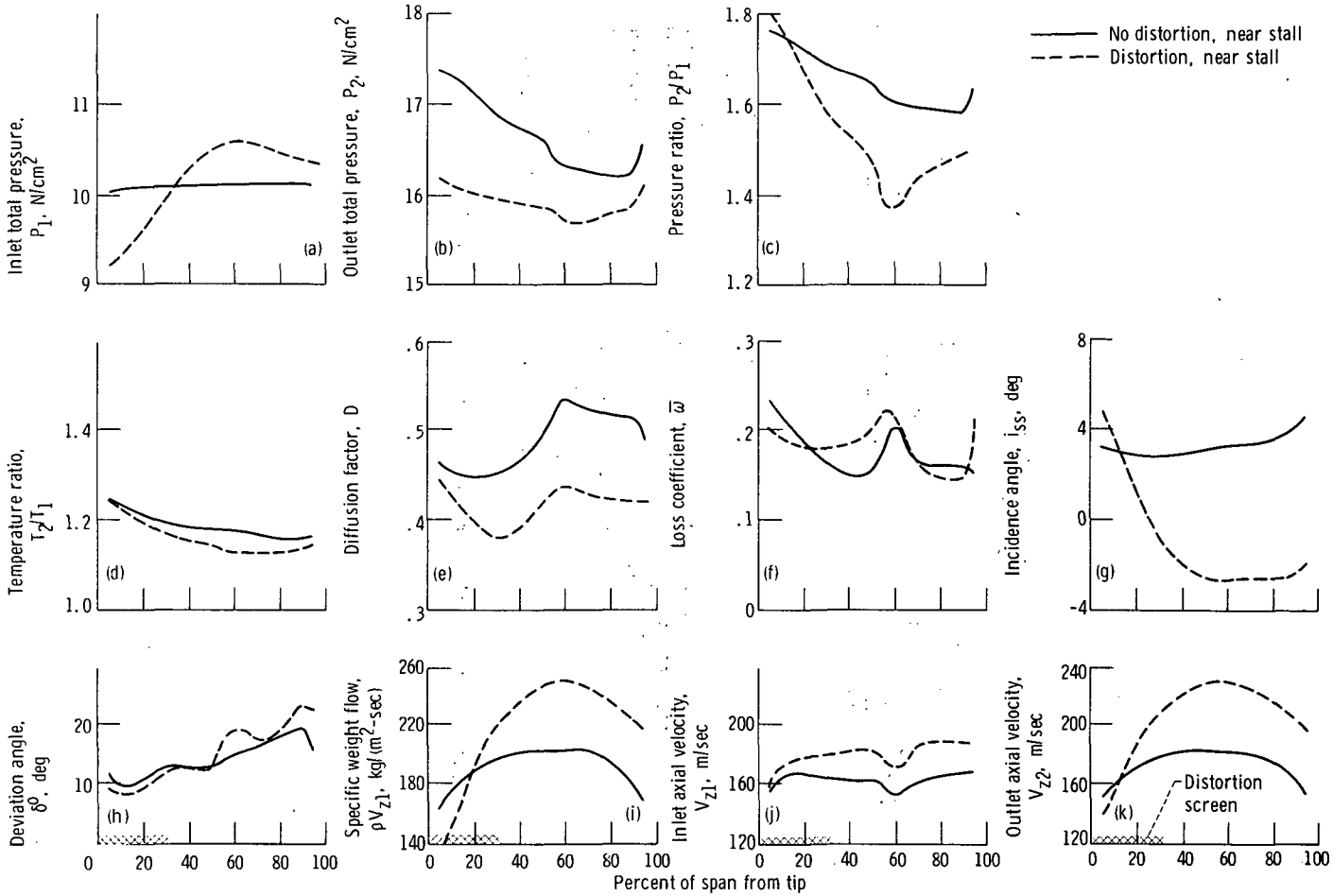

Figure 24. - Radial distributions of selected flow parameters with radially distorted and undistorted flows in low MVR rotor 20. Design speed; magnitude of distortion, 0.18.

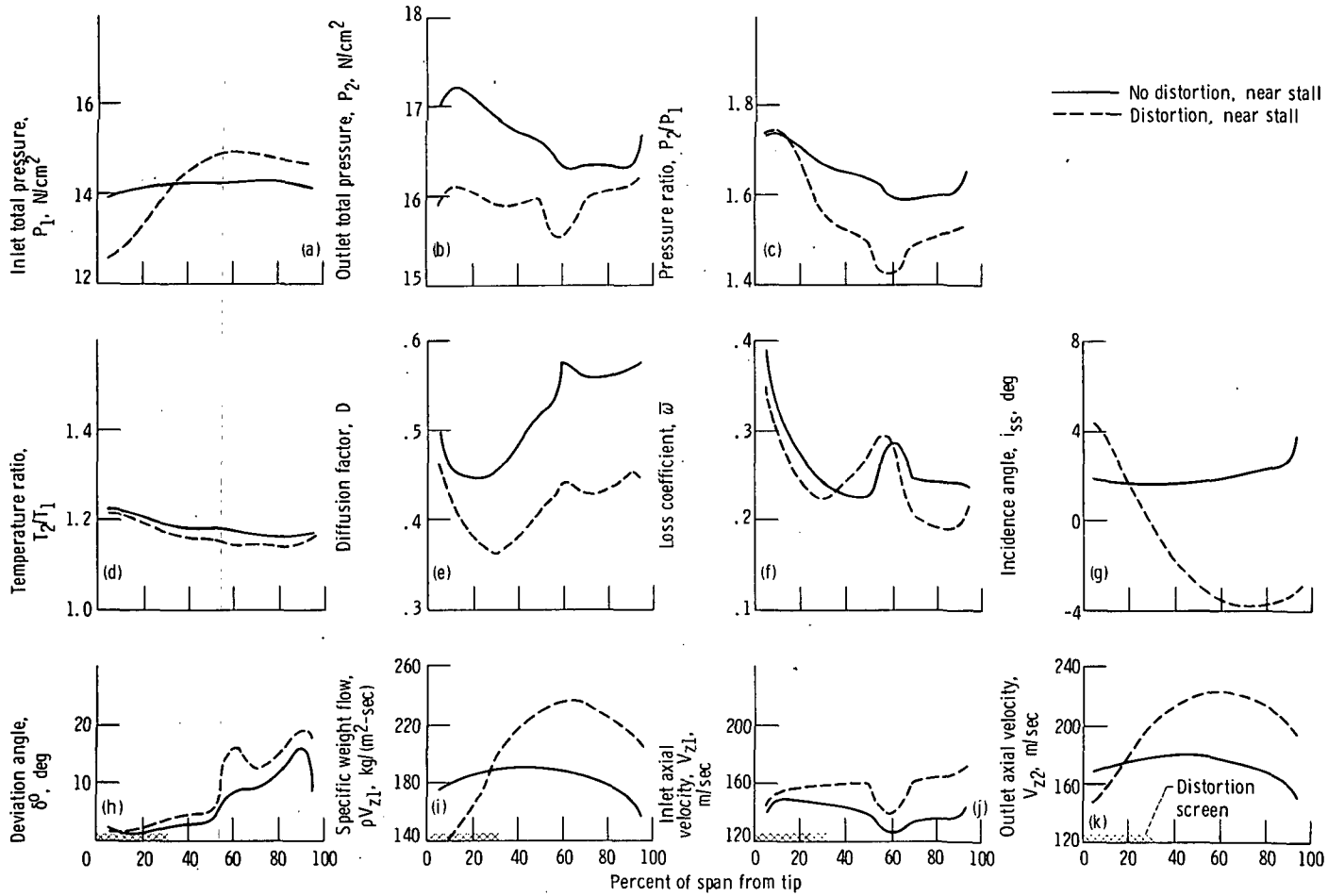

Figure 25. - Radial distributions of selected flow parameters with tip radially distorted and undistorted flows in high MVR rotor 19. Design speed; magnitude of distortion, 0.16.

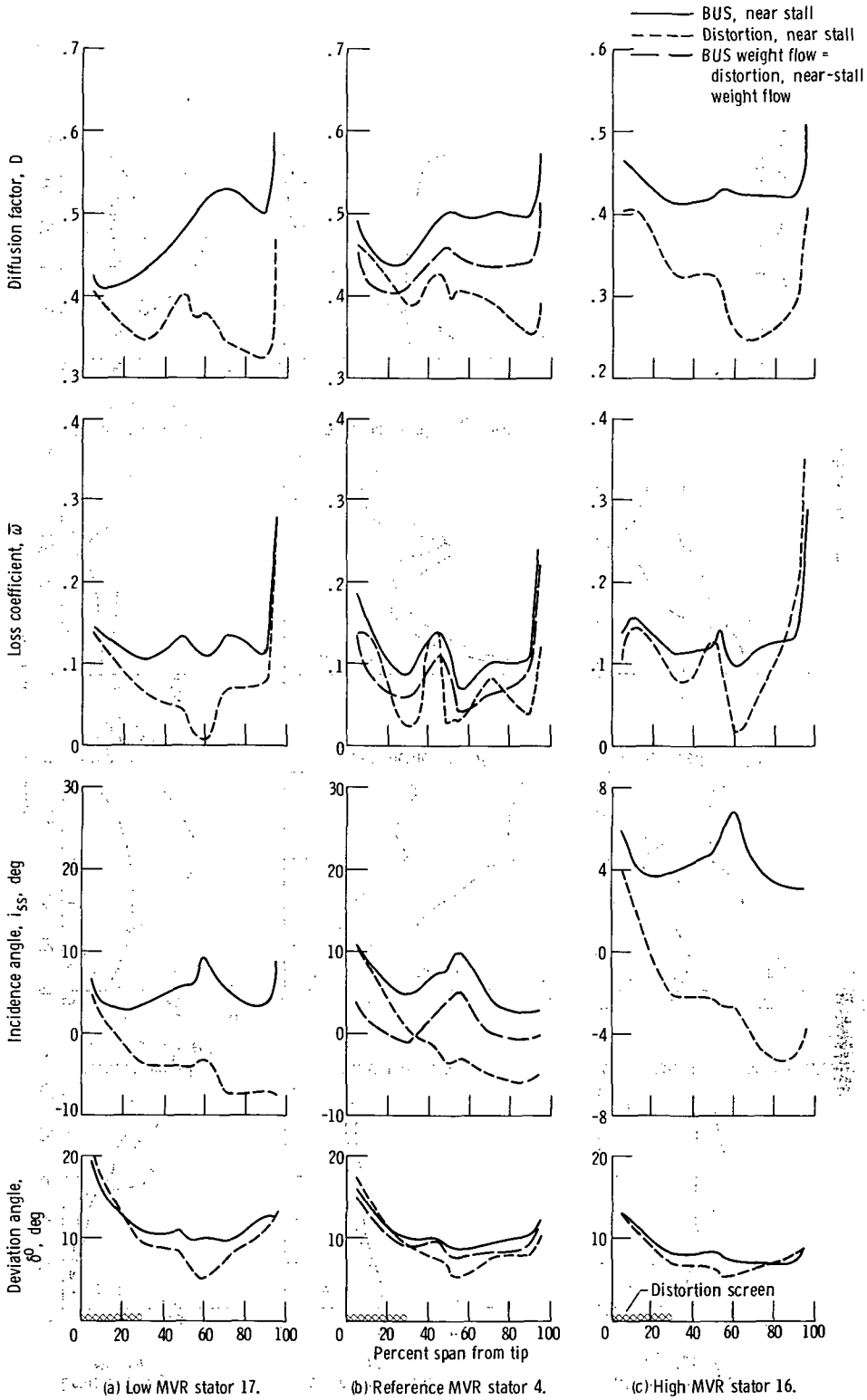

Figure 26. - Radial distributions of selected flow parameters with tip radially distorted and undistorted flows in stators. Design speed; magnitude of distortion, 0.16.

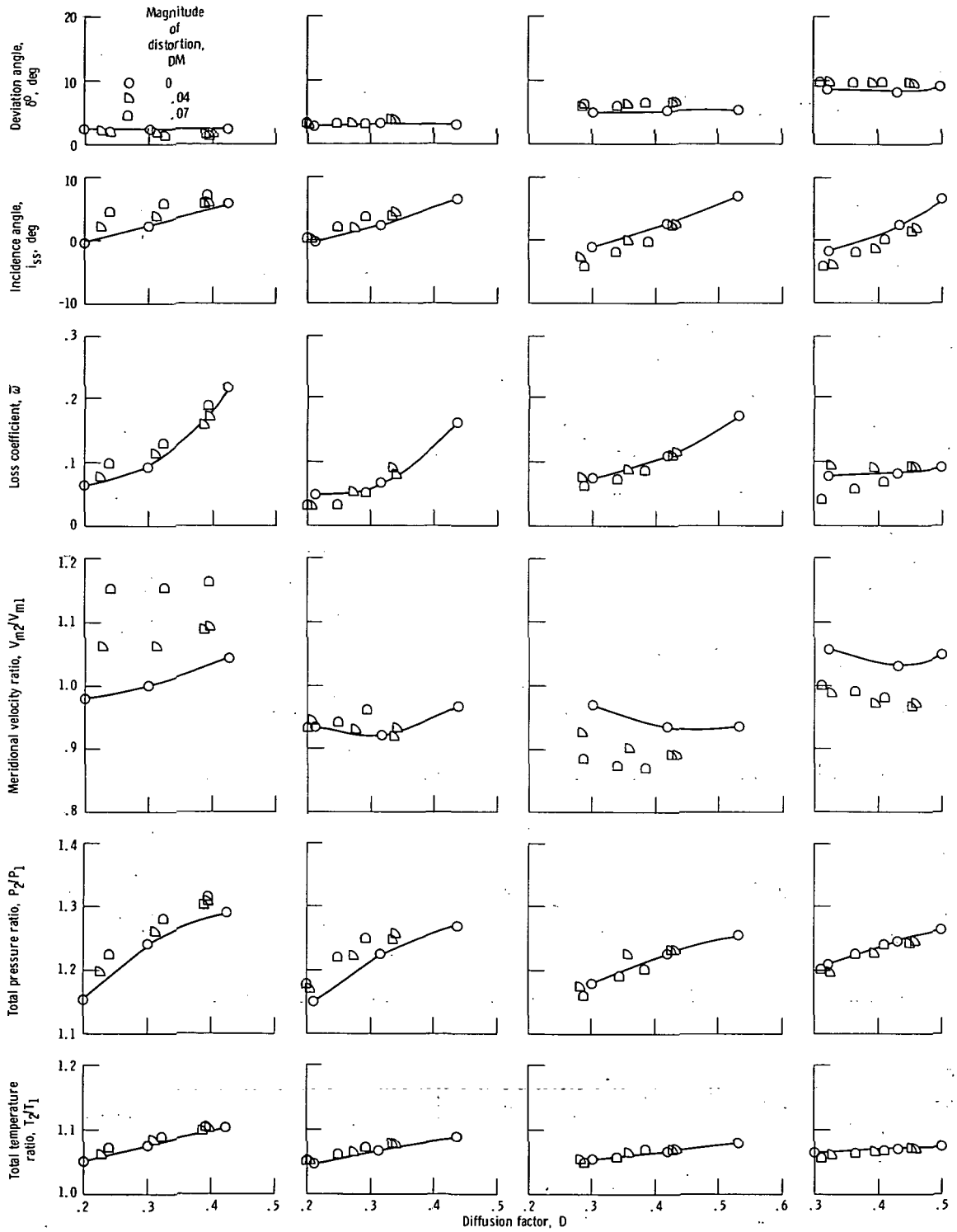

Figure 27. - Low MVR rotor 20 blade-element performance at 70 percent of design speed.

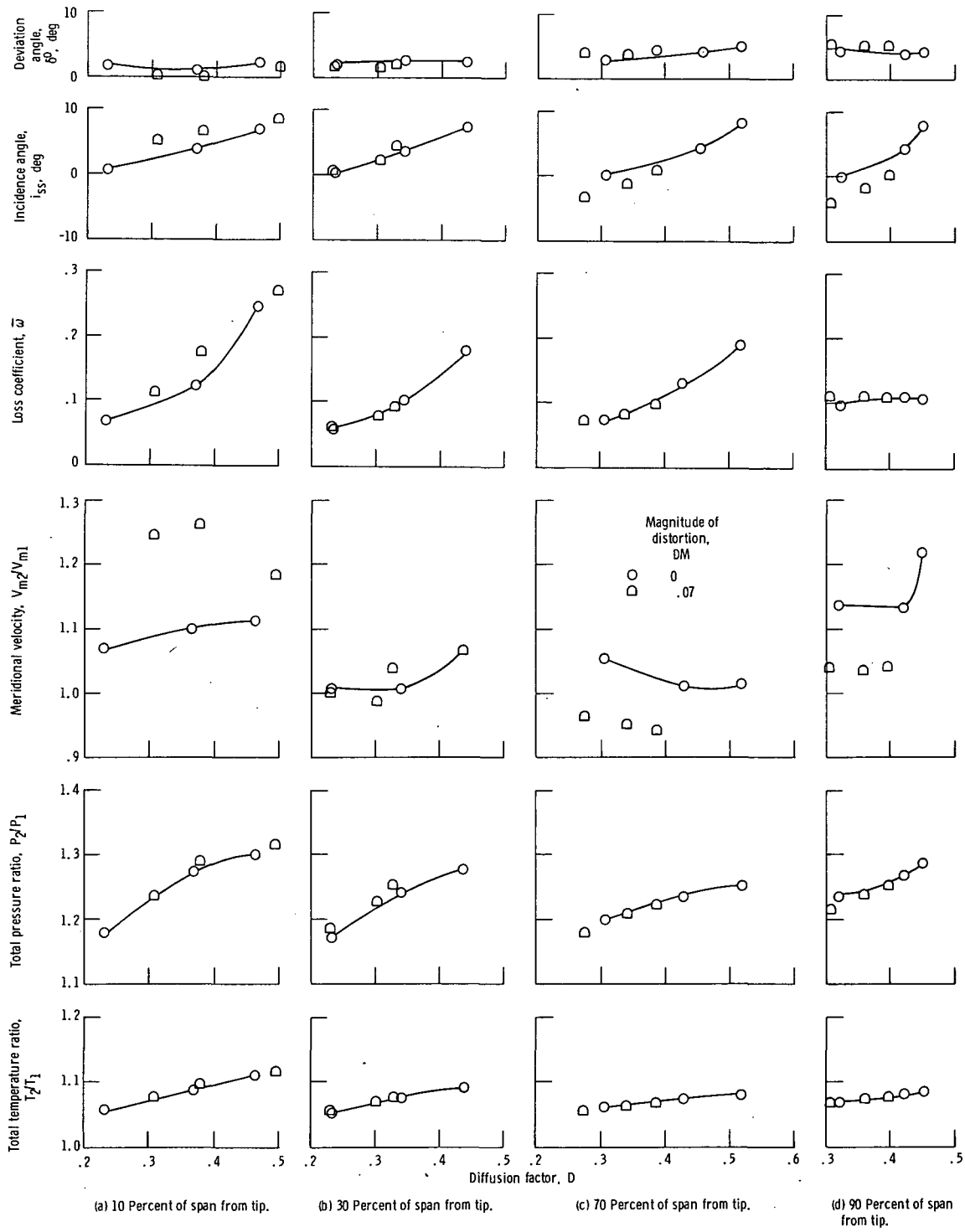

Figure 28. - Reference MVR rotor 11 blade-element performance at 70 percent of design speed.

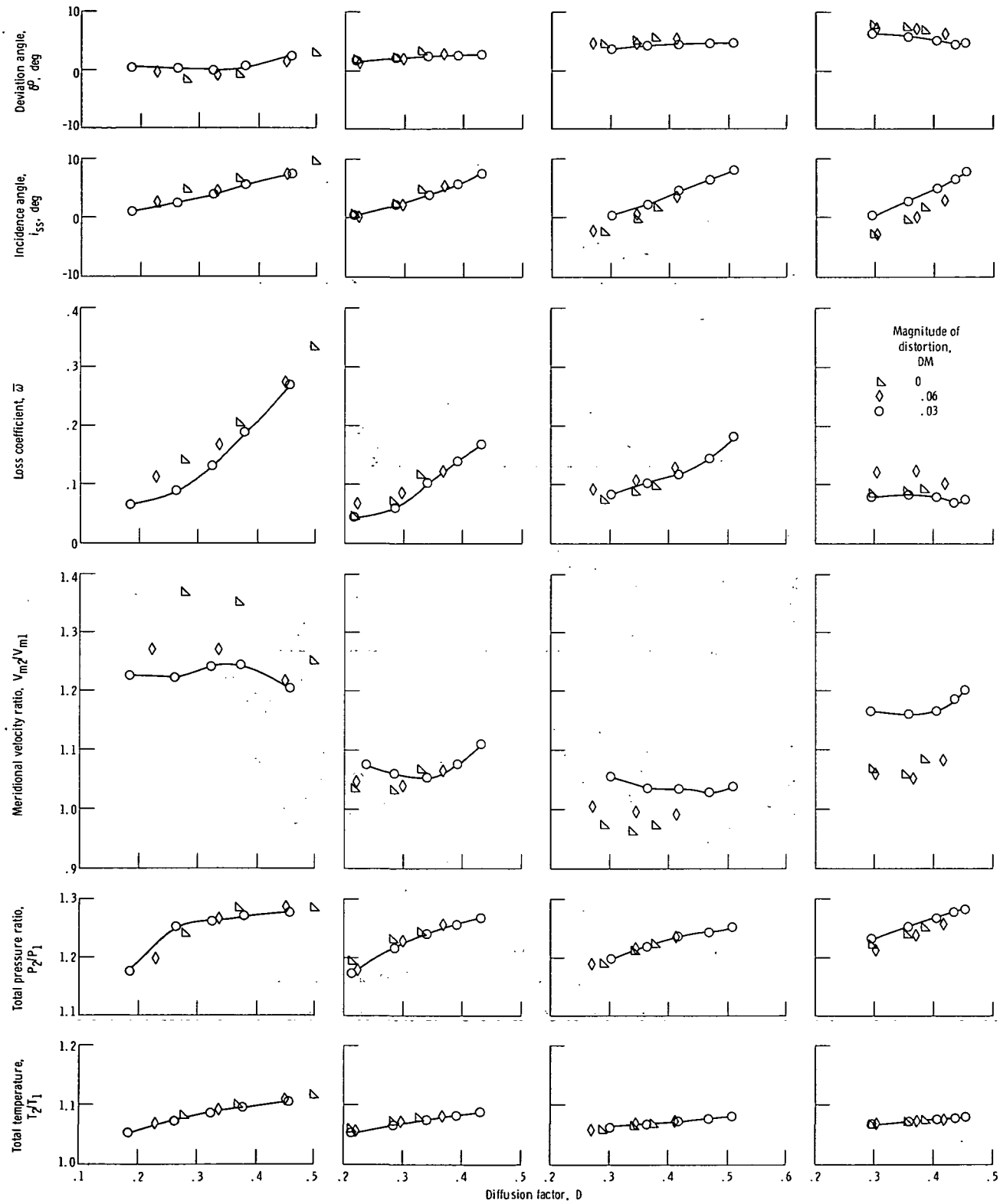

(a) 10 Percent of span from tip. (b) 30 Percent of span from tip. (c) 70 Percent of span from tip. (d) 90 Percent of span from tip.

Figure 29. - High MVR rotor 19 blade-element performance at 70 percent of design speed.

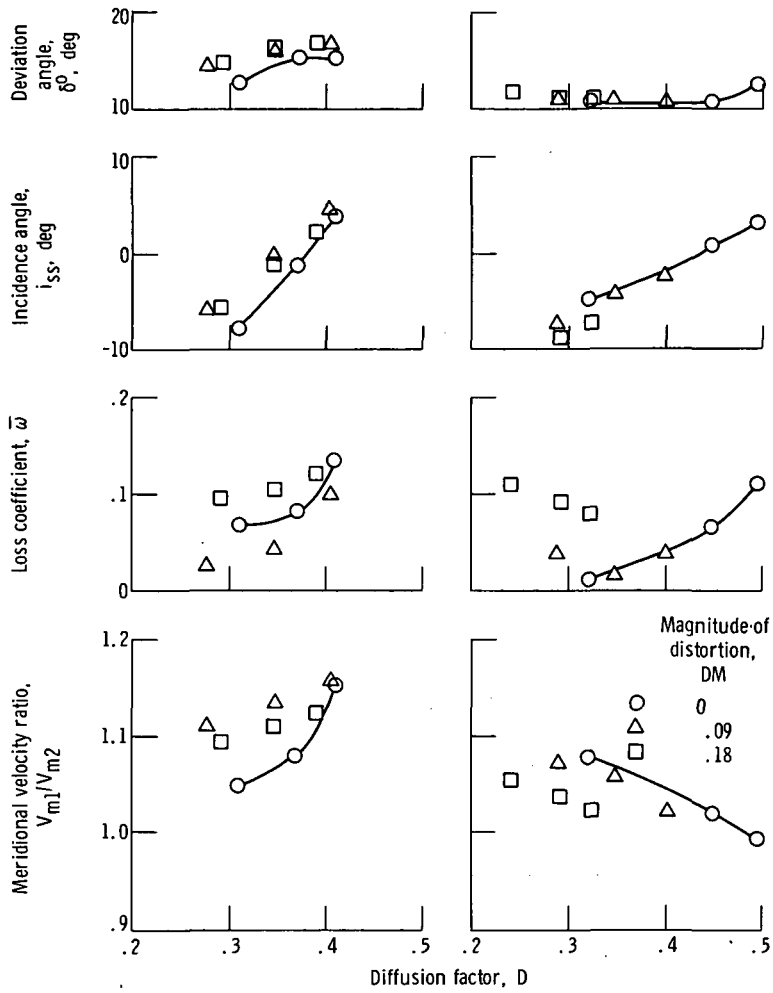

(a) 10 Percent of span from tip. (b) 90 Percent of span from tip.

Figure 30. - Stator 17 (low MVR stage 20-17) blade-element performance at design speed.

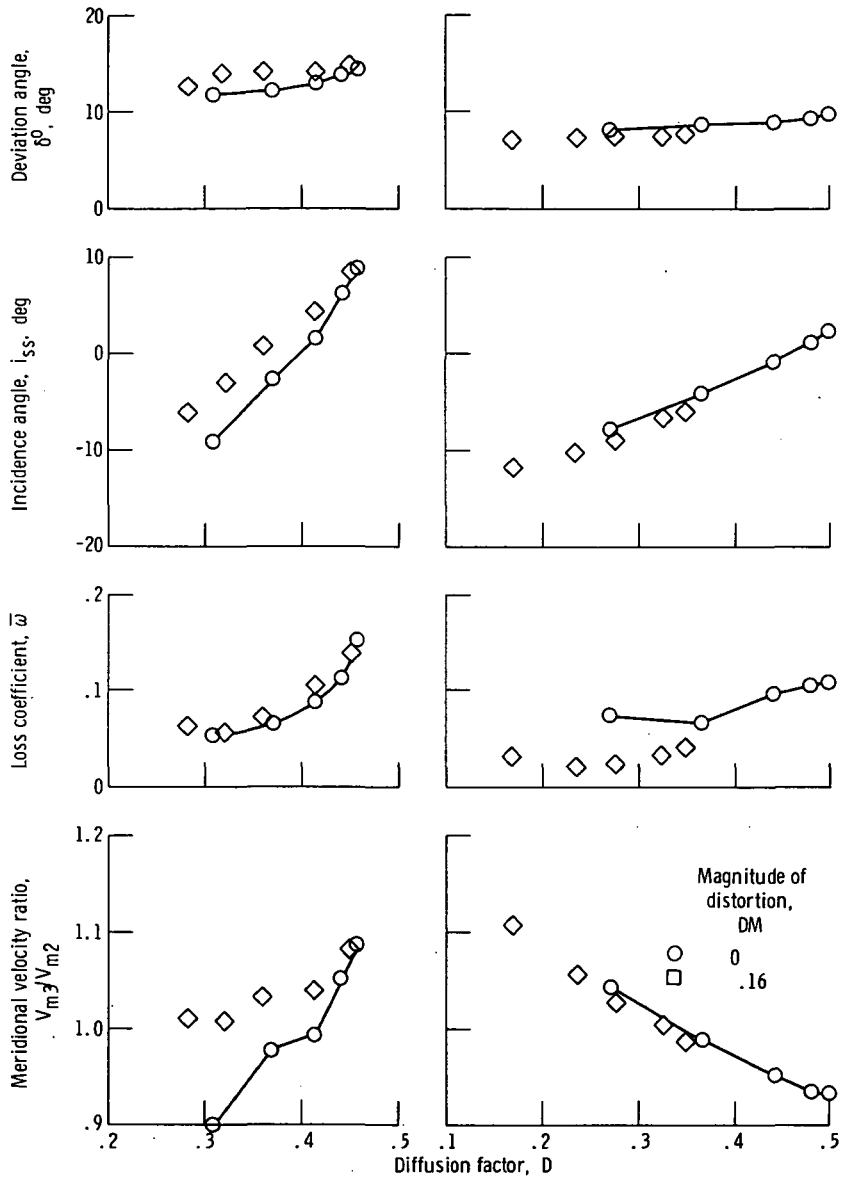

(a) 10 Percent of span from tip. (b) 90 Percent of span from tip.

Figure 31. - Stator 4 (reference MVR stage 11-4) blade-element performance at design speed.

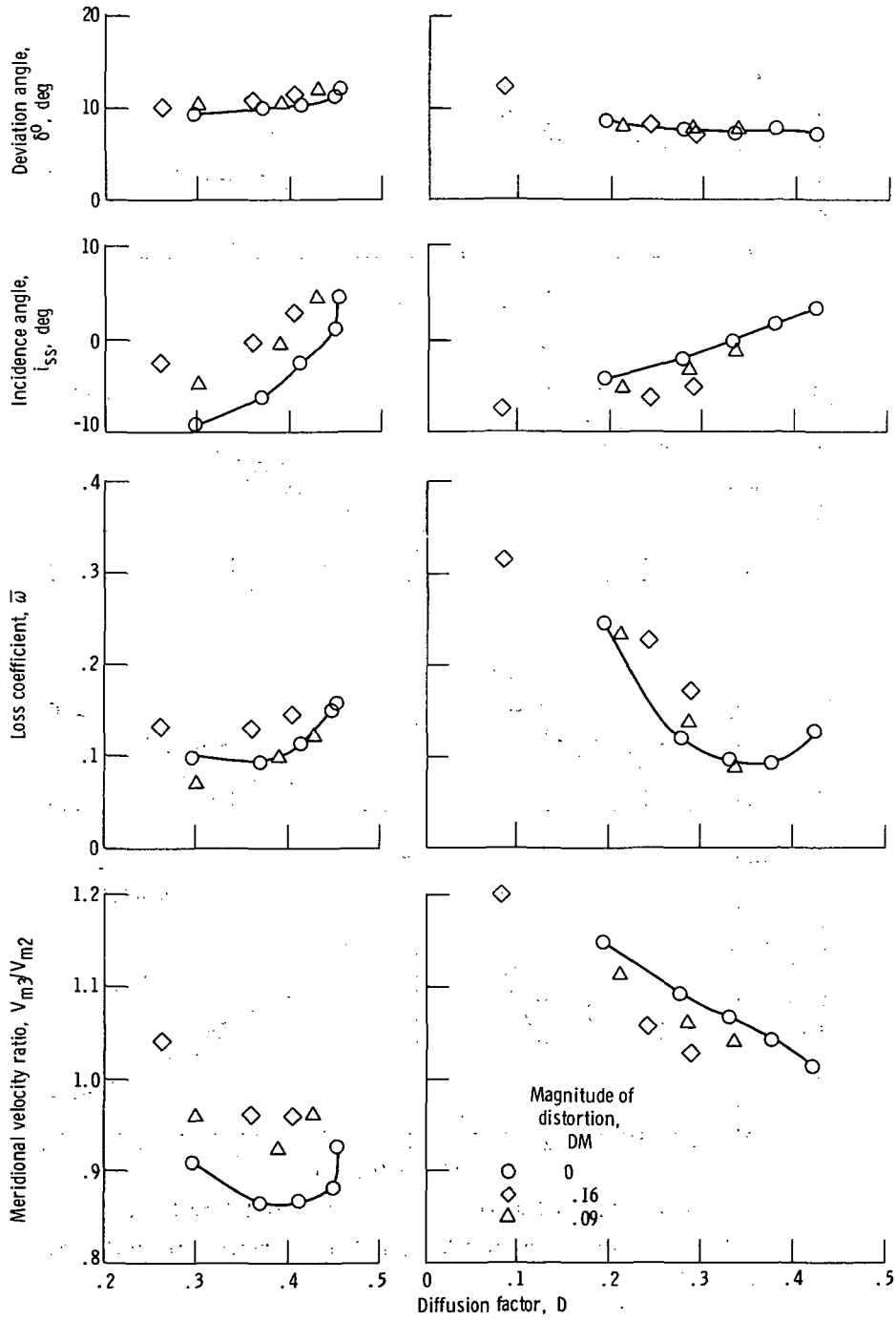

(a) 10 Percent of span from tip. (b) 90 Percent of span from tip.

Figure 32. - Stator 16 (high MVR stage 19-16) blade-element performance at design speed.

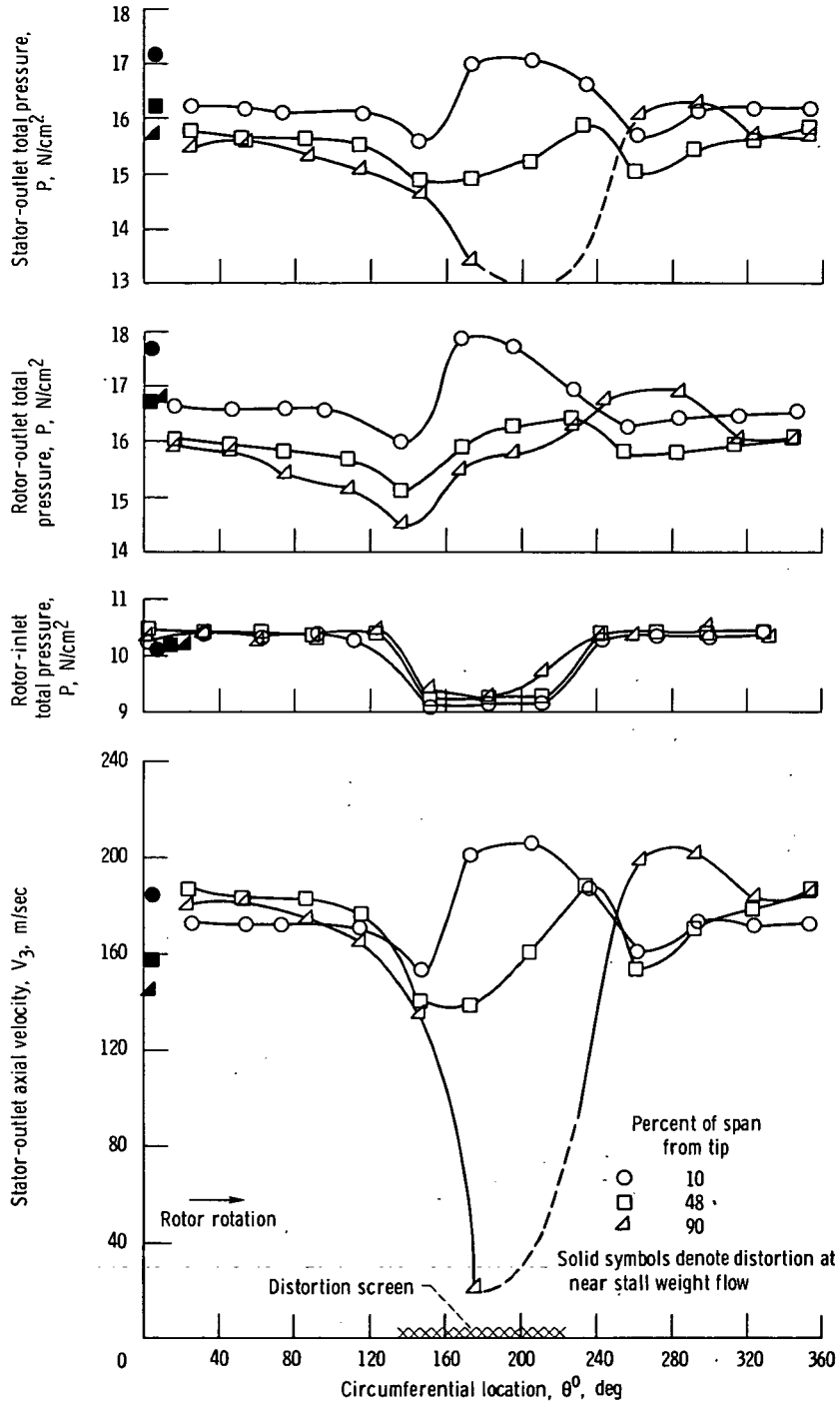

Figure 33. - Circumferential distributions of flow parameters at rotor inlet, rotor outlet, and stator outlet planes in low MVR stage 20-17. Near-stall conditions; design speed; 90° circumferential distortion.

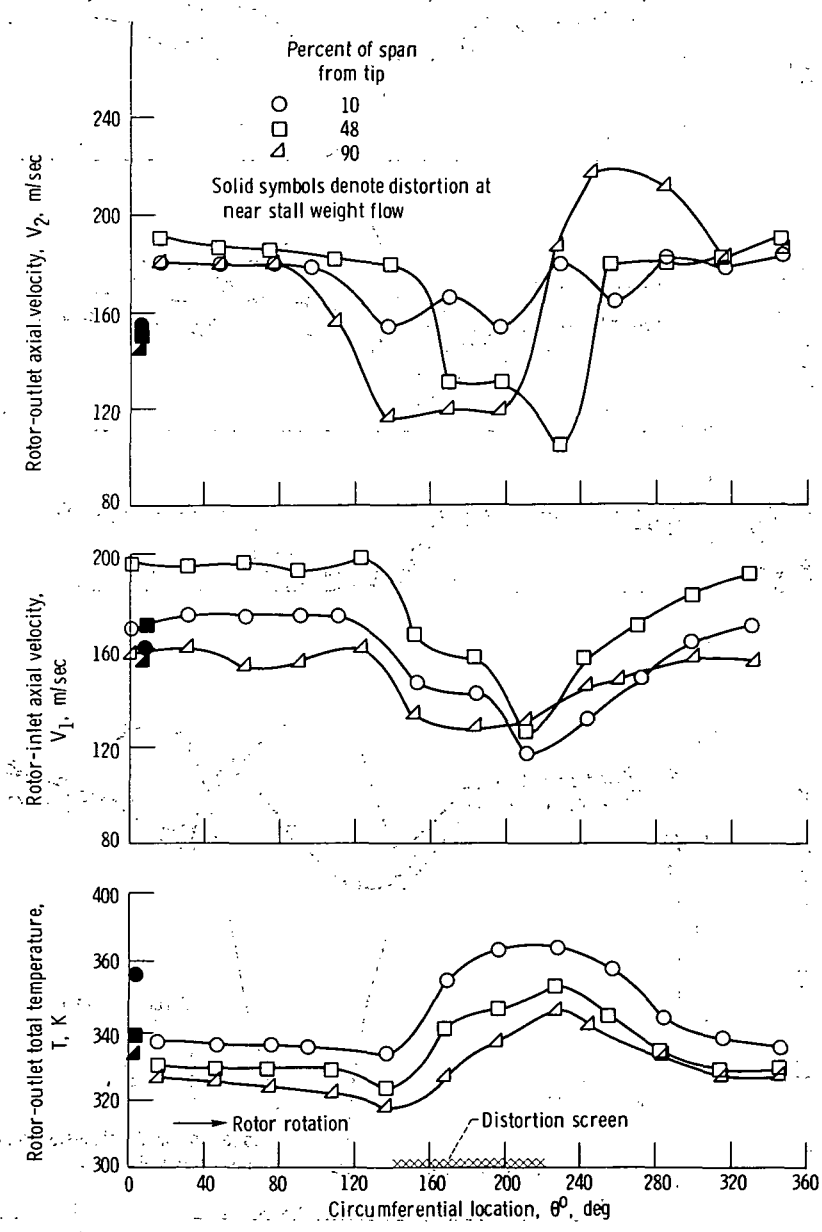

Figure 33. - Continued.

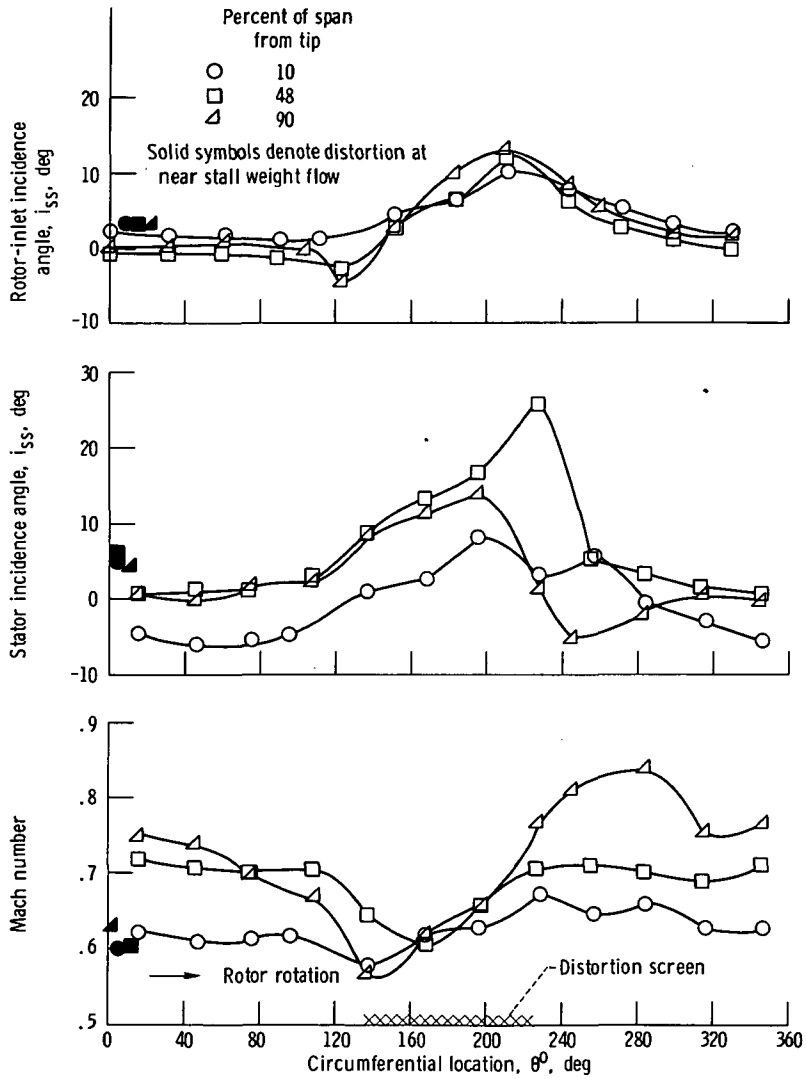

Figure 33. - Concluded.

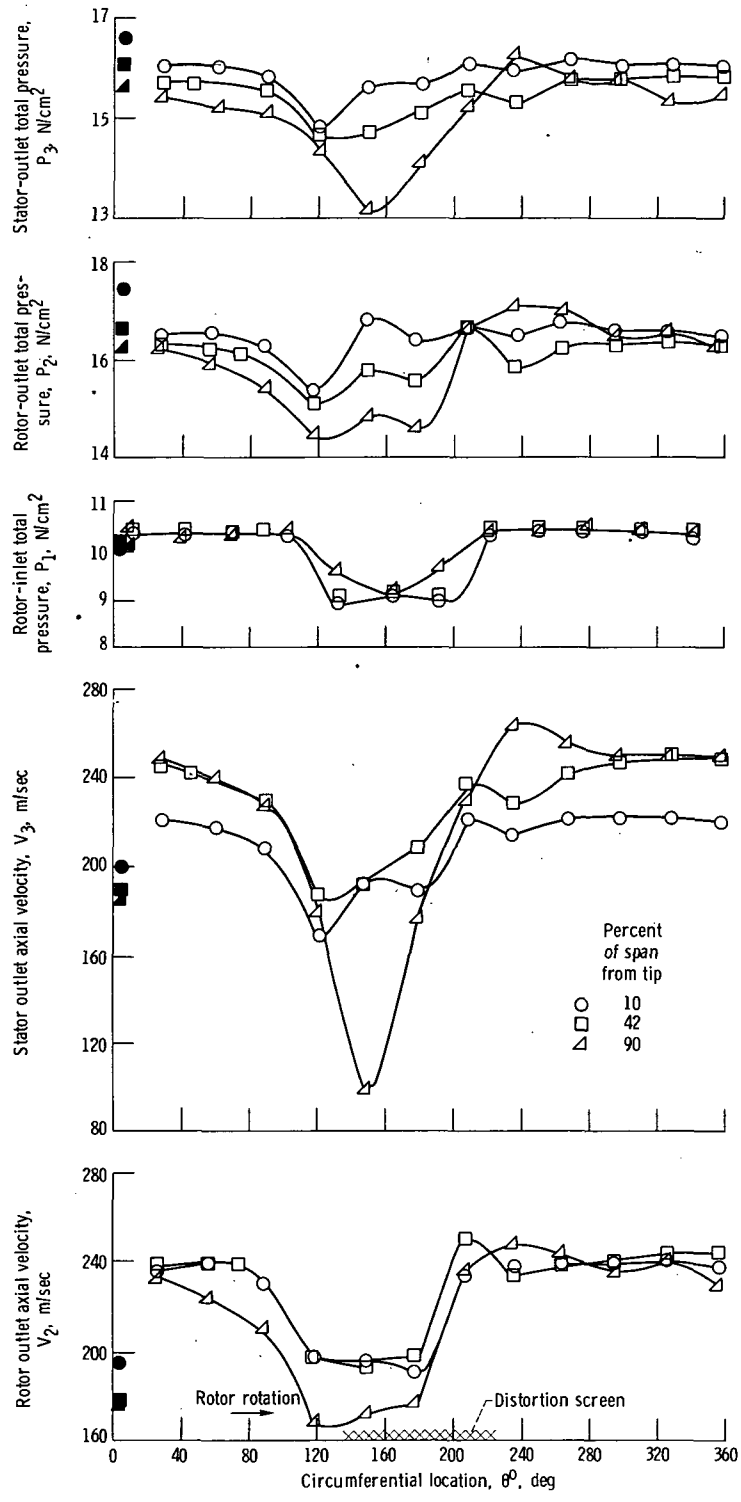

Figure 34. - Circumferential distribution of flow parameters at rotor inlet, rotor outlet, and stator outlet planes in high MVR stage 19-16. Near-stall conditions; design speed; 90^0 circumferential distortion.

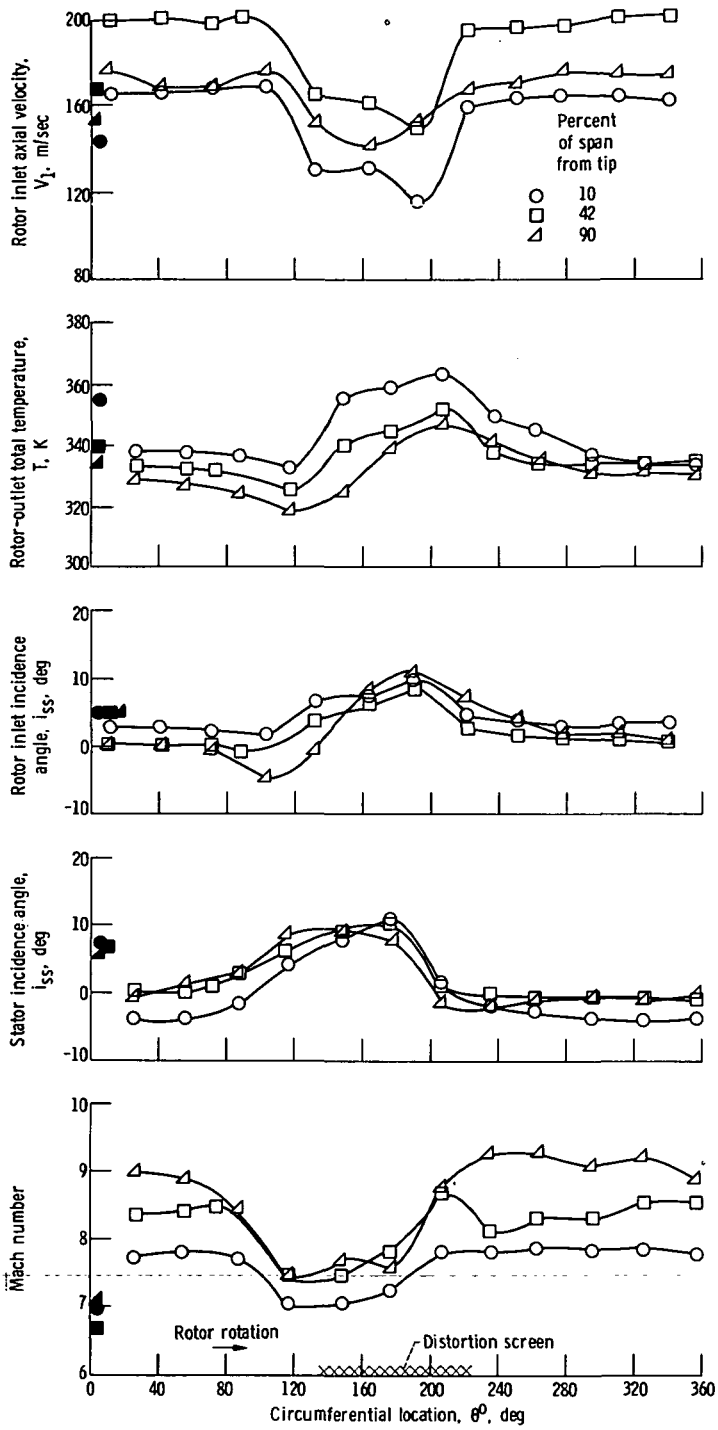

Figure 34. - Concluded.

1. Report No.	2. Government Accession No.	3. Recipient's Catalog No.
NASA TP-1278		

4. Title and Subtitle	5. Report Date
EFFECT OF ROTOR MERIDIONAL VELOCITY RATIO ON RESPONSE TO INLET RADIAL AND CIRCUMFERENTIAL DISTORTION	July 1979
	6. Performing Organization Code
7. Author(s)	8. Performing Organization Report No.
Nelson L. Sanger	E-8987
	10. Work Unit No.
9. Performing Organization Name and Address	505-04
National Aeronautics and Space Administration Lewis Research Center Cleveland, Ohio 44135	11. Contract or Grant No.
	13. Type of Report and Period Covered
12. Sponsoring Agency Name and Address	Technical Paper
National Aeronautics and Space Administration Washington, D.C. 20546	14. Sponsoring Agency Code

15. Supplementary Notes

16. Abstract

Three single transonic fan stages, each having a different meridional velocity ratio across its rotor, were tested with two magnitudes of tip radial distortion and with a 90^{o} circumferential distortion imposed on the inlet flow. The rotor with the lowest meridional velocity ratio (less than 0.9 at the tip) demonstrated the least degradation of performance due to these distortions. Loss and deviation angle data (as needed for performance prediction with radial distortion) calculated along actual streamlines for radially distorted flow and correlated against diffusion factor, showed consistent agreement with data calculated along design streamlines for undistorted flow.

17. Key Words (Suggested by Author(s))	18. Distribution Statement
Turbomachinery	Unclassified - unlimited STAR Category 07

19. Security Classif. (of this report)	20. Security Classif. (of this page)	21. No. of Pages	22. Price*
Unclassified	Unclassified	73	A04

* For sale by the National Technical Information Service, Springfield, Virginia 22161

NASA-Langley, 1979

National Aeronautics and
Space Administration

Washington, D.C.
20546

Official Business
Penalty for Private Use, $300

THIRD-CLASS BULK RATE

Postage and Fees Paid
National Aeronautics and
Space Administration
NASA-451

POSTMASTER: If Undeliverable (Section 158 Postal Manual) Do Not Return